The Thesis Committee for James Robert Kleineck
Certifies that this is the approved version of the following thesis:

Galvanizing Crack Formation at Base Plate to Shaft Welds of High Mast Illumination Poles

APPROVED BY

SUPERVISING COMMITTEE:

Supervisor:

Todd Helwig

Michael Engelhardt

Galvanizing Crack Formation at Base Plate to Shaft Welds of High Mast Illumination Poles

by

James Robert Kleineck, B.S.

Thesis

Presented to the Faculty of the Graduate School of

The University of Texas at Austin

in Partial Fulfillment

of the Requirements

for the Degree of

Master of Science in Engineering

The University of Texas at Austin

August, 2011

This thesis is dedicated to my family and extended family. You all have always been a source of strength and encouragement for me as I pursued my dreams. Your love, care, and prayers have meant more to me than words can do justice.

Acknowledgements

Abstract

Galvanizing Crack Formation at Base Plate to Shaft Welds of High Mast Illumination Poles

James Robert Kleineck, M.S.E.

The University of Texas at Austin, 2011

Supervisor: Todd Helwig

High mast illumination poles (HMIPs) are tall cantilevered structures used to efficiently illuminate large portions of highways and interchanges. Great interest in the performance of HMIPS has arisen from the discovery of extensive premature cracking at the toes of base plate to pole shaft welds of poles currently in service. These cracks, in some cases, have become so severe that HMIPs have actually collapsed, and therefore present a great threat to public safety.

Previous research at the University of Texas at Austin sought to solve the design problems posed by these pole failures by conducting both full-scale and analytical tests on optimized designs of HMIPs for fatigue loads. These studies indicated that using full penetration welds to connect 3" thick base plates to relatively thin shaft walls minimized warping of the base plate during fatigue loading, and maximized fatigue performance.

Toward the end of these studies when researchers sought to test an uncoated optimized HMIP back-to-back against a galvanized HMIP of the same design and material, researchers discovered the galvanized specimen had cracked during the galvanizing

process. This finding prompted an in-depth study to determine the cause of these cracks, and to determine if practices could be implemented to prevent crack formation.

Initially, bend radius, chemistry, and shaft to base plate thickness studies were conducted to find how these parameters affect HMIPs during galvanizing. These parameters were found to play a minor role in the cracking of HMIPs relative to the thermal effects induced during the galvanizing process. Full-scale and analytical tests verified the impact of thermal straining within HMIPs during galvanizing. Instrumenting HMIPs and smaller HMIP stub sections with thermocouples and strain gages provided temperature and initial strain gradients resulting from exposure to the molten zinc bath. This data, as well as observations of cracks in the tested HMIP sections, aided the development of a finite element parametric study comparing HMIPs of the same 150' length and 80 mph design but varying shaft thicknesses. This research concludes that reducing the pole shaft diameter to thickness ratio reduces the likelihood of galvanizing crack formation.

Table of Contents

List of Tables

List of Figures

xvii

xviii

CHAPTER 1. INTRODUCTION

1.1 Origin of Problem

High mast illumination poles (HMIPs) are often used to provide lighting for large areas around freeways and interchanges, as shown in Figure 1-1. These steel poles are fabricated in segments that are galvanized to improve the long-term corrosion performance. The geometry of the poles is dependent on the height requirements as well as the design wind speed, and can typically vary from 100' to 175'. A major concern within TxDOT is the relatively recent finding that several HMIPs across the state have cracks at weld toes between the pole shaft and base plate. Due to the potential for fatigue damage from wind loads acting on the poles, the cracks pose a major safety concern for the public. TxDOT has funded a number of studies in recent years to improve the fatigue resistance of HMIPs. The most recent study has focused on the cause of cracks that have been found in relatively new poles. The research is focused on answering two questions about these cracks: 1.) Why are these cracks forming? and 2.) How much fatigue life is left in these HMIPs?

Figure 1-1: High masts at a freeway interchange (Rios, 2007)

Seeking answers to these questions led researchers to understand that cracks can form in HMIPs by two separate mechanisms. After focusing research efforts on the fatigue performance of HMIPs, researchers at the University of Texas were aware of the potential for crack growth due to fatigue loads. But studying the fatigue performance of HMIPs also led researchers to become aware of cracks that formed during galvanizing, prior to loading in the field, as shown in Figure 1-2.
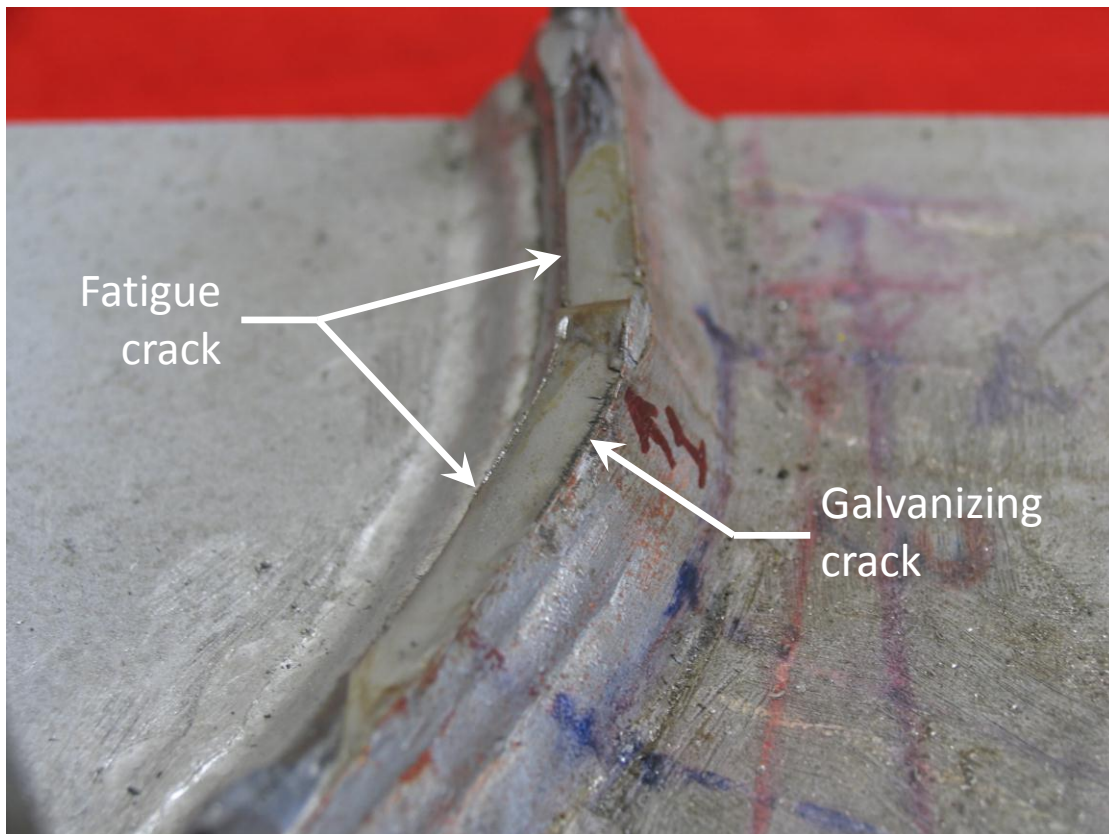
Figure 1-2: Crack at bend from high mast illumination tower after fatigue testing

1.2   Scope of Research

Building on this previous work, researchers at the University of Texas broadened their research to not only evaluate the design of poles, but to better understand their loading conditions as a means of answering the questions raised by TxDOT. The research was split into two topics: the evaluation of wind loads on HMIPs (Magenes, 2011), and the evaluation of performance during the galvanizing process, which is the focus of this thesis.

Research on the performance during galvanizing included monitoring HMIP sections during the galvanizing process and also conducting parametric finite element analyses to better understanding the cause of the cracking and also to propose methods of mitigating the cracking problem. The field instrumentation consisted of instrumenting pole sections with thermocouples to measure the thermal gradients to which the HMIPs are subjected during the galvanizing process. In the last round of these tests, strain gages were also used to gain a measure of the thermally induced strains that occurred during dipping of the pole section in the galvanizing bath.

The field data proved valuable for validating the accuracy of finite element models developed to simulate the dipping procedure. These models were used to conduct parametric analyses on HMIP sections, allowing evaluation of the thermal and structural response to the galvanizing process. From these analyses, hotspots were located where large thermal strains may be contributing to crack formation in the weld between the base plate and the shaft. The combined field monitoring and parametric analyses were used to develop recommendations that might mitigate the cracking problems that have occurred during the galvanizing process.

1.3   Organization of Thesis

The thesis has been divided into eight chapters. Following this introduction, Chapter 2 provides an overview of fatigue research on HMIPs, the galvanizing process, and the state of the art in approaching cracks during galvanizing. Chapter 3 provides an overview of the testing that led to the decision to evaluate thermal loads on HMIPs during galvanizing. An overview of the instrumentation that was used in the field studies as well as methods used to set up the instrumentation is presented in Chapter 4. Chapter 5 discusses the geometries of each field test and the results from these field tests. An overview of the finite element model development is provided in Chapter 6 and the results from the subsequent parametric investigation are provided in Chapter 7. Finally, the conclusions and recommendations from this study are summarized in Chapter 8.

CHAPTER 2.   BACKGROUND INFORMATION

2.1   Introduction

There have been a number of studies on high mast illumination poles (HMIP) over the past several years. Research on the poles at the University of Texas began around 2003 and focused on the fatigue performance of various shaft to base plate details. The initial research included full scale testing and analytical modeling to determine failure mechanisms for HMIP systems. The results were used to develop design recommendations for improving pole fatigue performance. After researchers arrived at design recommendations in the initial phases of the studies, additional laboratory tests were conducted to verify the design recommendations. Fatigue test failures indicated that significant differences existed between earlier analytical models and the full scale test results. Initially through ultrasonic testing (UT), and later through destructive testing, researchers determined the origin of this loss in fatigue resistance stemmed from initial cracks that formed during the galvanizing process in the HMIPs.

This chapter summarizes the origins of this phase of research, describes the current state of the art of hot dip galvanizing, and explores theories concerning the formation of initial cracks in steel high mast illumination poles during the galvanizing process.

2.2   High Mast Illumination Pole Fatigue Design and Recommendations

The fatigue behavior of high mast illumination was studied in depth at the University of Texas over the past several years. The work includes large scale experimental testing as well as parametrical finite element analysis and is summarized by Rios (2007), Stam (2009), and Pool (2010). These researchers undertook their work in response to a growing concern among several departments of transportation following failures in high mast illumination poles well before the end of the design lives. Some of these failures consisted of cracks that propagated and resulted in brittle fractures leading to collapse of the HMIP (Conner et al., 2005). Stam (2009) reported on several HMIP failures documented in the literature (Rios, 2007) (Ocel, 2006) (Warpinski, 2006).

The danger of a high mast illumination pole collapsing across an interstate highway or road produces a hazard to the public that led to the creation of a multi-state department of transportation Pooled Fund Study to evaluate the design adequacy of current fabrication details and potential design solutions. Results from the different phases of this study are listed below.

The investigation began with a review of typical HMIP design practices. According to Rios (2007), the 2001 AASHTO Specification, resulted in a poor design that led to potential early failures at the toe of the baseplate to pole shaft weld under service loading. AASHTO Specification Section 11.5 governs the design of the baseplate to shaft connection, as noted by Pool, "which states that all components shall be designed to accommodate fatigue stresses within their constant amplitude fatigue limits (CAFL) (2010)." Obviously, these provisions were not being met by available design techniques and typical details. Rios (2007) and Stam (2009) focused their research on developing solutions to these issues.

2.2.1 Phase I and Phase II Pooled Fund Fatigue Study Results

The experimental work completed by Rios and Stam in the respective Phases I and II of the pooled fund study at The University of Texas at Austin, comprised four types of connections— the fillet welded socket connection, full penetration weld connections, denoted "Wyoming Detail" for the case which included a backup bar, and "Texas Detail" for the case without a backup bar, and a stool-stiffened baseplate-shaft connection (Stam 2009). The Texas and Wyoming connection details are shown in Figure 2-1 and Figure 2-2. Despite the connection detail differences, the overall geometry of the poles used for full-scale testing remained fairly consistent: every pole in the test matrix maintained a shaft flat-to-flat diameter of 24 inches while varying the baseplate thickness from 1.5 inches to 3 inches. Pool, in Phase III, completed the full scale experiments by testing Texas details on high masts with 32.625" diameter shafts and 3 inch baseplates (2010). An explanation of the naming scheme used for the completed tests is given in Figure 2-3. To maintain consistency, the same naming convention is employed throughout the subsequent chapters of this thesis. Results from all previous high mast tests are shown in Figure 2-4, Figure 2-5, and Figure 2-6.
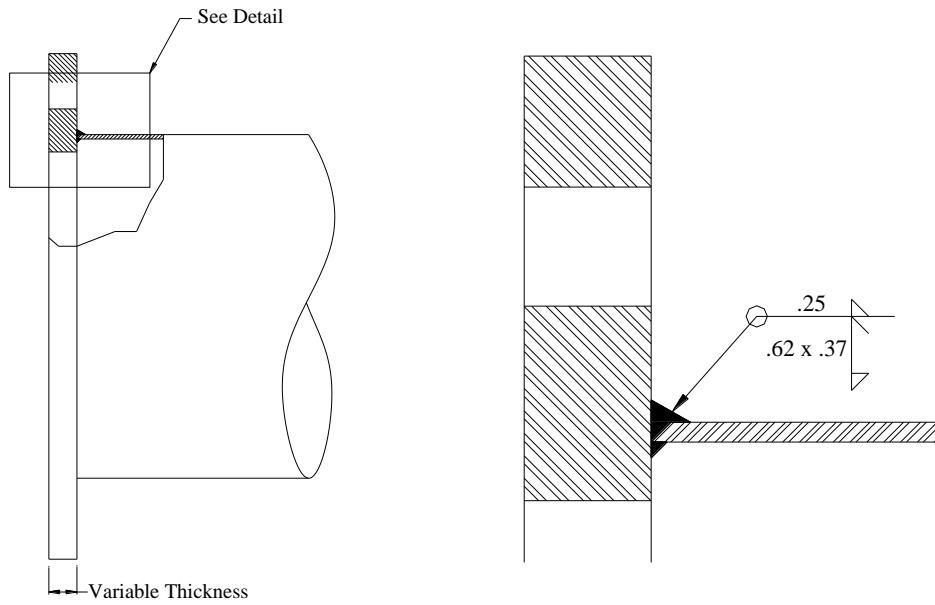
Figure 2-1: Typical "Texas" HMIP weld detail (Stam, 2009)
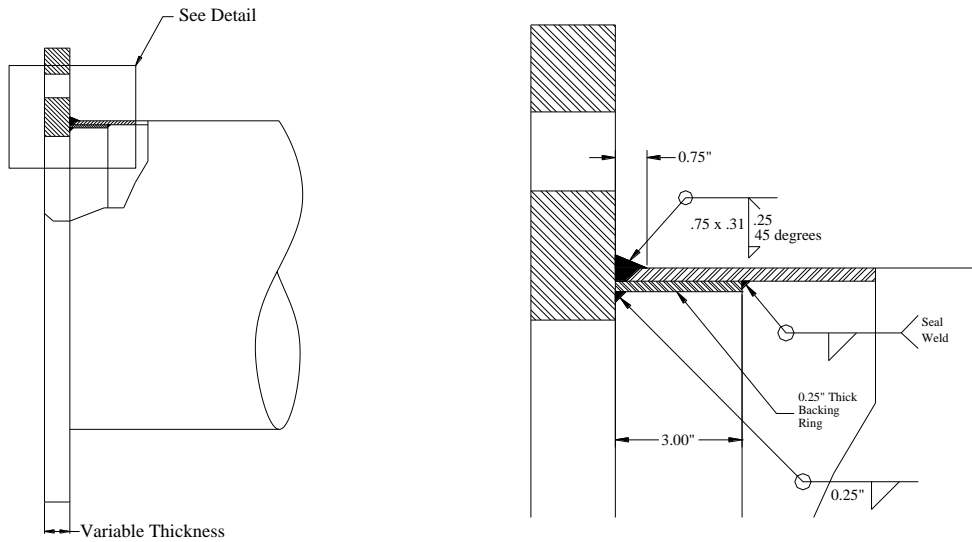
Figure 2-2: Typical "Wyoming" HMIP weld detail (Stam, 2009)

Figure 2-3: Typical naming scheme (Stam, 2009)

Figure 2-4: S-N plot of fatigue test results for Phase I of Pooled Fund Study (Rios, 2007)

Based on the experimental data, the University of Texas concluded that the Wyoming and Texas details performed best in fatigue due to the stiffness of the full penetration weld, particularly when fitted with an external collar. All tested specimens were fabricated with a consistent 5/16″ shaft wall thickness as per the typical design practice.

Figure 2-5: S-N plot of fatigue test results for Phase II of Pooled Fund Study (Stam, 2009)

Analytical research completed by Stam (2009) indicates that the stress concentration factor (SCF) defined as the maximum hotspot stress divided by the nominal stress at the baseplate weld, decreases as the section modulus decreases. By increasing the section modulus, the double curvature of the shaft near the baseplate weld is reduced. Stam came to this conclusion after analytically and experimentally investigating several different connection details primarily comprising full penetration connections and socket details. First demonstrated by Warpinski (2006), Stam showed analytically that by increasing the baseplate thickness, the SCF decreases, though not linearly. Figure 2-6 demonstrates this relationship by showing how the SCF changes on different Socket welded high mast poles with varying shaft thicknesses. It would be logical to assume that this decreasing trend holds true for all baseplate to shaft weld connection details and shaft thicknesses, since socket connection details have been shown experimentally to display worse fatigue performance due to the lower section modulus and the lower resultant stiffness.

Stam (2009) also conducted a literature review to determine the significance of changing the shaft thickness relative to the baseplate thickness for improving fatigue performance. From his investigation, he concludes that increases in the baseplate thickness provide a greater advantage

for improving the section modulus than increasing the shaft thickness. At the end of the first two phases of the Pooled Fund Study, the primary conclusion converged on the idea that fatigue life is a function of the SCF, and this SCF can be reduced most effectively by increasing the baseplate thickness, and where necessary, including an external collar.
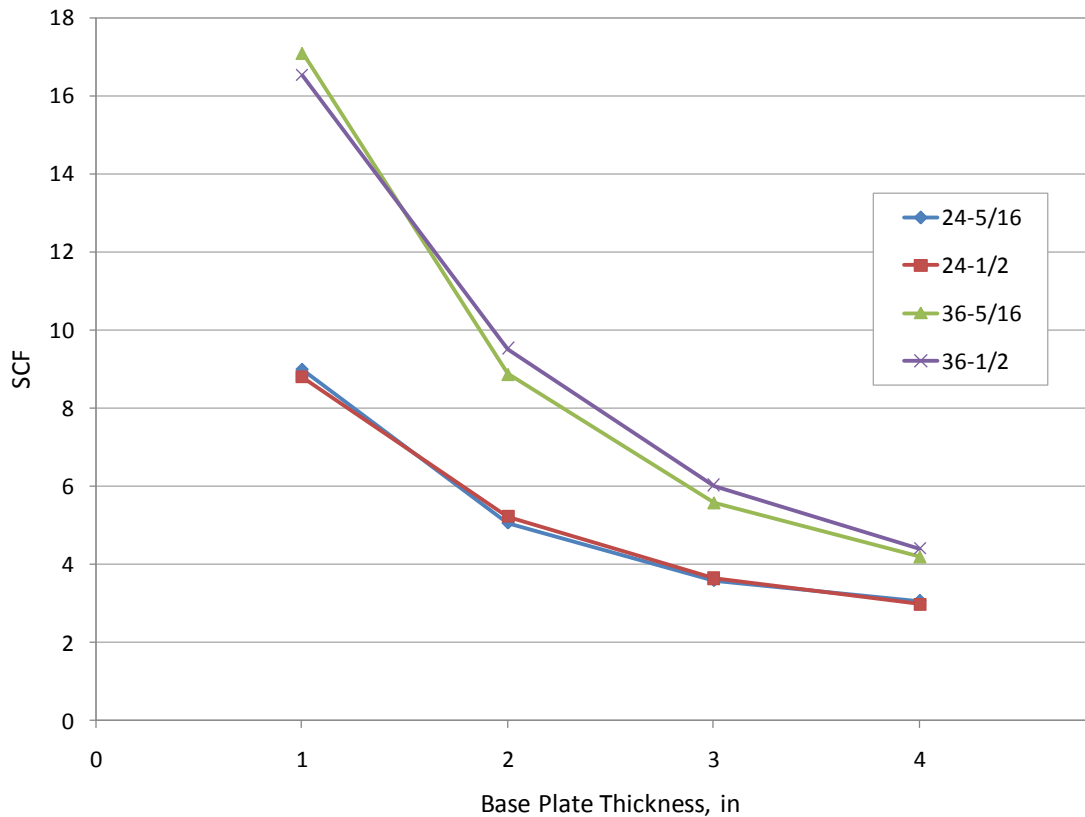
Figure 2-6: SCFs for Socket Details in Wall Thickness and Shaft Diameter Parametric Study (Stam, 2009)

2.2.2   Phase III Pooled Fund Fatigue Study Results

The final phase of the Pooled Fund Study was intended to confirm that the results from the 24″ diameter specimens in Phase II were also applicable for larger sections. Therefore tests were conducted on 32.625″ diameter specimens. On the contrary, researchers found a distinct difference in the fatigue performance of the 32.625″ specimens, which indicated a worse case than what was observed in the 24″ tests. This observation was counter-intuitive when juxtaposed to the parametric work completed by Stam in Phase II. Though Ocel (2006) had shown that the SCFs in mast arms can increase when a diameter is increased beyond a certain threshold value,

Stam (2009) demonstrated that increasing the shaft diameter from 24″ to 36″ decreases the hotspot stresses at the weld toe and, by deduction, the SCF as well. As Figure 2-7 indicates, the opposite held true when subjected to full scale testing.
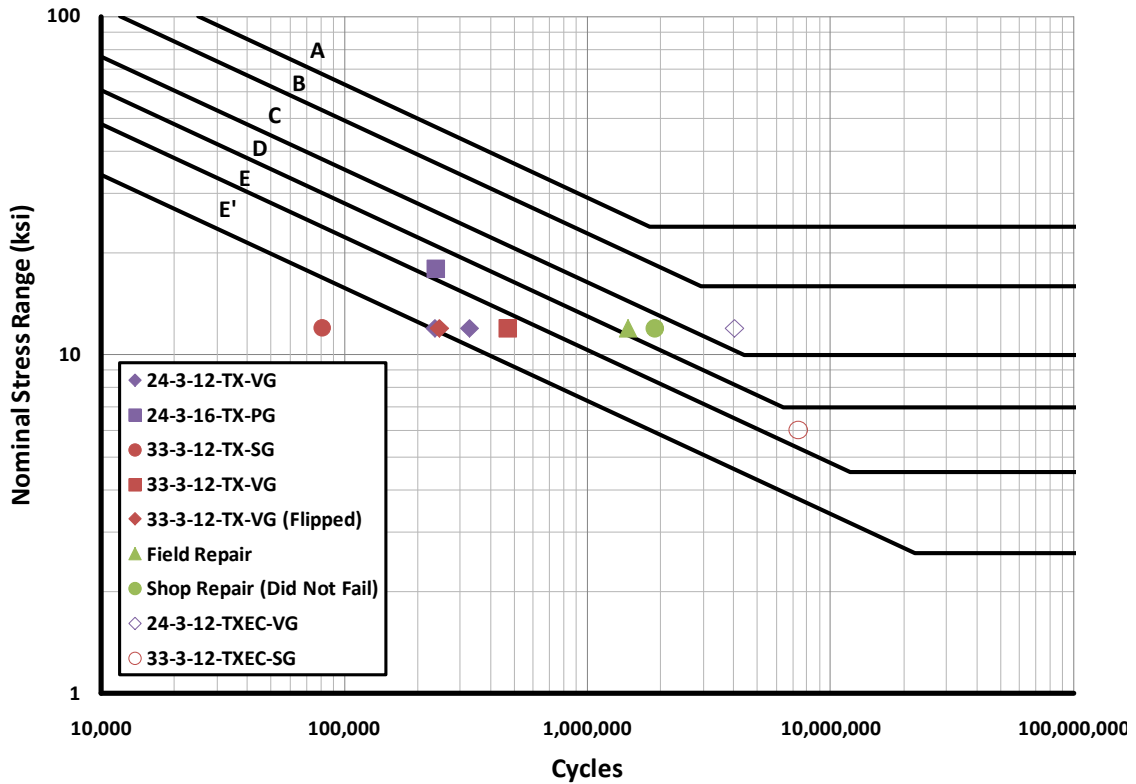
Figure 2-7: Fatigue results from 32.5" test specimens relative to 24" test specimens (Pool, 2010)

Upon reviewing these findings, Phase III shifted emphasis from validation of the recommended fatigue detail to determining the reason for the premature failure of these large diameter high mast illumination poles. The culmination of this study indicated that small cracks had formed in the high masts prior to fatigue loading likely due to the galvanizing procedure.

2.3   Initial Crack Observation

The first observations of initial cracks within the context of the Pooled Fund Study originated with a set of high masts which were intended to validate the results from full scale testing and finite element work. The test was meant to determine the fatigue life of 32.625″ diameter high mast illumination poles with the "Texas" weld detail, and to verify that a suitable fatigue

10

performance could be achieved with the connection detail. Along with the weld detail, the effect of galvanizing on the fatigue behavior was also to be reflected by this pair of HMIPs (Pool, 2010). The effect of the galvanizing on the fatigue performance was measured by testing ungalvanized, or "black", poles. The motivation for testing black poles compared to galvanized poles stems from research performed by Richman (2009) as well as research by Koenigs (2003). Based on his research, Koenigs asserted that the galvanizing procedure hinders fatigue life in mast arms with socket connections (2003). Richman sought to verify this fact with mast arm connection details. Testing a series of black mast arms against galvanized specimens, Richman (2009) reported no significant reduction in fatigue performance. Both specimens in Richman's tests had the Wyoming connection detail.

In the next step of the Texas study, Pool was preparing to test a black HMIP specimen back-to-back against a galvanized specimen of the exact design, but a significant difference was noticed prior to testing. The researchers asked Texas Department of Transportation (TxDOT) to use ultra-sonic testing (UT) techniques to inspect the test specimens prior to the fatigue tests. After checking all the bends of each high mast, designated 33-3-12-TX-SG-A and 33-3-12-TX-SB-B, TxDOT determined that the black specimen had no initial defects, whereas the galvanized specimen was riddled with small crack indications at the toe of the full penetration baseplate-to-shaft connection at every location of a cold bend. A schematic drawing of the crack locations on the two pole cross sections is shown in Figure 2-8. The UT evaluations showed that some of the cracks penetrated as much as 1/8″ into the 5/16″ thick shaft and extended between 1/2″ to 1 5/8″ on either side of the bend. The fatigue performance of 33-3-12-TX-SG-A suffered accordingly, as demonstrated in Figure 2-7, whereas 33-3-12-TX-SB-B showed no signs of deteriorating fatigue performance at the same number of cycles and stress range (Pool, 2010).
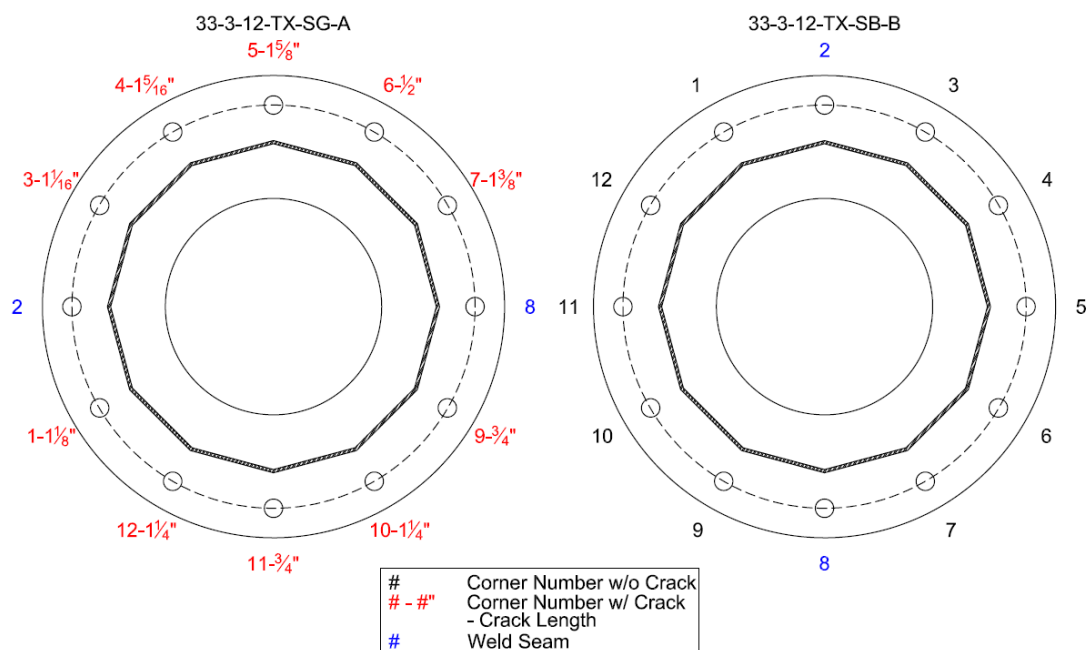
Figure 2-8: Initial Crack Locations and Lengths in Specimens 33-3-12-TX-SG-A and 33-3-12-TX-SB-B (Pool, 2010)

After fatiguing specimen 33-3-12-TX-SG-A to the point of failure, bends containing initial cracks were opened to examine the crack surface for potential clues pertaining to the crack indications noticed by TxDOT and the poor fatigue performance. Photographs of bend 5 are depicted in Figure 2-9 and Figure 2-10. Pool notes that several details of the crack regions provide an indication of the nature of the cracking. The roughened black surface visible in Figure 2-8 is attributed to the initial cracking phenomenon, whereas the smooth, rounded surface is a sign of growth of the crack during the fatigue testing. Also worthy of noting, the roughened black surfaces were present at all opened bend locations where initial ultra-sonic testing indicated the presence of cracks prior to the fatigue tests. The different crack surfaces verified that a significant failure mechanism was introduced prior to fatigue loading and contributed to the earlier-than-expected fatigue failure of the test specimen and connection detail (Pool, 2010).
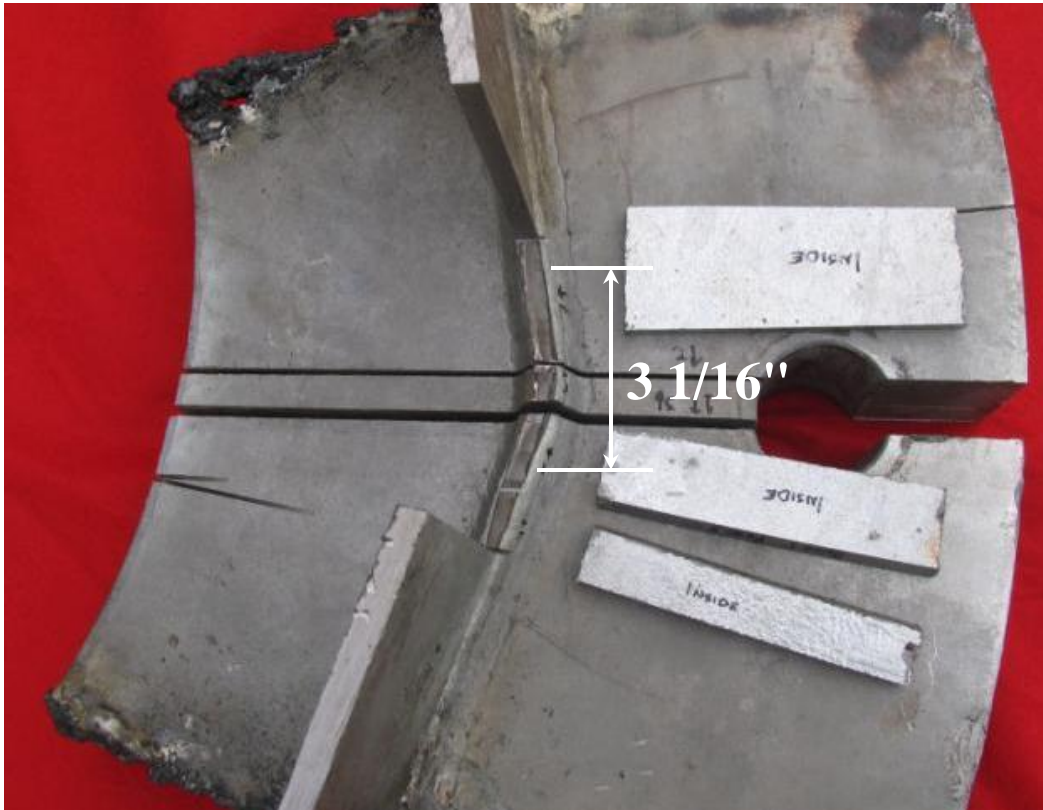
Figure 2-9: View of Bend 5 after sectioning. Length of observed initial crack is labeled (Pool, 2010).

Though the initial cracks varied in both length and penetration depth into the wall thickness, their presence and subsequent effect on fatigue life were alarming: this was a phenomenon not observed on the 24″ diameter specimens tested by Stam (2009). Because TxDOT has several hundred of the 32.625″ diameter poles in the field, researchers realized the potential severity of the problem with respect to TxDOT's HMIP inventory. Pool, therefore, spent the remainder of his research investigating the location of initial cracks in 32.625″ diameter poles with various shaft to baseplate connection details, how to identify the initial cracks, and the corresponding impact on fatigue life.
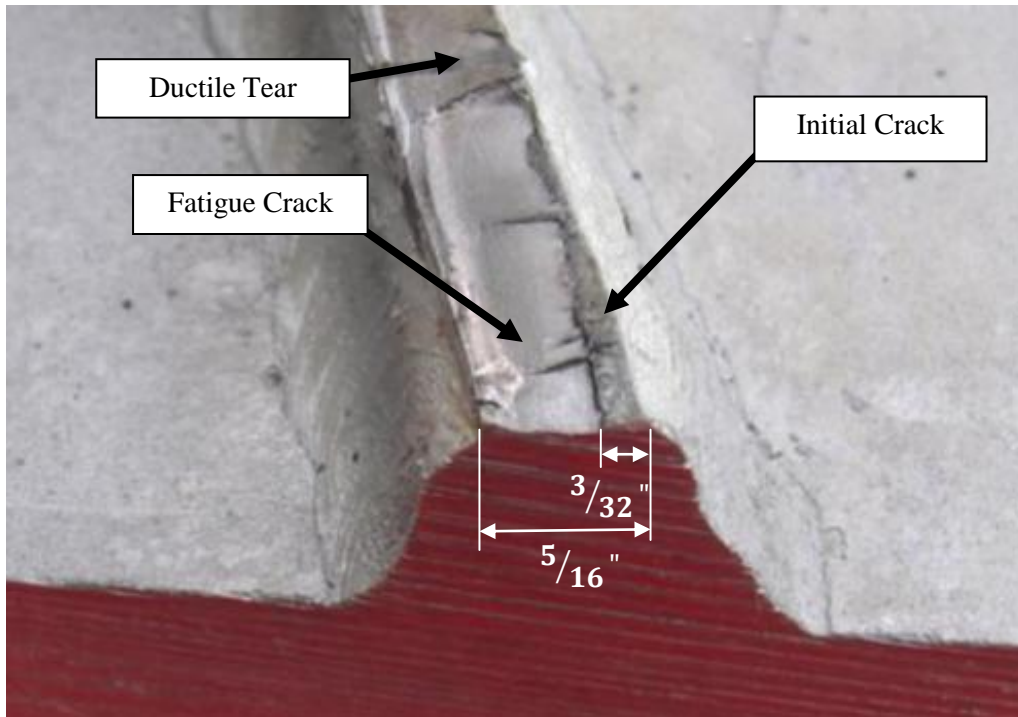
Figure 2-10: Depth of initial crack at weld toe of bend 5 from 33-3-12-TX-SG-A (Pool, 2010)

The interesting aspect of these initial cracks, which seemed to hold true throughout the rest of Pool's research stemmed from the unpredictability of the cracks: their existence and the extent to which they penetrated the shaft wall section seemed to vary from fabricator to fabricator. Another pair of poles of the same design as 33-3-12-TX-SG-A was ordered from a separate galvanizer, and Pool observed that while initial cracks were present, there were significantly fewer, and their lengths and depths were lessened. Instead of finding initial crack indications at nearly every bend in these twelve-sided poles, specimens 33-3-12-TX-VG-A and 33-3-12-TX-VG-B were cracked at only 3 and 4 bend locations, respectively, and in both cases, the severity of the cracks in terms of length and depth were less than the poles previously tested (Pool, 2010).

2.4 Galvanizing Process

The cracking that was observed in the galvanized specimens occurred somewhere between the completion of pole fabrication and arriving at Ferguson Structural Engineering Laboratory. Since the shipping and handling methods for the black poles and the galvanized poles did not differ, the initiation of the cracks likely occurred sometime during the galvanizing process. To better

understand the cracking phenomenon, it is useful to understand the galvanizing process. According to the American Galvanizers Association, AGA, there are three specific aspects of the hot dip galvanizing process (in chronological order): surface preparation, galvanizing, and inspection (AGA, 2008).

2.4.1   Surface Preparation

As the black specimen arrives on site from the fabricator, the first action in the galvanizing processes is to prepare the surface to ensure a strong bond forms between the zinc and steel. This surface preparation is accomplished by dipping the poles into three distinctive baths. A clean bond, free from surface contaminants, is assured by first dipping the poles in a hot alkaline solution. The hot alkaline solution acts as a degreaser and caustic cleanser, removing grease, dirt, oil, and soluble markings. Once free from these contaminants, the specimen is ready to enter into a picking bath, mainly comprised of either hydrochloric or sulfuric acid, to remove mill scale and rust. After degreasing and pickling, the pole is ready for fluxing. Fluxing removes oxides, and also prevents oxidation prior to immersion in the molten zinc. The fluxing can either be applied in its own distinctive bath (dry galvanizing process), or it can be floated on top of the molten zinc (wet galvanizing process). Once cleaned, pickled, and fluxed, the pole is chemically ready to receive its zinc coating (AGA, 2008).

2.4.2   Galvanizing

The next step in the galvanizing process is for the pole to be immersed in molten zinc. This portion of galvanizing is rather variable due to its dependence on typical practices of specific galvanizers. Generally speaking, HMIP's are dipped at an angle with the baseplate entering the 815°F to 850°F zinc bath first, and allowed to sit submerged until the galvanizer deems the chemical reaction to have finished. This process culminates in the formation of a series of zinc-iron alloy layers, commonly topped by a layer of pure zinc (AGA, 2008).

Galvanizing generally serves two basic purposes: 1) to function as a means of mitigating rust and 2) to provide an aesthetically desirable finish for the owner of the part. The application of zinc satisfies the need to mitigate oxidation, but a proper and uniform surface also needs to be ensured. Galvanizers ensure surface quality through both mechanical and chemical means. Mechanically, galvanizers remove excess zinc on high mast poles through draining and vibrating the poles

(AGA, 2008). This draining process often dictates the angle of removal from the molten zinc bath.

Chemically, many different elements may be alloyed with the molten zinc to obtain desirable surface finishes. It should be noted that while this thesis does not seek to focus on many of the chemical considerations that go into the galvanizing process and their effects on steel, a topical understanding of the process is useful to better understand the complexity of the problem addressed by this thesis.

Galvanizers seek to minimize the thickness of the zinc layer deposited on the surface of steel as a means of both saving money, and to gain a more pleasing surface finish. Particularly as silicon-killed steels became more popular, Reumont et al.(1998) notes that "the galvanizer was confronted with excessive coating thickness, a grey surface appearance and poor adhesion, when using the normal galvanizing procedures". As a solution, many galvanizers add between 0.06% to 0.15% nickel to the zinc bath (by weight) to counteract the effects of the silicon present in the steel base material. Further, Reumont et al. (1998) reveals that alloying the zinc bath with other transition metals such as manganese, titanium, aluminum, or tin achieves a similar effect as the addition of nickel. Because of this research, and similar work, it is typical practice for galvanizers to alloy their baths with several other elements.

Following removal of the HMIP from the galvanizing bath, the galvanized pole is set aside to cool to an adequate handling temperature. Cooling can either be achieved through air cooling, or by quenching in liquid (AGA, 2008).

2.4.3   Inspection

The final step in the galvanizing process is inspection. The extent to which poles are inspected are often times specified by the owner. Galvanizers will check coating thickness and other surface conditions to ensure an acceptable product prior to delivering the galvanized pole to the owner (AGA, 2008).

2.5   Previous Studies on Galvanizing-Induced Cracking

Cracking in galvanized structures is a phenomenon which has been widely reported, though the issues governing the generation of this phenomenon are still in greater need of clarity. This section highlights some of the documentation of the problem as well as investigations on the

causes of the cracking. Aischinger and Higgins (2006) provide an overview of potential causes of toe cracking in welds of HMIP systems. They further discuss methods that might minimize the chances of crack initiation. Although the problem with cracking has gained a significant amount of attention in recent years, the galvanizing industry has been aware of such problems for several years. Aichinger and Higgins (2006) discuss a study on weld toe cracking conducted by Valmont for a utility company in 1974. While no absolute cause for the cracking was determined, Valmont originally identified galvanizing, braking, welding, and material selection as possibly contributing factors to the likelihood of initial crack development at the weld toe of tubular structures.

Writing from the position of having gained 30 years of experience since these cracks were originally reported, Aichinger and Higgins seek to shed additional light onto the nebulous topic of these cracks. Despite reporting that toe cracks occur only on galvanized structures, and that poles from the communication and transportation industries exhibit cracks at a less frequent level than other owner entities, no central issue was identified as the catalyst of these cracks. Instead, the authors focus on five areas that may play a part in driving the cracking process: 1) welding and metallurgy, 2) purchasing, 3) galvanizing, 4) product design, and 5) manufacturing and shop practice. To evaluate these different parameters, Valmont relied on data from each of their four large pole fabrication sites from the years 1998, 2000, and 2002.

Aichinger and Higgins subsequently describe the different tests conducted to determine the impact that these different parameters might have played. Despite a lack of hard scientific conclusions, the authors discuss a series of provisions to reduce the possibility of the formation of galvanized-induced cracks based on results gained from small tests conducted to investigate welding and metallurgy, purchasing, galvanizing, product design, and manufacturing and shop practice.

Kinstler (2006) conducted a synthesis study on the topic of cracks that form in steel structures following galvanizing and prior to loading. Like the report published by Aichinger and Higgins, this document primarily seeks to explain the formation of cracks due to liquid metal embrittlement. Though not giving a specific catalyst for these types of cracks, Kinstler provides valuable insight into the breadth of the galvanizing problem.

First, Kinstler notes that the process of galvanizing has not changed significantly in the past 100 years. Because of this, and the lack of data suggesting the cracks seen widely today have always been present in the industry, new variables must have been added to the galvanizing process to result in these failures. Particularly, Kinstler emphasizes how the bath and steel chemistries have been altered relatively recently with other elements to aid in continuous casting in steel, and to give more desirable zinc coatings during galvanizing. This is an interesting point: Kinstler notes that Prime Western Zinc, which consists of 1% lead, an alloying metal that reportedly contributes to liquid metal embrittlement, has been the standard for galvanizers to use in their bathes up until the early 2000s. He then sites that as of 2003 galvanizers began shifting to zinc rated lower in lead concentrations.

Other research completed by Kinstler indicates that steel becomes less ductile while in contact with liquid zinc. Figure 2-11 depicts a tensile test completed in a zinc environment, then in an air environment. Though the curves seem to match up fairly well, the fracture strain of the steel immersed in zinc is significantly lower. Kinstler points out that despite this mechanical phenomenon, which must have also occurred 100 years ago, galvanizing cracks were not reported. However, it is possible that cracks at the toes of base plate to pole shaft welds were not noticed due to their small size and difficulty to identify without use of specific ultra-sonic testing techniques. Nevertheless, it stands to reason that if the problem did not occur when the standard practice was to galvanize with Prime Western Zinc, then the more extreme examples of galvanizing cracks more recently observed must be a result of a change in bath or steel chemistries.
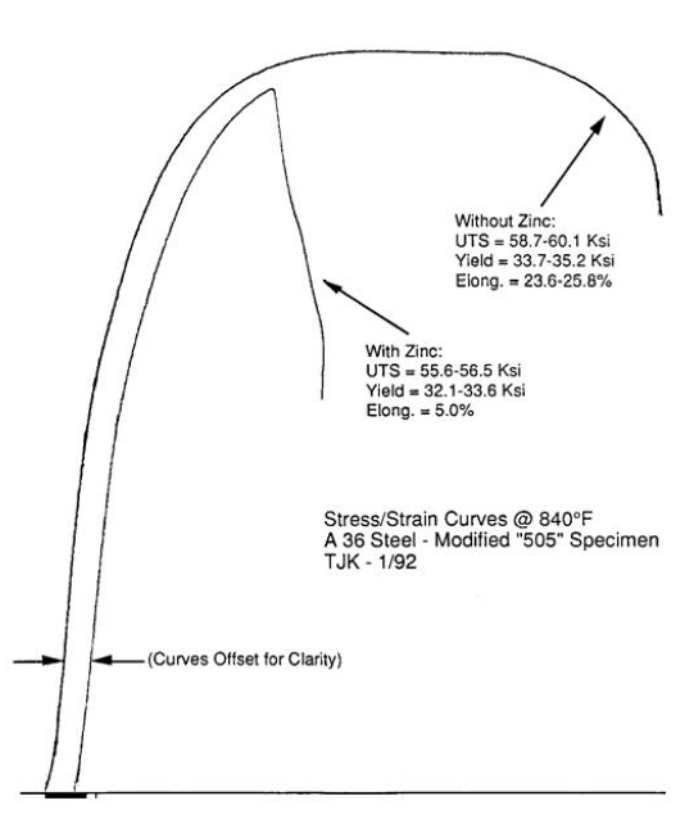
**Figure 2-11: Stress strain curve with and without zinc at 840°F
(Kinstler, 2006)**

The breadth of Kinstler's investigation covers a wide array of topics and several sources. Kinstler covers chemistry with galvanized coatings, chemistry of base metal, thermal gradients, stress-strain relationships, residual stresses, cold working considerations, flame cutting, and many more topics. Despite this exhaustive synthesis of previous research in so many areas, most of that which is reported pertains to either steel girders or HSS members, with unfortunately sparse discussion of poles with heavy base plates. Kinstler does report, however, that "stresses/strains induced in the galvanizing thermal transient has been studied by many," though University of Texas researchers have been unable to locate these reports. Kinstler indicates that the Japanese have conducted many studies on galvanizing cracks, but much of their work has not been translated into English.

Steel cracking during the galvanizing is a relatively far reaching problem that is not unique to the only the United States. In fact, it is apparent from research and reports that this cracking is such a

significant issue that European codes are attempting to develop provisions to address the problem. Feldmann et al. (2010) developed a guide entitled "Hot-dip-zinc-coating of prefabricated structural steel components" which was written for design engineers and fabricators on how to design steel components and control galvanizing baths in such a means that cracking during galvanizing does not occur. The types of cracks observed and addressed by this report are consistent with cracks noticed in the United States and characteristically seem to start from locations where stress concentrations occur due to residual stresses from fabrication. Figure 2-12 depicts examples of the cracks that the guide from Feldman et al. seeks to mitigate.

Feldmann et al. observes in this report that since 2000, contractors have been noticing an increased number of galvanized structural members with premature fractures that can compromise the safety of structures. Further, these types of cracks are typically discovered after erection and loading due to the fact that these cracks are often filled with zinc after galvanizing. After loading, the poor bond between the zinc and steel fractures and reveals the larger defect present within the structural member.

Focused on the fact that these cracks occur when base metal is galvanized in baths that contain higher concentrations of tin (Sn) along with other alloying metals in an attempt to reduce coating thicknesses, this report attributes these cracks to liquid metal embrittlement (LME) or liquid metal assisted cracking (LMAC) and a resultant ultimate strain capacity of steel in hot-zinc bath. Figure 2-13 presents a crack of this characterization. Note how the crack in the base steel is filled with zinc melt, and demonstrate that these cracks must form during the galvanizing process. This photograph also depicts the surface roughening caused by additives to the zinc melt such as Sn. Upon closer examination, as shown in Figure 2-14, one can see that the cracks occur at the steel grain boundaries. This penetration of the zinc melt into these boundaries is what causes the embrittlement and results in the reduction in ultimate strain capacity.
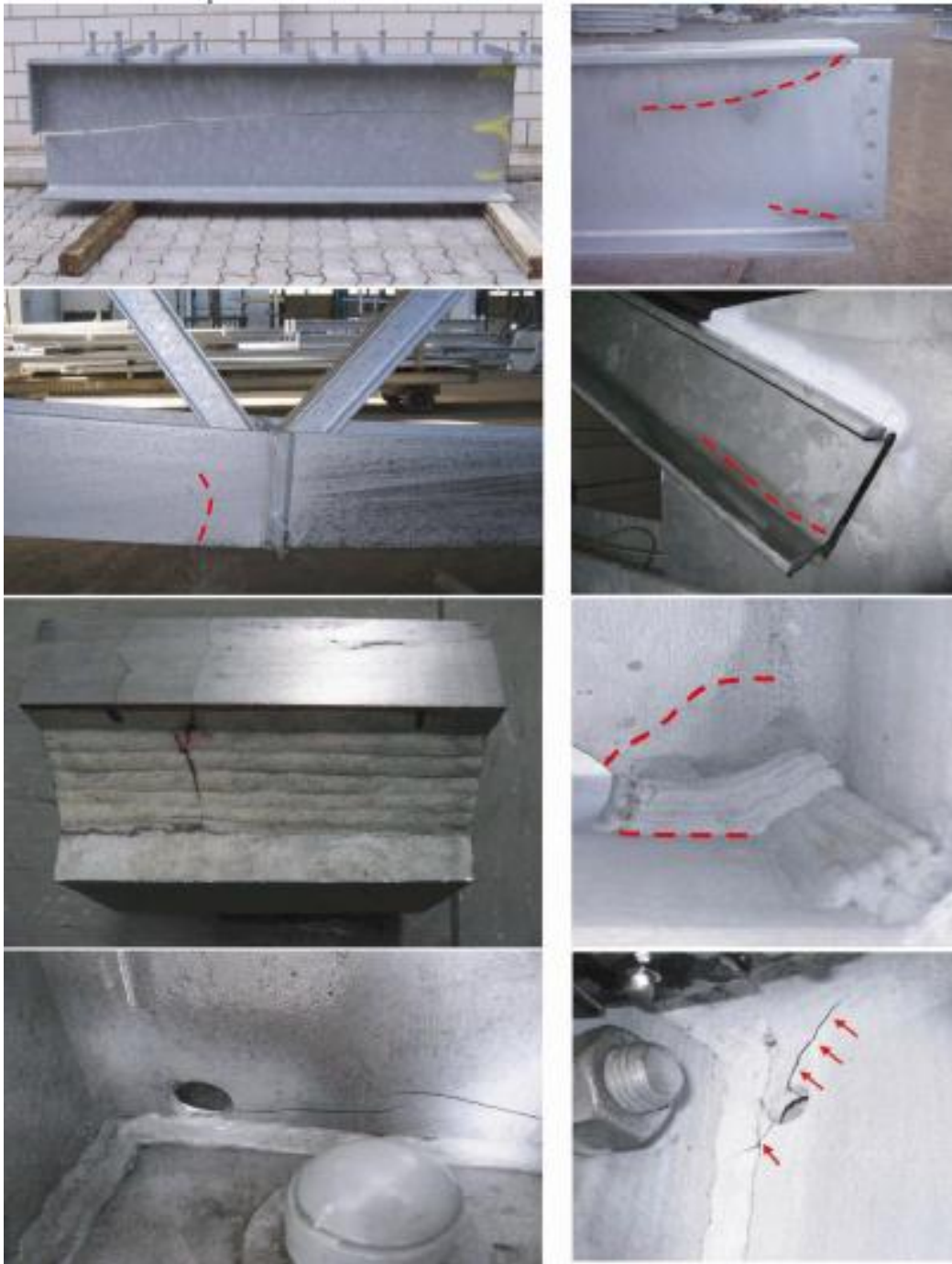
Figure 2-12: Damages observed after zinc coating or after erection of hot-dip-zinc-coated structural components (Feldmann et al., 2010)
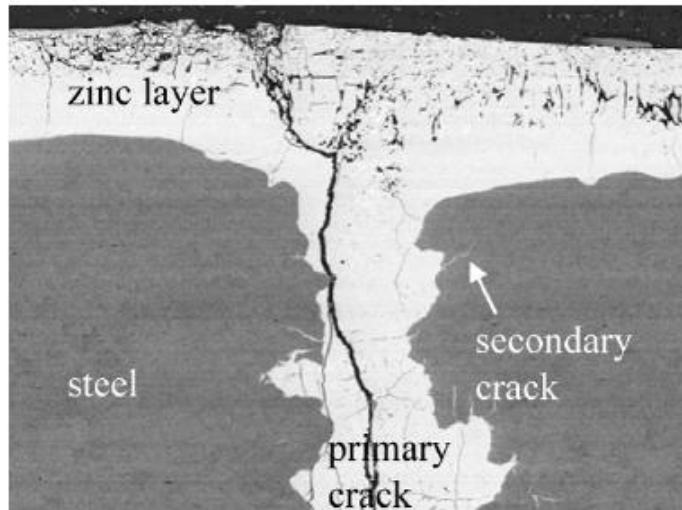
Figure 2-13: Primary crack and secondary crack (200x) (Feldmann et al. 2010)
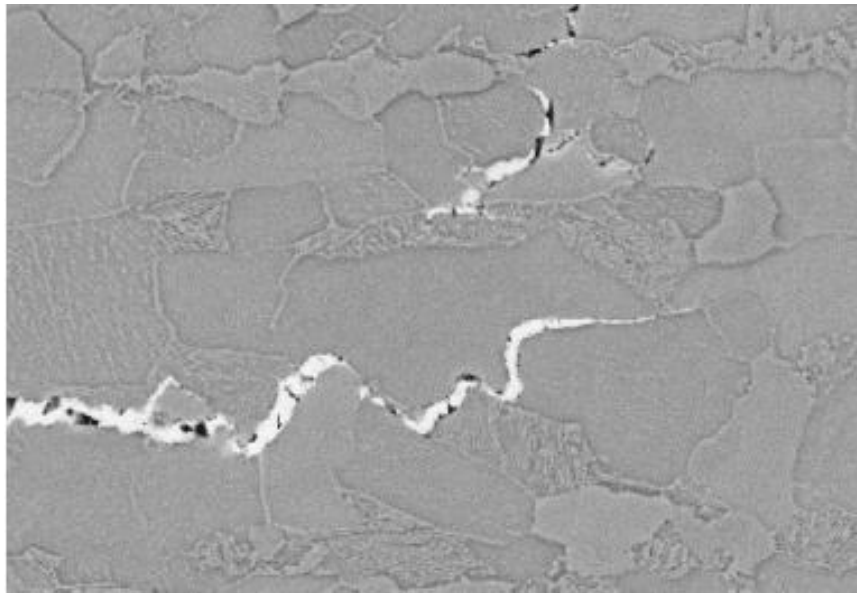
Figure 2-14: Intergranular crack in ferrite-pearlite structure (5000x) (Feldmann et al. 2010)

Feldmann et al. (2010) utilize the knowledge of LME to establish a standardized test to produce an "equivalent plastic strain"-resistance in a zinc bath depending on composition and temperature

of the zinc bath, the quality of the steel, microstructure and surface conditions of the steel product, and strain rate.

2.6 Summary

Due to the reduction in fatigue life which has been found to be associated with the initial cracks formed after galvanization at weld toes, the University of Texas has undertaken research to determine what driving factor has contributed greatest to this phenomenon. While a plethora of material and resources detail the considerations and likelihood of crack formation as the result of flame cut surfaces, cold bends, and extreme bath chemistry issues, few resources which discuss the small initial cracks that develop at weld toes in high masts after galvanizing are currently available. The subsequent chapters of this thesis compare recommendations and observations from the listed reports to an investigation by the University of Texas to determine the source of these cracks.

CHAPTER 3.   INITIAL TESTING

3.1   Introduction

The cracks that were found at the toe of baseplate to shaft welds on the galvanized 32.625"
HMIPs introduced a significant problem into the study on the fatigue resistance of HMIP
systems. As noted in Section 2.5, many different possible characteristics are attributed to
enabling cracking during galvanizing. To narrow down the scope of potential failure modes,
several smaller studies were conducted to isolate a particular characteristic unique to the 32.625"
diameter galvanized HMIPs that might results in their cracking, as opposed to the characteristics
of the 24" diameter specimens that did not crack. To evaluate the interaction of failure
mechanisms observed from the established literature, tests were conducted on specimens to
determine the impact of chemical reactivity between the galvanized coating and base metal,
extent of cold working in bends, and characteristics of baseplate to shaft thickness ratios on crack
development.

3.2   Bend Radius Study

Through observations of the HMIP sections which had cracked after galvanizing, researchers
found that cracks only formed at shaft bend locations. These cracks did not seem to initiate at
any of the flat locations, nor in the shaft seam-welds that run longitudinally along the length of
the pole. Because of this, researchers hypothesized that some sort of relationship might exist
between the cold bending of the HMIPs during fabrication to form the shaft shape and the
initiation of these initial cracks.

Cold working is a common practice in the fabrication of structural tube sections. Since these
shapes are galvanized from time to time, researchers searched for ASTM standards which might
govern the fabrication and coating procedures to mitigate cracking from galvanizing.
Researchers found that ASTM A143/4 1433/M-07 linked embrittlement in hot-dipped galvanized
structural steel to four factors: strain-aging, atomic hydrogen absorption (hydrogen
embrittlement), loss of ductility in cold-worked steel, and low service temperatures. After
observing chemistry reports listed in Section 3.3 and noting the characteristically warm climate of
Texas (where the poles were fabricated and galvanized), hydrogen embrittlement and low service
temperatures were ruled out as a governing mechanism in the cracking phenomenon. This left
strain-aging and loss of ductility as the potential instigator of cracks.

Fabricating HMIPs necessitates cold-working of structural steel to achieve the necessary pole geometries. During cold-working, a press brake is used to introduce the desired bends into two separate sheets of structural steel such that each sheet is formed into a half of a cylinder. These two halves are then welded together to form the complete HMIP. This processes significantly impacts the strength of the steel being worked as the steel deforms plastically. During the cold-working, the steel is often deformed well into the strain-hardening region which increases strength and hardness while decreasing ductility. While strain-hardening is often used for many standard structural applications, ASTM A143 notes that cold-worked steel is subject to strain-aging, or a delayed and gradual further increase of hardness and strength and loss of ductility and impact resistance, and that the effects of strain-aging are related to temperature. The rate of strain-aging increases as cold-worked steel is subjected to high temperatures, such as those achieved during galvanization.

While reviewing ASTM A143, researchers also noticed that as a control on embrittlement, this standard recommends increasing the cold bend radii in tubular shapes to greater than three times the thickness as a safeguard against the harmful effects of embrittlement during galvanizing. Measurements were taken on all HMIP and mast arm specimens present at Ferguson Structural Engineering Laboratory to determine the bend radius to shaft thickness ratio at the base plate to compare against the recommended bend radius of three times the shaft thickness. The results from these tests are provided in Table 1 and Table 2. Note that the HMIP with pole thicknesses of 5/16" should have bend radii of no less than 0.9375" to satisfy the ASTM provision.

The results from this study indicate two significant details: the average bend radius for specific sizes of poles vary by fabricator, and quality controls used in ensuring bend radius consistency when fabricating a specific size of pole can also vary significantly per manufacturer. What is most interesting, though, is that the poles that cracked from the galvanizing process all complied with the ASTM bend radius to shaft thickness ratio. Three other HMIPs and several mast arms did not comply with this ratio and did not experience cracks (as indicated in red in Table 1 and Table 2).

Table 3-1: Bend radius to shaft thickness ratios study for HMIPs

Specimen Name	Thickness (in)	Avg. Inside Bend Radius (in)	Radius/Thickness
33-3-12-TX-SG-A*	0.313	1.45	4.64
33-3-12-TX-SB-B	0.313	1.35	4.32
33-3-12-TX-VG-A*	0.313	1.28	4.08
33-3-12-TX-VG-B*	0.313	1.23	3.92
24-3-16-WY-PG	0.313	0.66	**2.11**
24-3-16-TX-PG	0.313	0.69	**2.20**
24-3-16-SEC-PG-A	0.313	0.40	**1.29**
24-3-16-SEC-PG-B	0.313	1.09	3.49
24-2-8-STL-VG-A	0.313	4.00	12.80
24-2-8-STL-VG-B	0.313	4.00	12.80
VII-6	0.250	0.79	3.17
VII-7	0.250	0.83	3.32

*Asterisk denotes existence or indication of initial cracks

Table 3-2: Bend radius to shaft thickness ratios study for mast arms

Specimen Name	Thickness (in)	Avg. Inside Bend Radius (in)	R/T
10-2R-EC-PG-A	0.179	0.48	**2.67**
10-2R-EC-PG-B	0.179	0.35	**1.98**
10-2S-WY-PG-A	0.179	0.65	3.60
10-2S-WY-PG-B	0.179	0.67	3.72
10-3R-WY-PG-A	0.179	0.42	**2.33**
12-2R-EC-PG-A	0.179	0.42	**2.32**
12-2R-EC-PG-B	0.179	0.35	**1.98**
12-3R-WY-PG-A	0.179	0.42	**2.32**
VII-1	0.188	0.47	**2.49**
VII-2	0.188	0.47	**2.49**
VII-3	0.188	0.47	**2.49**
VII-6	0.188	0.68	3.61
VII-7	0.188	0.65	3.49

These results tend to indicate that while the bend radius might contribute to initial crack formation, it is not likely the catalyst. This conclusion seems to be consistent with galvanizing crack observations as well since cracks would likely exist along the entire length of the shaft if

the bend ratio were the primary contributor. Instead the cracks were only found at the base plate and shaft connection.

3.3 Chemistry Studies

Perhaps the most commonly identified parameters governing the early cracking of steel structures during galvanizing are the chemistry of the base metal and galvanizing bath. Many references site high levels of lead, tin, nickel, and other low melting point temperature metals in galvanizing baths as primary contributors to cracking during galvanizing. In most cases, these sorts of cracks, which are characteristic of those viewed in Figure 2-10, tend to involve areas of high local residual stresses from flame cutting or coping, or excessive cold working. Also, the characteristic crack is usual on the order of many inches long and penetrates all the way through the thickness of the base material. The cracks in Figure 2-10 are much more severe than those found at the toes of the HMIPs, as depicted in Figure 2-7, but researchers were still interested in learning more about the chemistry of the base material and galvanizing coating to determine whether the data would indicate susceptibility to cracking. These chemistry analyses were conducted by chemical sampling, and electron microscopy.

3.3.1 Chemical Sampling

Chemistry specimens were taken from HMIP sections by using a large diameter annular cutter to remove a slug from the shaft of each specimen of interest. Specimens were chosen from the shaft to find out material properties from zones of the shaft that demonstrated the greatest propensity to crack. After smoothing edges, these slugs were packaged and mailed for analysis to Chicago Spectro Service Laboratory, Inc.

The results in Table 1 show a side by side comparison of similar HMIPs that were tested to assure chemical uniformity within the steel test specimen and galvanized coating. A total of five HMIPs were tested. Specimens Pelco 1 and Pelco 2 came from the same HMIP from Phase II, 24-3-16-WY-PG-B, which did not exhibit initial cracking, S&S 1 and S&S 2 are the respective test poles 33-3-12-TX-SG-A and 33-3-12-TX-SG-B that were fabricated at the same time and galvanized approximately four months between one other at the same galvanizing plant. The two respective entries Valmont 1 and Valmont 2 correlate to 33-3-12-TX-VG-A and 33-3-12-TX-VG-B that were fabricated and galvanized at the at the same time. The results are broken up into base metal

and coating chemistries and detail chemical concentrations of elements known to play a part in the galvanizing cracking phenomenon.

Table 3-3: Chemistry Test Results

Chemistry		Pelco 1	Pelco 2	S&S 1	S&S 2	Valmont 1	Valmont 2
Base	Carbon	0.15	0.15	0.05	0.04	0.15	0.15
	Manganese	1.18	1.07	0.98	0.94	1.13	1.05
	Phosphorus	0.005	0.009	0.011	0.013	0.005	0.008
	Sulfur	<0.005	<0.005	<.005	<0.005	0.005	<0.005
	Silicon	0.03	0.02	0.28	0.21	0.02	0.02
	Nickel	0.04	0.04	0.04	0.05	0.04	0.04
	Chromium	0.03	0.03	0.03	0.03	0.03	0.04
	Molybdenum	0.01	0.01	0.01	0.01	0.01	0.01
	Copper	0.03	0.02	0.06	0.03	0.03	0.04
	Aluminum	0.04	0.04	0.02	<0.01	0.05	0.04
	Nitrogen	0.004	0.004	0.002	0.004	0.002	0.005
	Boron	N/A	<0.0005	N/A	<0.0005	N/A	<0.0005
	Vanadium	N/A	<0.01	N/A	<0.01	N/A	<0.01
	Titanium	N/A	<0.01	N/A	<0.01	N/A	<0.01
	Niobium	N/A	<0.01	N/A	<0.01	N/A	<0.01
	Iron	Balance	Balance	Balance	Balance	Balance	Balance
Coating	Cadmium	N/A	<0.001	N/A	<0.001	N/A	<0.001
	Aluminum	<0.005	<0.001	<.005	<0.001	<.005	0.001
	Lead	N/A	<0.005	N/A	<0.005	N/A	0.005
	Tin	<0.005	<0.005	0.03	<0.005	0.03	<0.005
	Nickel	<.001	<0.001	0.1	<0.001	0.14	0.001
	Indium	N/A	<0.005	N/A	<0.005	N/A	<0.005
	Bismuth	<0.005	<0.005	<.005	<0.005	<.005	<0.005
	Iron	N/A	<0.005	N/A	0.005	N/A	0.005
	Copper	N/A	0.001	N/A	0.005	N/A	0.005
	Zinc	Balance	Balance	Balance	Balance	Balance	Balance
	SLM400	82.68	91.64	125.88	134.02	86.58	91.24

Several interesting observations can be made by examining the chemistries shown above. First, the chemistries comply with ASTM 572 by specification, as shown in Figure 3-1. By comparing the chemistries of each specimen, researchers found that the steel and coating chemistries are similar between specimens. The most significant change appears to be in the amount of nickel in the coating chemistries of S&S1 and S&S2 and of Valmont 1 and Valmont 2. This change could be explained for the S&S pairing due to the large amount of time between galvanizing 33-3-12-TX-SG-A and 33-3-12-TX-SG-B, but cannot be explained for the difference in the Valmont

specimens, which were fabricated and galvanized together.
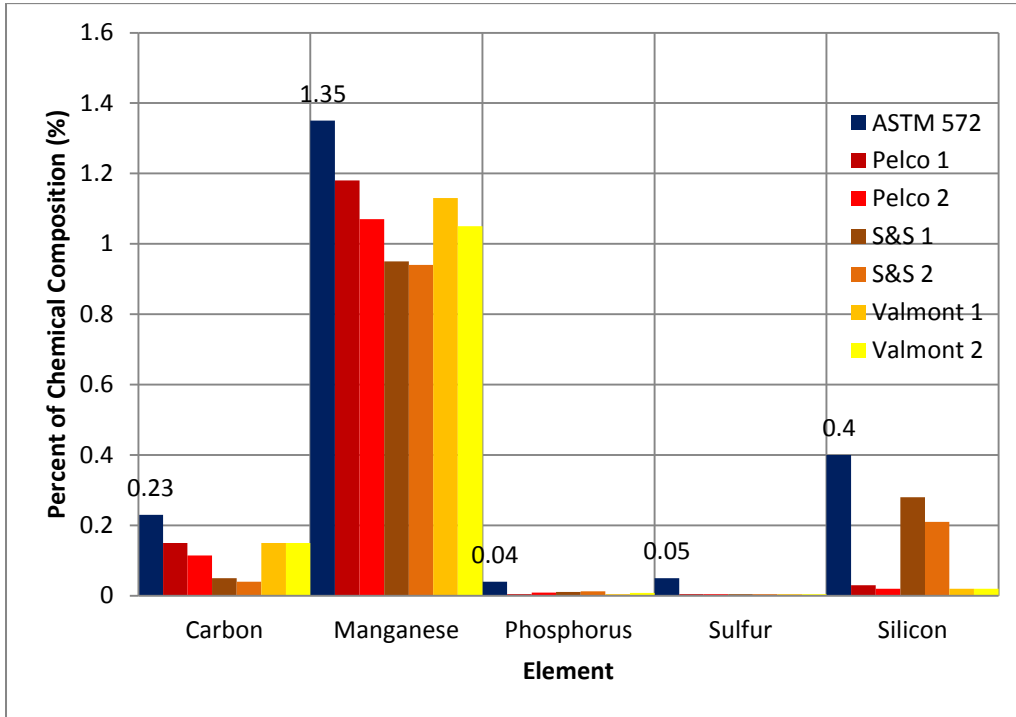
Figure 3-1: Base steel chemistry compositions relative to ASTM 572 specification
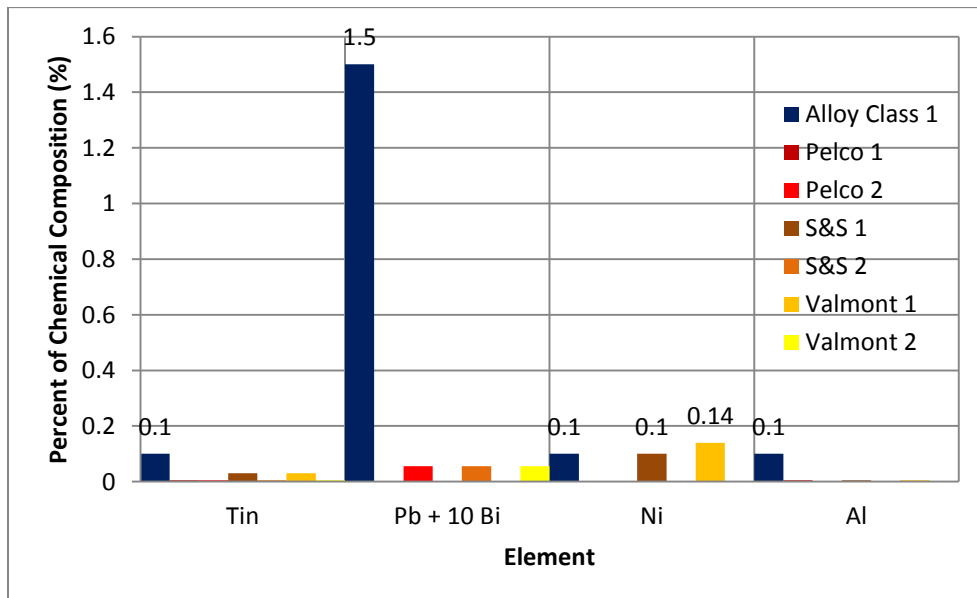
Figure 3-2: Zinc bath chemical compositions relative JRC Scientific and Technical Report Alloy Class 1

When comparing the chemistry analysis against the JRC Scientific and Technical Report "Hot-dip-zinc-coating of prefabricated structural steel components," the coatings seem to most closely match the recommendations given for an "Alloy Class 1" designation, less the greater quantity of nickel than that accounted for in any bath. One other element content category that was listed in the JRC report is the sum of other elements not listed (excluding zinc and iron), which was not to exceed 0.1%. Other elemental weights in the galvanizing coating besides those requested were not measured, but based on the results displayed Table 3, the remaining unweighed elements are assumed to be negligible. However, if these designations are to be applied to these HMIP specimens in most cases, the Alloy Class 1 parameters largely dwarf the chemical contents measured in the coating by Chicago Spectro Service Laboratory, Inc., as demonstrated in Figure 3-2.

The means of assessing vulnerability to cracking in this report, however, seems to focus predominantly on the maximum tin content to equate a maximum plastic strain resistance, and a correlated effective heat transfer coefficient to bath chemistry. If the assumption of an Alloy Class 1 is true, which holds for all but the 33-3-12-TX-VG-A pole (Valmont 1), the galvanizing baths would result in the mildest case of straining due to chemical considerations. In fact, the uncracked 24" Pelco specimens and cracked 32.625" specimens all fall in the same straining category. This seems to hint at a greater set of issues than those of which chemical considerations alone can explain. This notion is further reinforced by the calculation of the SLM400, which is a calculation sited by Aichinger et al. serving as an indicator of susceptibility for liquid metal embrittlement.

The values of the SLM400 have been calculated as completely as possible for the given elements analyzed in each specimen from the chemical study in the final row of Table 3. Interestingly enough, both the Pelco and Valmont specimens match most closely in their chemical contributions to the galvanizing bath, and should have experienced the most cracking as a lower SLM4000 value indicates a greater likelihood of cracking. However, the samples originating from the Structural and Steel fabricator experienced the worst cracking despite having a significantly larger SLM400. Though no doubt chemistry plays a large part in the premature failure of these light poles, based on evaluation of the SLM400 and comparisons with the JRC report, extreme chemical reactions have been eliminated as the source of the crack initiation.

3.3.2 Electron Microscopy

Apart from examining shaft and coating chemistry at shaft locations, researchers were also interested in observing chemistry at the location of an existing initial crack. Images of an initial crack from specimen 33-3-12-TX-SG-A, bend 10 were taken to evaluate localized chemical concentrations. Figure 3-3 shows the initial crack from the outside weld toe of bend 10.
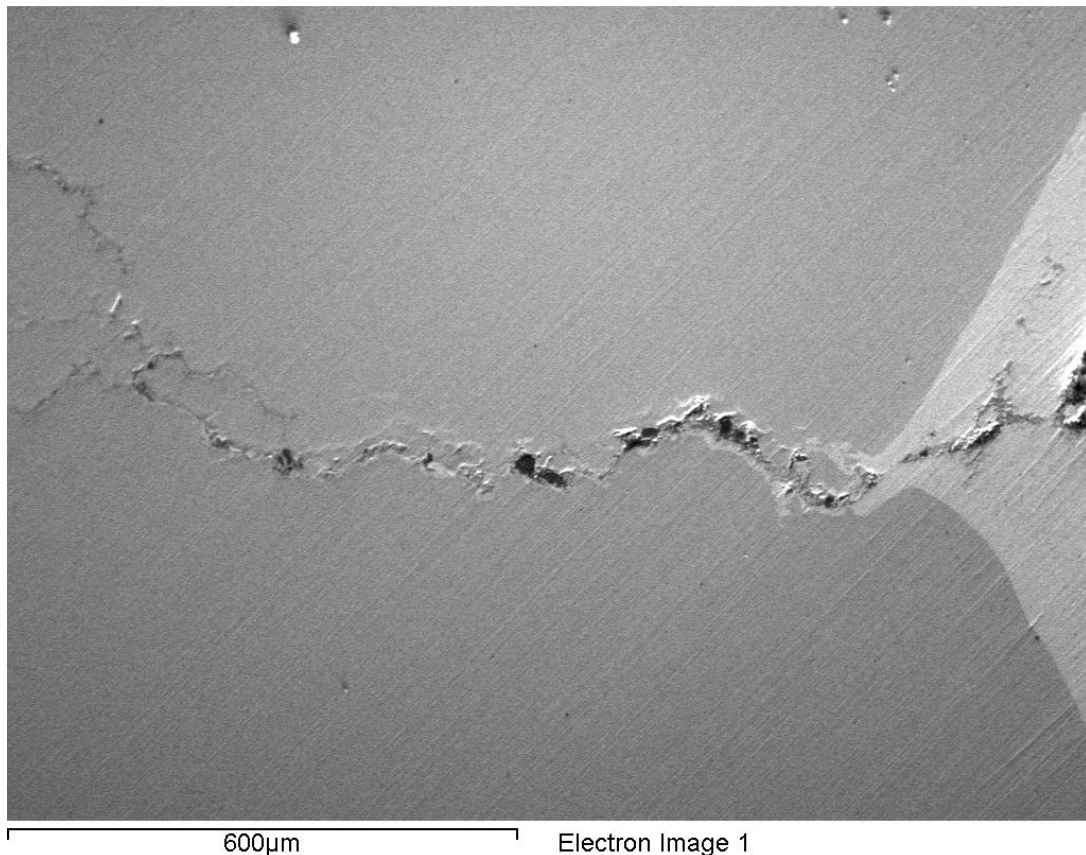
Figure 3-3: Initial crack from bend 10 of 33-3-12-TX-SG-A (Courtesy of TxDOT)

By analyzing the section of the initial crack observed in Figure 3-3, several details stand out. First of all, the crack seems to spread in multiple directions, and seems to follow a more erratic path, perhaps grain boundaries, rather than propagating in a strain line like those seen due to fatigue. Also, there appear to be alloy regions at the surface of the cracks that indicate the penetration of chemicals deeper into the base metal during galvanizing. These beliefs were verified when TxDOT created dot maps to indicate the presence of various elements superimposed on the section of bend 10 as depicted in Figure 3-4, Figure 3-6, and Figure 3-5.

31
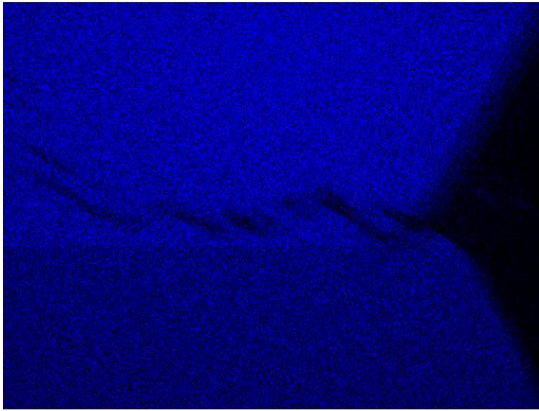
Fe Ka1

**Figure 3-4: Fe dot map of bend 10
(Courtesy of Edward Morgan TxDOT
Construction Division)**
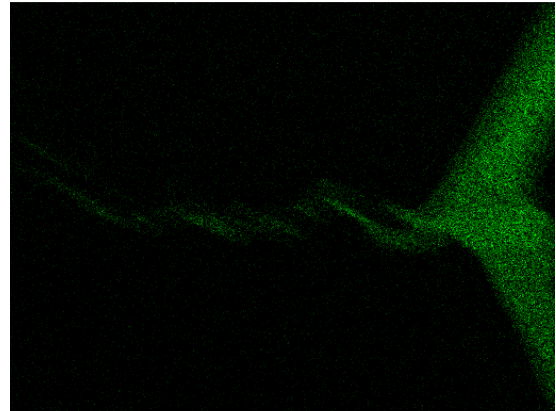
Zn Ka1

**Figure 3-6: Zn dot map of bend 10
(Courtesy of Edward Morgan TxDOT
Construction Division)**
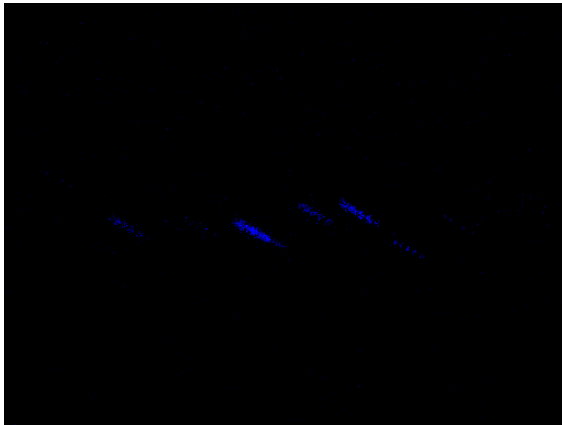
Si Ka1

**Figure 3-5: Si dot map of bend 10 (Courtesy
of Edward Morgan TxDOT Construction
Division)**

Of particular interest are Figure 3-6 and Figure 3-5, which show the depth of penetration of zinc into the base metal of upwards of about 1.2 mm. This indication verifies that zinc must have remained in the fluid phase after the formation of the crack, as also seen in photos from the JRC Report (see Figure 2-13 and Figure 2-14). It also seems to indicate some relationship between silicon and the formation of these cracks, as the presence of silicon in the cracked region appears

to be rather concentrated. Noting that silicon is known to increase the thickness of the galvanizing coating, presence of silicon in the crack region could potentially play a part in the initial cracking phenomenon. More research specific to this type of concern is warranted to verify this claim.

3.3.3 Chemistry Summary

The results from the chemistry analysis verify that while the source of the cracking does not necessarily stem from particularly reactive chemical components within the galvanizing bath, it is likely that cracking occurs while the specimens are submerged in the zinc bath. Particularly, this means that liquid metal embrittlement may be playing a part in the formation of these cracks, though, as discussed in section 3.3.1, not necessary in a way that independently results in cracking. Some other external factor is apparently controlling the origination of the initial cracks.

3.4 Comparison of Design Ratios

The final consideration reported in literature as an instigator of initial cracks were geometric ratios relating thicknesses of various HMIP components. Researchers looked at two different ratios to evaluate whether the ratios might be related to the formation of initial cracks.

3.4.1 Baseplate to Shaft Thickness Ratio

From the earliest detection of initial cracks in HMIPs at the University of Texas, design geometry has been at the forefront of researchers' minds as a contributing factor. After all, while the 80 mph, 100 ft. HMIP designs with 24.625" shaft diameters were being tested, these cracks were not developing. The following tests were performed to determine the effects of geometry on the development of initial cracks, and whether any trends became apparent.

A factor reported in research by Valmont is the volumetric shaft to baseplate ratio. According to the earlier referenced Valmont report, as the thickness of the baseplate increases relative to that of the shaft, the likelihood of developing cracks during galvanizing increases. Pool (2010) addressed this observation in his thesis by presenting the graph shown in Figure 3-7. The line shown on the graph represents the trend indicated by Valmont, and the individual points indicate specific HMIPs which were evaluated for initial cracks by using ultrasonic testing.
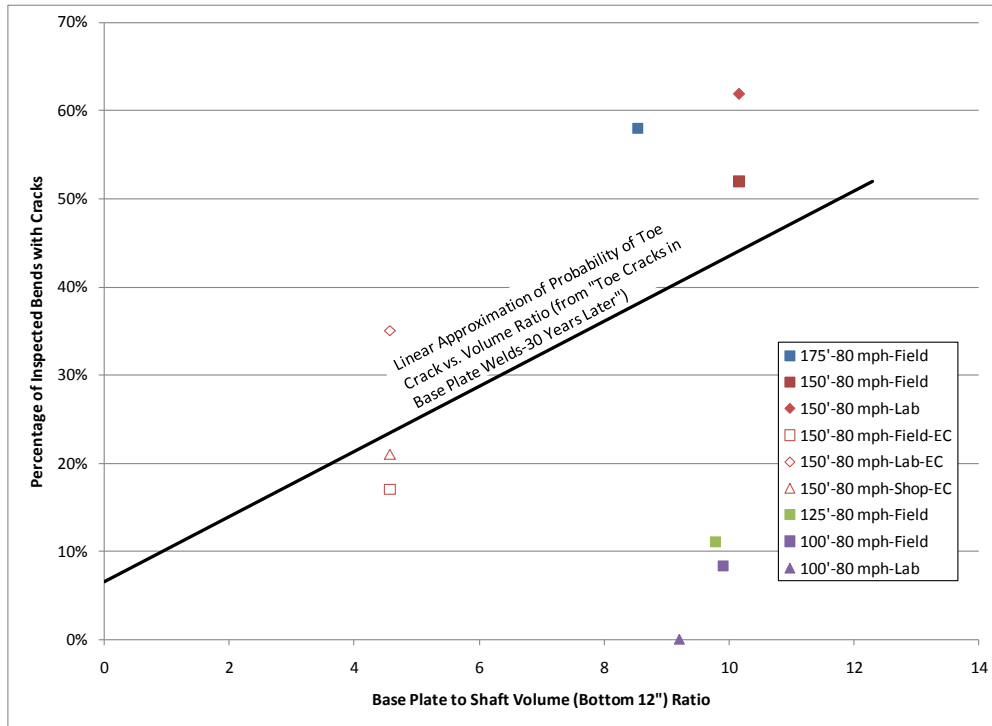
Figure 3-7: Percentage of cracks found compared to ratio of the volume of the base plate to the volume of the shaft (Pool, 2010)

The greatest observation from this graph is the correlation between particular designs of HMIPs and their percentage of cracked bends, rather than a strictly observed correlation between the actual baseplate to shaft volumetric ratio. Either way, Figure 3-7 depicts a correlation linking geometry to the likelihood of crack formation. This observation later inspired the examination of thermal effects as a principle culprit in the development of initial cracks in HMIPs during galvanizing.

3.4.2   Shaft Diameter to Shaft Thickness Ratios

In recognition of a correlation between HMIP geometry and the formation of initial cracks during galvanizing, Texas Department of Transportation began to inventory these towers across the state to determine which have cracked in the field relative to the type of pole design. The standard 80 mph TxDOT design specifies a shaft diameter of 36.250 in. and shaft thickness of 0.375 in. (measured from flat to flat) for the 175 ft. tall poles, a diameter of 32.625 in. and a thickness of 0.313 in. for the 150 ft. tall poles, and a diameter of 24.625 in. and a thickness of 0.313 in. for the

100 ft. tall poles. Figure 3-8 graphically depicts the results from this study. Through this study, a clear correlation appears between shaft diameter to thickness ratios and the development of cracks. It should be noted, however, that every pole evaluated by UT testing by TxDOT had already been installed in the field, and could have been subjected to wind loading for years. Despite the variability in loading and load duration, a direct relationship between the shaft diameter to shaft thickness ratio (d/t ratio) and the likelihood of crack formation in poles that were otherwise thought to be safe clearly exists. Particularly, the study indicates that should the d/t ratio be increased above 66, HMIP designs may be at risk of developing cracks at the toes of the base plate to pole shaft weld.
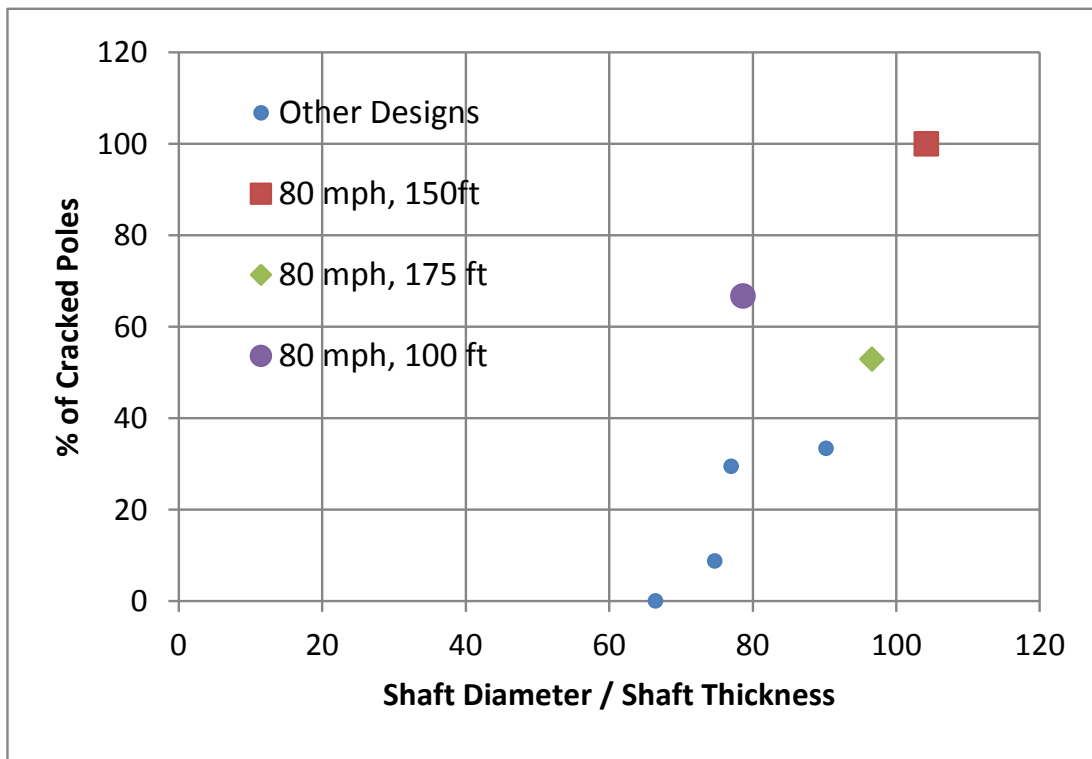
Figure 3-8: Percent of cracked poles of a given TxDOT design relative to shaft diameter to thickness ratio (Figure courtesy of Luca Magenes)

3.5   Conclusions

While these tests and studies did not conclusively establish the cause of initial crack formation, implications of thermally induced stresses and strains due to the galvanizing process seemed most

plausible due to the orientation of cracks at the weld toe, relative chemical uniformity of material, non-reactivity of bath chemistry, and involvement of design geometry relative to the formation of cracks. Based on the results of these tests, subsequent chapters focus on evaluating the performance of specific types of TxDOT HMIP designs as they are subjected to thermal stresses and strains due to galvanizing.

CHAPTER 4. FIELD INSTRUMENTATION

4.1 Introduction

From initial testing and initial studies, thermal effects on design geometry stood out as the most likely catalyst to initiate cracking during galvanizing. To test this hypothesis, a full scale testing program of HMIP designs was developed to measure the temperature gradient across the pole sections, and to determine the impact of different design geometries on crack formation during galvanizing. The full scale testing was completed by instrumenting poles so that data could be gathered while the HMIPs were being dipped. Tests were conducted at two different galvanizers so that the effects of variations in the dipping process could be measured. The tests were conducted on full size specimens as well as reduced sections, which are referred to in this thesis as stub pole sections. This chapter addresses the considerations and processes utilized to instrument and measure temperatures at various points on high mast illumination poles during galvanizing.

4.2 Data Acquisition

To measure the impact of thermal gradients on crack initiation HMIPs were instrumented and monitored during the galvanizing process. The field measurements were used to validate the accuracy of finite element models which were developed to conduct parametric studies on the thermal behavior of HMIP sections during galvanizing. A major task in the field monitoring was developing the instrumentation configuration to obtain temperature readings at specific points on the HMIP. Configuration decisions included the types of sensors, the geometrical sensor layout on the HMIP, the data acquisition system that was used to monitor the sensors, and the method of protection for the entire monitoring system to prevent damage from the hot galvanizing bath. The following sub-sections detail the configuration of the instrumentation that was used for the field monitoring.

4.2.1 Thermocouples and Connection Configurations

The extreme temperatures from the hot zinc bath necessitated a robust temperature measurement system. The system needed to accurately measure temperatures throughout the duration of the hot-dipping process.   Although thermal imaging was initially considered, researchers realized that the gradients on the HMIP would not be recorded once the HMIP was submerged in the bath. Instead, thermal sensors would need to be placed on the poles to continuously monitor

temperature throughout the dipping process.   The sensors needed to be adequately distributed on the section to ensure good measurement of the thermal gradients on the shaft and base plate would be obtained.

Type K thermocouples were selected since the wire provides the adequate temperature range for the galvanizing process. The thermocouple wire has two layers of high temperature glass insulation on both the individual thermocouple leads, and around the exterior of both thermocouples, which provides adequate protection so that the leads are not damaged during galvanizing. A relatively small gage wire was selected to enable embedment of the thermocouple junction into the steel shaft and base plate to measure the internal temperature. Omega HH-K-24 Type K thermocouple wire was selected for the instrumentation.

Once the proper thermocouple wire and insulation had been selected to monitor the HMIP temperature during galvanizing, the instrumentation locations were selected and a means of fastening thermocouples to the high mast specimens was developed. To best understand the effects of the thermal gradients across the high mast section, temperature measurement locations were chosen in the base plate as well as in the pole shaft. A more complete discussion of the instrumentation locations is provided in Chapter 5.   Over the course of the study, two different methods of fastening thermocouples to high masts were implemented: 1) screw connections and 2) adhesive connection. The screw connection is shown in Figure 4-1 in which 3/16" diameter holes were drilled and tapped with threads into the exterior of the high mast. A large-headed screw was used to hold the end of the thermocouple flush against the surface of the high mast. The screw detail was only used on the shaft thermocouples. The adhesive connection that was used to fasten the thermocouples to the HMIP was executed by drilling a 3/16" diameter hole and embedding the thermocouple in the hole with a fast-curing high-temperature adhesive, as shown in Figure 4-2.
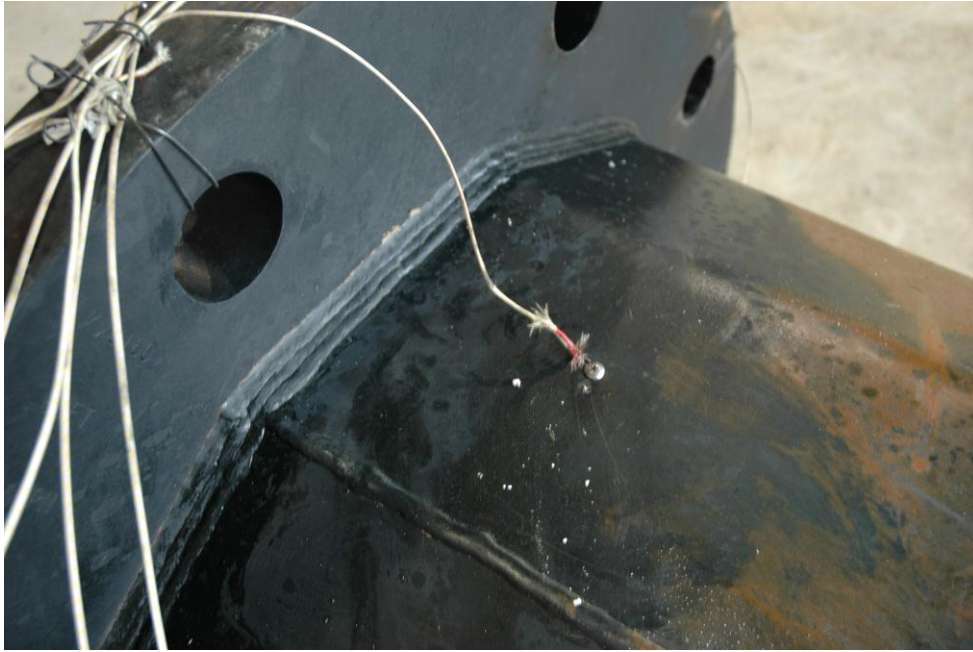
Figure 4-1: Screw thermocouple connection at HMIP shaft location
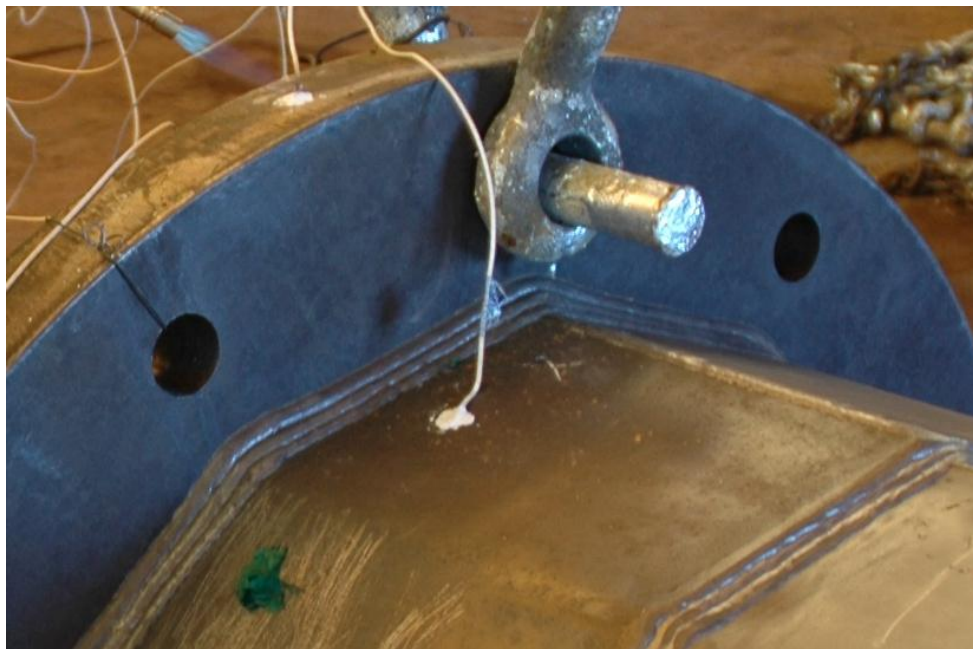
Figure 4-2: Adhesive thermocouple connection at HMIP external collar location

Of the two methods previously described for attaching thermocouples at the shaft locations, the high temperature adhesive proved most effective. Intuitively, this makes more sense: when thermocouples are clamped to the surface of a high mast during hot-dipping, enough molten metal flows over the surface of the shaft to keep the temperature of the molten bath significantly warmer than that of the steel, resulting in little useful information about the actual temperature at the exterior of the pole. For this reason, embedded thermocouples seemed to give more realistic and useful measurements of temperature.

4.2.2   Hardware

One of the challenges in conducting full scale thermal tests at the galvanizing plants involved logging data in a high temperature, and relatively inaccessibly environment. The dangers of galvanizing procedures are relatively apparent—large pieces of fluxed steel are being lowered into molten metal averaging nearly 830°F. The actual galvanizing procedure can produces violent reactions which resemble a boiling pot of water on a stove and often results in hot liquid zinc flying through the air as the steel element is lowered into the zinc bath. To safeguard workers, the galvanizing baths observed by researchers were surrounded by a protective barrier that closes around the bath at the time of pole submergence. It was therefore necessary to attach the data acquisition system onto the lifting system that was used to support the HMIP during the galvanizing procedure.
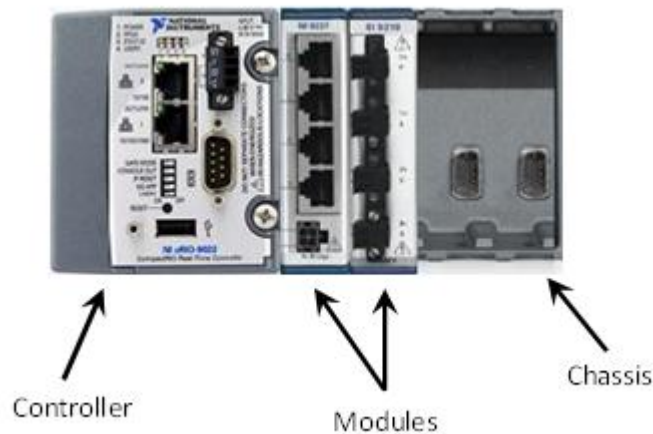
Figure 4-3: CompactRIO component diagram

The data acquisition system consisted of a National Instruments CompactRIO controller, chassis, and several modules, as depicted in Figure 4-3. Thermocouples and strain gage wires were hardwired into the screw terminals of the CompactRIO modules and data was recorded directly into the controller. A non-spillable motorcycle battery with a 1 Amp fuse was used to power the system.

The data acquisition system and battery were housed within a box that was suspended from the rigging used to dip the HMIPs as shown in Figure 4.2. Since electronic equipment typically performs poorly at higher operating temperatures, care was taken to ensure the box holding the CompactRIO was well insulated against heat; the box was fabricated out of wood and coated in ventilation duct insulation, which was held in place by aluminum tape. Originally icepacks were also placed inside the instrumentation box to keep operating temperature low, but after recording acceptable temperatures within the box, ice packs were no longer deemed necessary. Temperatures within the instrumentation box remained consistent with ambient room temperatures for the duration of the dipping process.
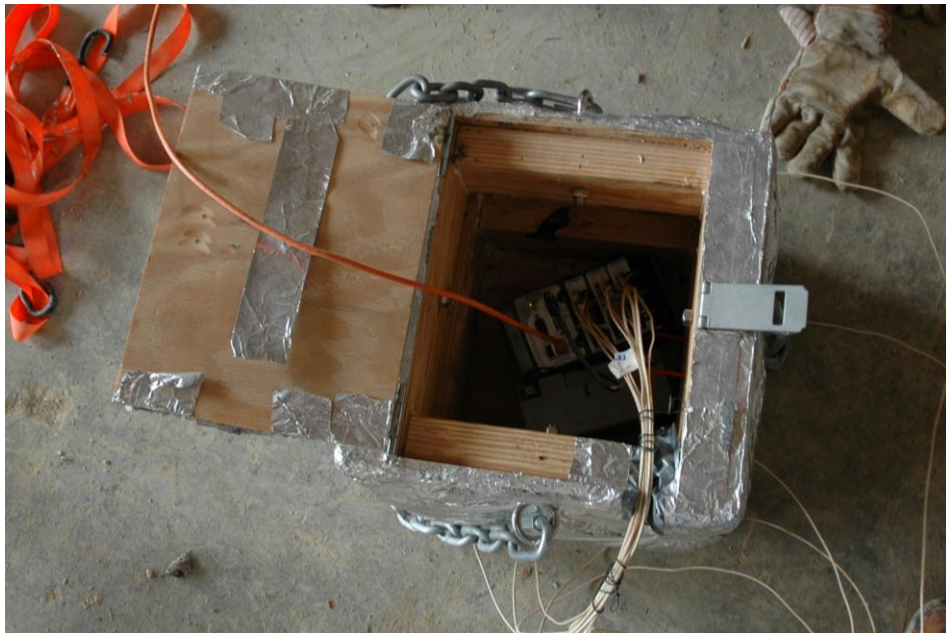
Figure 4-4: Data acquisition box with CompactRIO and battery inside

4.2.3   Software

The program Labview from National Instruments was used to develop the data acquisition instructions to collect and store the data. Labview allowed for easy interfacing between controller and thermocouple or strain gage modules, and also enabled researchers to specify durations of time between data measurements. This proved particularly useful when taking simultaneous thermocouple and strain gage data since each module could be set to take data readings at specific frequencies. In the case of all thermal experiments, thermal data was taken at a frequency of 1 Hz and when strain data was simultaneously taken, researchers logged data at a frequency of 50 Hz.

4.3   Implementing Data Acquisition System

The demands of instrumenting HMIPs in the field prior to hot dip galvanizing require rapid implementation and flexibility to ensure accurate results with minimal interference to the galvanizer dipping schedule. The procedures outlined in this section describe the process by which the high mast illumination poles and stub sections were instrumented with thermocouples and strain gages at the galvanizing plants.

4.3.1   Phasing

Instrumenting pole and stub sections at actual galvanizer plants afforded invaluable opportunities to learn more about the industry standards used by hot dip galvanizers regarding HMIPs. In order to take data in such an environment, however, certain restrictions were placed on the time frame during which researchers could instrument specimens. As described in Section 2.4.2 the process of galvanizing involves the use of several chemical baths to facilitate cleaning and fluxing of the base metal, prior to even entering the molten zinc bath. These cleaning and fluxing procedures often take several hours to complete, which restricted when the sections could be instrumented to directly after fluxing and prior to hot-dipping.

While this time frame afforded researchers the greatest chance to adequately instrument the high mast illumination poles, because this period of time is in the middle of the galvanizing process the researchers had to complete the instrumentation in a timely fashion to avoid slowing down the galvanizing line. Also, fluxed steel has a tendency to "flash rust" when exposed to the air for longer than approximately 30-60 minutes after completion of the fluxing process. Flash rusting reduces coating quality, and might also affect the heat flow characteristics between the

galvanizing bath and base steel. For this reason, an instrumentation strategy was developed to minimize the amount of time that would take between instrumenting and hot-dipping.

Thermocouple locations required specially drilled holes in the base metal to embed a thermocouple. All base plate hole locations were drilled by the fabricator prior to the arrival of the HMIP at the galvanizing plant. In the case of drilling the holes in the external collars, holes were initially drilled on site following the fluxing process. On the final round of testing, all shaft locations were drilled by the fabricator prior to arrival at the galvanizing plant.

4.3.2   Thermocouple Instrumentation

As previously stated, type K thermocouples with glass weave insulation were used to measure the thermal gradients on the HMIP during galvanizing. Several of the thermocouples were connected to the poles by embedding the sensor into a hole and using an insulating adhesive to protect the thermocouple leads during galvanizing and to ensure contact with steel at points of interest. The first step in attaching the thermocouples was to prepare the high temperature adhesive. The adhesive came in a liquid activator and a granular compound which needed to be mixed to activate as shown in Figure 4-5. Once mixed in the recommended proportions, the adhesive was poured into a syringe injector, which was used as the applicator.

Figure 4-5: Resbond 940HT fast curing adhesive

To further expedite instrumentation, thermocouple leads were pre-measured and labeled for connection to the test specimen. Thermocouples were wired into the respective CompactRIO modules beforehand to minimize the amount of time needed for instrumentation. The thermocouple wire was measured to ensure about 10 feet of separation between the DAQ box and the test specimen.

Prior to application of the adhesive, drilled thermocouple holes were cleaned by swabbing with a Q-Tip and a thermocouple was inserted into its respective drilled hole. After insertion, the adhesive was applied into the top of the thermocouple hole, and around the exterior opening in such a way that sealed the hole closed, as shown in Figure 4-6. By sealing the holes, researchers could guarantee that temperatures being measured were of the base steel and not the liquid zinc. Maintaining the integrity of this data was essential to ensuring the proper evaluation of temperatures. To protect the thermocouple wires during the galvanizing process, which can be rather volatile, researchers provided extra slack in thermocouple wires near embedment locations to provide some strain relief. All of the thermocouple wires met at a common point at the top of the baseplate, from which the wires were run back to the DAQ box as shown in Figure 4-10.

Figure 4-6: Researcher applies adhesive paste to seal thermocouple hole

The greatest points of concern with the instrumentation of the high masts were how curing time for the adhesive could be minimized, whether the adhesive could sustain the temperatures in the

galvanizing baths, and whether the adhesive would be able to block the passage of molten zinc from penetrating into a drilled hole. These considerations were the driving parameter in selecting Resbond 940HT, a fast curing alumina adhesive rated at 2800°F, made by Cotronics. The thermal properties of Resbond 940HT as compared against steel are listed in Table 4.

Table 4-1: Thermal Properties of Adhesive and Steel

Parameter		Resbond 940HT	Steel
Conductivity	$\left(\dfrac{Btu \times in}{hr. \times °F \times ft^2}\right)$	15	300
Thermal Expansion Coefficient	$\left(\dfrac{in \times 10^{-6}}{in \times °F}\right)$	4	7.3

Another beneficial property of Resbond 940HT is that with the application of 200°F temperatures, the adhesive cures in five to fifteen minutes. Researchers applied this heat with propane torches, as shown in Figure 4-7. By using two researchers to place the thermocouples and adhesive and one or two researchers to assist with the data acquisition system and wiring, the entire specimen could be instrumented in approximately thirty minutes.
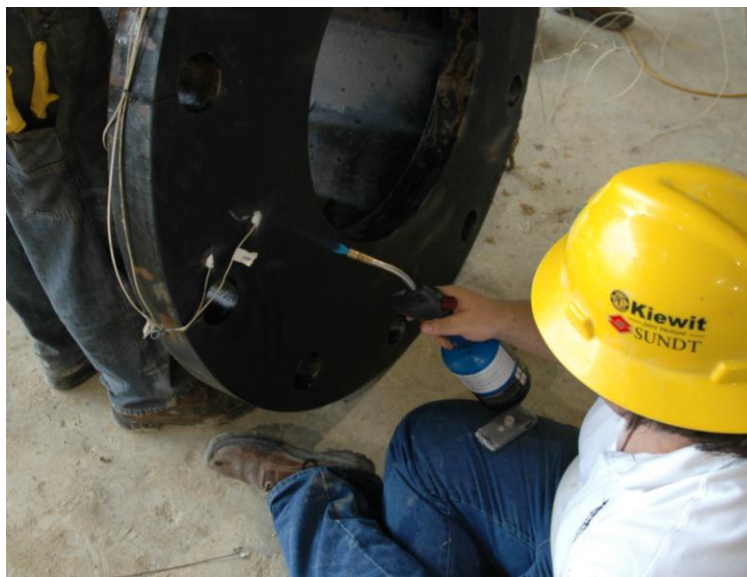
Figure 4-7: Researcher heats adhesive paste with propane torch to decrease curing time

4.3.3   Strain Gage Instrumentation

The purpose of instrumenting these HMIPs to measure thermal gradients as a function of time during dipping is to gain an understanding of the thermally induced stresses and strains within the section. Combined with the finite element studies, the gathered data was to be used to determine a correlation between these stresses and strains, and the likelihood of crack initiation during galvanizing. In recognizing that strain gaging would not yield much information prior to burning up in the zinc bath, the captured experimental data focused primarily on recording temperatures within the high masts. However, for the final round of testing, strain gages were placed on the three HMIP sections to be galvanized for the sake of capturing whatever amount of strain data possible. This data was later used to aid in verifying the thermally induced strains reported by ABAQUS. Although the gages would not survive the galvanizing process for long, the sensors would provide some indication of the strain gradients that develop in parts of the HMIP during the dipping process.
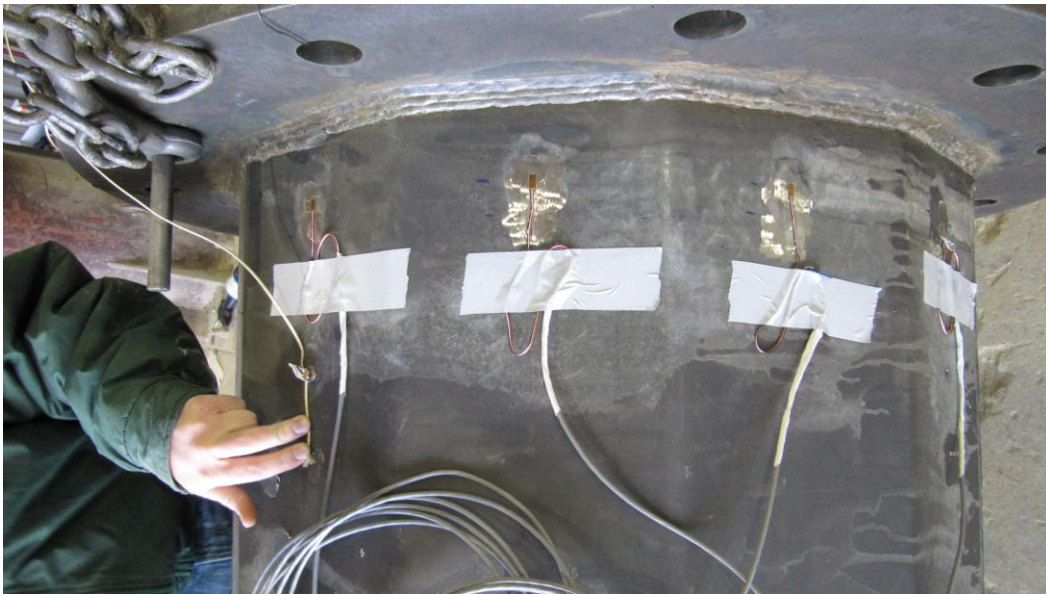
Figure 4-8: Strain gages attached to high mast prior to galvanizing

Vishay Micromeasurement foil strain gages, model number CEA-06-250UN-350/P2 were used to capture strains in the longitudinal direction of the pole shaft during dipping. These strain gages were attached at flat locations along the outer perimeter of the pole shaft. Instrumentation sites were first ground smooth and degreased to provide a good bond between the steel and foil

backing. The strain gages were then oriented along the longitudinal direction of the shaft at a specifically measured location and glued to the shaft as shown in Figure 4-8. A piece of tape was placed over the top of the strain gages to ensure the strain gage remained undisturbed prior to galvanizing. Because the gages were introduced into the galvanizing bath within 30 minutes after application, no additional environmental protection was used since the bonding adhesive would not degrade during that time period.

4.3.4 Initiating Data Capture

Once all the thermocouples and strain gages were fastened into place, a laptop computer was used to activate the Labview program on the CompactRIO as shown in Figure 4-9. Labview enabled data capture frequencies to be specified by each module, which could receive input from up to four leads. The majority of the sensors that were used were thermocouples, but HMIP stub sections were also instrumented with four strain gages in three of the tests. In this case, three modules were used to take thermocouple data, and set to take measurements at a frequency of 1 Hz, while the strain gage module was set to take measurements at a frequency of 50 Hz. Taking measurements at different frequencies for different parameters helped to create data files that were more manageable.

Figure 4-9: Researcher activates CompactRIO data acquisition system

47

Once activated, the DAQ was sealed inside the DAQ box, and then fastened to the galvanizing rigging as shown in Figure 4-10. The HMIP was then moved to the galvanizing bath. The results of these dipping experiments are recorded and discussed in Chapter 5.

Figure 4-10: Instrumented high mast stub and DAQ box prior to galvanizing

CHAPTER 5.   FIELD INSTRUMENTATION RESULTS

5.1   Introduction

Over the course of three trips, a total of eight high mast illumination pole sections were monitored during galvanizing to determine the effects of varying pole geometry on the developments of thermal gradients and the formation of cracks in the weld between the shaft and baseplate.   This chapter describes observations from the tests. The three trips to the galvanizing plant were conducted in January and June of 2010 and February of 2011. The results that are provided are identified by the date of the visit to the galvanizing plant. For each test, the pole geometry is discussed along with the temperature profile that was measured from the thermocouples as well as the resulting crack distribution. Strain data is presented and discussed for tests performed during February of 2011.

Figure 5-1: Suspended HMIP section with external collar and DAQ box after galvanizing

5.2   January 2010 Test

In the first test conducted to measure thermal gradients in HMIPs during galvanization, two full length 33-3-12-TXEC specimens, as shown in Figure 5-1, were instrumented and hot-dip galvanized at two separate galvanizing plants. The purpose of this round of testing was to see whether substantial differences in crack formation resulted from using two different galvanizers. Both of these specimens were of the same design and material. The results of these tests are discussed in the following subsections.

5.2.1   Design Details

The first high mast illumination poles tested for development of initial cracks were TxDOT 80 mph 150' designs with an external collar. TxDOT selected this type of high mast, with the external collar, as an effort to determine the effect of the external collars on the development of cracks during galvanizing. Researchers had previously also noticed that the length and quantity of galvanizing cracks differed on the 80 mph 150' poles by galvanizer, and therefore ordered that these poles from the same fabricator. The poles were then galvanized at two separate plants.

5.2.1.1   Pole Geometry

Two specimens were fabricated by Structural and Steel Products, and each specimen was sent to a separate galvanizer for coating. A profile drawing of the specimens is presented in Figure 5-2. These twelve-sided specimens were constructed with a 5/16" pole shaft wall, and a 3/8" inch thick external collar, and a 3" thick baseplate. The baseplate measured 47" in diameter and had a 22" diameter access hole cut from its center as shown in Figure 5-3. The out-to-out shaft diameter about opposite flat regions of the shaft measured 32-5/8". Unlike typical TxDOT designs, these poles had twelve anchor rod holes and an end plate welded onto the shaft so that the specimens could be tested in fatigue such as those fabricated in earlier phases of the research project. All full length sections tested were fabricated with twelve anchor rod holes, and an end plate. The end plates were socket welded to the end of the shaft. Details of the socket weld are shown in construction drawings in Appendix A.

Keeping with previous research suggestions, these poles were also fabricated with full penetration welds at the shaft to base plate connection. These full penetration welds maintained about a 2 to 1 aspect ratio to minimize the effects of stress concentrations in subsequent fatigue tests, as mentioned in Stam's thesis (2009), and as shown in Figure 5-4.
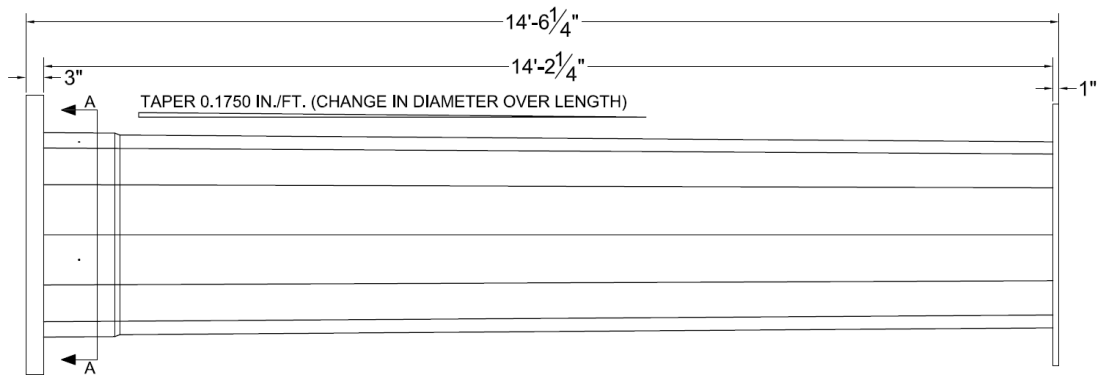
Figure 5-2: Profile of 33-3-12-TXEC-SG specimens
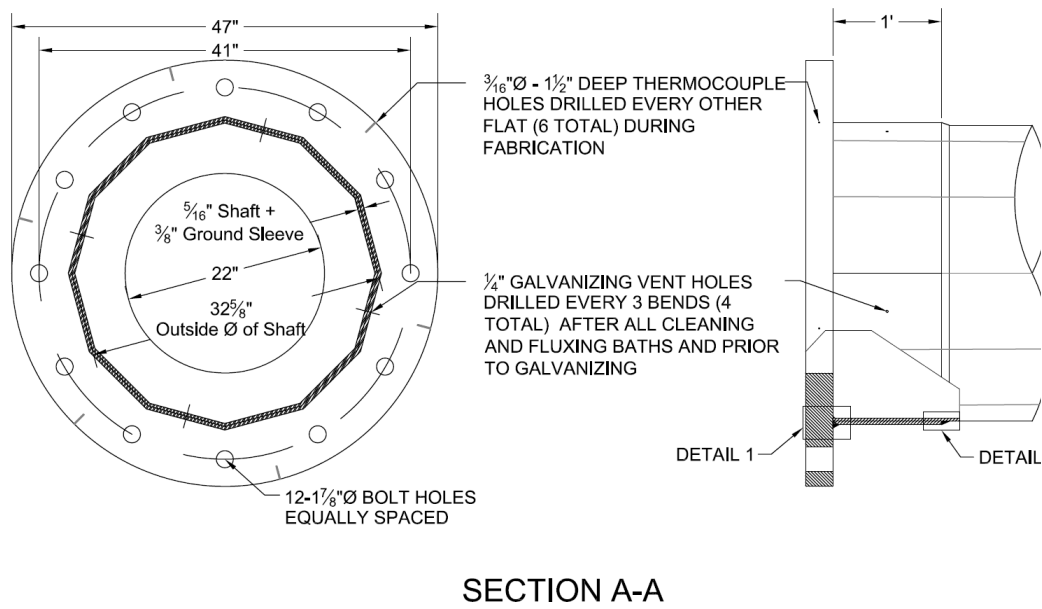
SECTION A-A

Figure 5-3: Section cut A-A with dimensions, as specified in Figure 5-2
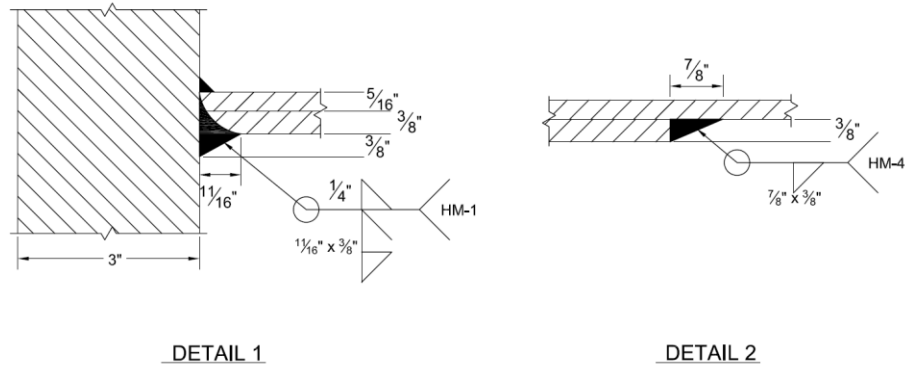
Figure 5-4: Weld details for baseplate and external collar, as called out in Figure 5-3

5.2.1.2 Instrumentation Locations

A particularly unique element to the fabrication of these high mast illumination poles were specified thermocouple locations which required special drilling. On the first two poles, these locations were chosen to provide researchers with radial temperature data corresponding to points along the baseplate. The thermocouple holes had a diameter of 3/16" and extended 1-1/2" into the base plate edge, as shown in Figure 5-3. Thermocouple holes in the baseplate were chosen to be equidistant from adjacent anchor rod holes to minimize the localized heating influence from liquid flowing into these anchor rod holes. Six thermocouple holes were drilled in the middle of the exterior edge of the base plate to make installation of thermocouple easier once researchers arrived on site for instrumentation. Only four of these locations were actually instrumented.

Two locations were instrumented in the shaft to record temperatures at the midpoint between the external collar and pole shaft. This temperature provided an indication as to the temperature of the coolest part of the pole shaft during galvanizing. These shaft locations were drilled on site on the flat edges of the shaft. The shaft locations were chosen equidistant from a bend and half way along the length of the external collar (six inches from the base plate). The layout of these thermocouple locations are displayed in Figure 5-5. In this figure, blue, italicized bend numbers correlate with the location of weld seams in the pole shaft, and underlined bend numbers indicate which bend was up while being hot dipped. This convention of designating bend locations is used throughout the rest of this thesis. Dimensions of independent thermocouple locations are shown in Figure 5-6.
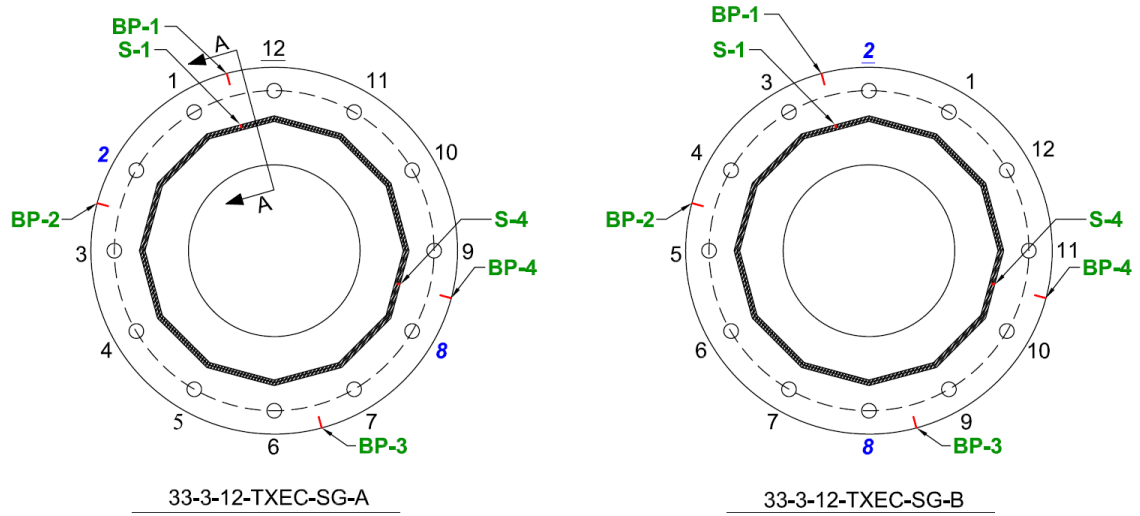
Figure 5-5: Thermocouple locations and bend designations for 33-3-12-TXEC-SG specimens in the up position during galvanizing
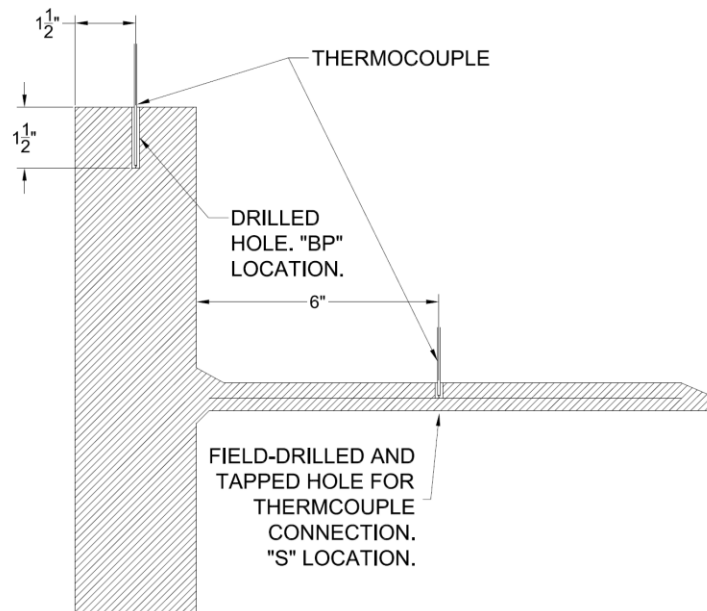
Figure 5-6: Typical thermocouple connection details for 33-3-12-TXEC-SG specimens as in section A-A of Figure 5-5

In the case of this first test, one can see from Figure 5-5 that the location of the weld seams for the pole shafts do not align between specimen dipping orientations: in the case of 33-3-12-

TXEC-SG-B, the weld seam is actually located at the up and down positions relative to the galvanizing bath. This was a beneficial orientation to choose for dipping because from previous experience opening galvanizing cracks, researchers found that these cracks are less likely to form at locations where the weld seam intersects the full penetration weld joining the baseplate to the shaft. Furthermore, researchers initial thought the up and down positions to be most crack-critical locations. These two orientations produced additional information regarding where cracks would most likely form relative to the weld seam.

5.2.2   Thermal Performance

Once instrumented in accordance with the procedures outlined in Chapter 4, temperature data was recorded at thermocouple locations with a frequency of 1 Hz. The HMIP was connected to the crane using a hole in the base plate and another in the reaction plate. Because the HMIP had cooled down during the instrumentation process, the crane operator positioning the section a few feet above the galvanizing bath for a number of minutes to heat the section. It should be noted that the temperatures achieved within the steel section through pre-heating is recorded in the data presented in Appendix B as the initial temperature shown prior to the start of dipping. This temperature is not highly variable, nor does it achieve much more than 115°F at any location. Relative to the 830°F of the galvanizing bath, this amount of heating above ambient temperature does not appear to yield significant results. After pre-heating, the steel section was hot dip galvanized at a rate and angle left to the discretion of the crane operator. Once the crane operator deemed that the high mast had been adequately submerged in the molten bath, the section was removed and allowed to air cool. At some galvanizers, high masts are quenched in a cooling bath before being allowed to air cool. Data was recorded from the time before galvanizing until several minutes after removal from the bath during the cooling process.

From the first round of testing, two separate graphs shown in Figure 5-4 were made showing the temperature at various node locations, with respect to time during dipping. Both of these data sets are presented in Appendix B. Figure 5-7 shows typical results from this round of thermal testing for this specific design type for thermocouple locations BP-1, BP-2, BP-4, S-1, and S-4. The other BP-3 location did not take reliable data due to errors and was omitted from the graph. Greater discussion on types of errors observed while monitoring temperatures with thermocouples is presented in Section 5.5. Thermocouple locations S-1 and S-4 were embedded

between the external collar and the pole shaft, and it can be seen that they gain temperature much more quickly than those embedded into the thicker baseplate.

Location S-4 seems to gain temperature the fastest, though it appears, by the roughening of the horizontal portion of the graph, the thermocouple came into contact with molten zinc once the zinc had worked its way between the shaft and the external collar. This seems plausible due to the fact that drain holes were drilled through the external collar and the shaft to inhibit the expansion of gases from accumulating between the shaft wall and external collar, which has been known to cause deformations in the shaft at times (Stam, 2009). The drain holes allow the liquid zinc to flow between the shaft and external collar. Later during destructive investigation of the sections hardened zinc was also found between the shaft and external collar, further giving credence to this hypothesis. More discussion of the impact of measuring molten zinc temperatures rather than base steel temperatures is given in Section 5.5.
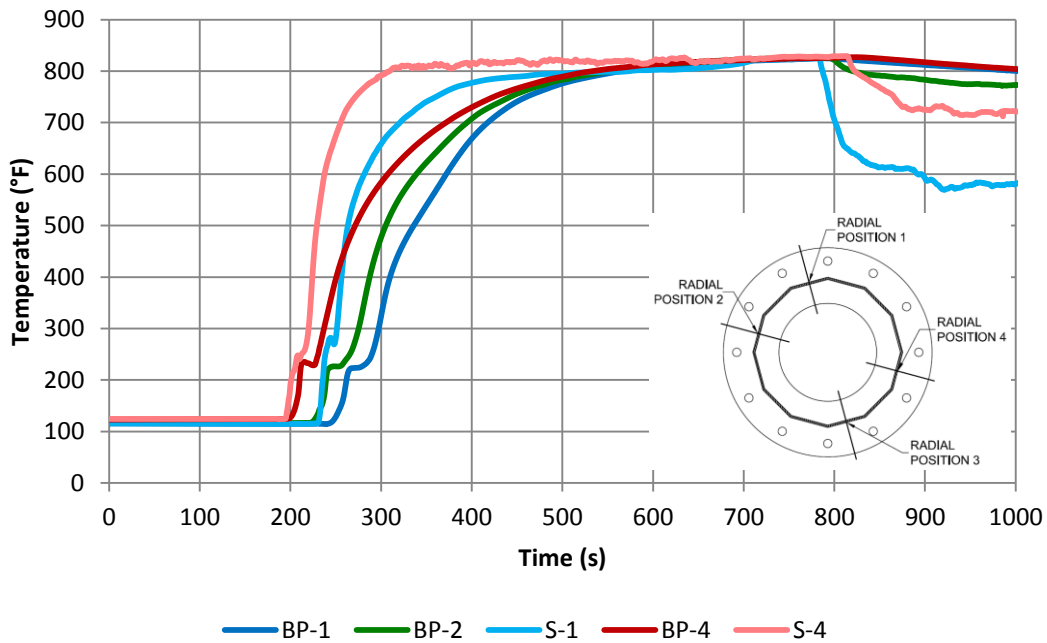
Figure 5-7: Typical thermal results from January 2010 specimen galvanizing trip
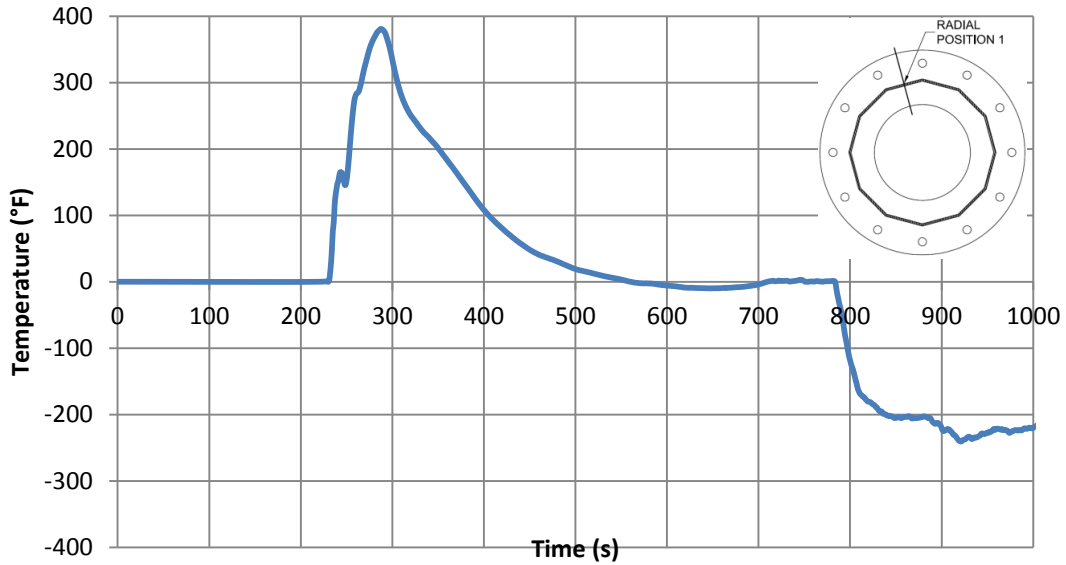
Figure 5-8: Thermal gradient between nodal locations BP-1 and S-1

The greatest and most useful observation from this set of data is the temperature difference between the nodal points at BP-1 and S-1, and between BP-4 and S-4. In measuring the difference in temperatures between the pole shaft and baseplate at the same radial position, it is apparent that a maximum thermal gradient of nearly 400°F can exist between corresponding radial locations, as shown in Figure 5-8.   The large thermal gradient is a likely source of the of the crack formation due to induced thermal stresses and strains during galvanizing. The measured gradients provided a valuable source of validation data for finite element models that were used to conduct parametric studies on the poles during galvanizing. The results from these studies are given in subsequent chapters.

5.2.3   Initial Cracks

To identify cracks in the poles a TxDOT technician evaluated the high mast illumination poles using ultrasonic testing at each pole shaft bend and weld seam. The poles were inspected before and after galvanizing to ensure that the cracking occurred during galvanizing. From earlier destructive testing, TxDOT verified that cracks at weld toes could be located using ultrasonic testing with satisfactory accuracy. The procedure and earlier evaluation of the effectiveness of ultrasonic testing is presented in greater detail in Pool's thesis (2010) and will not be discussed

here. The following section characterizes the location of cracks on high mast illumination poles 33-3-12-TXEC-SG-A and 33-3-12-TXEC-SG-B.
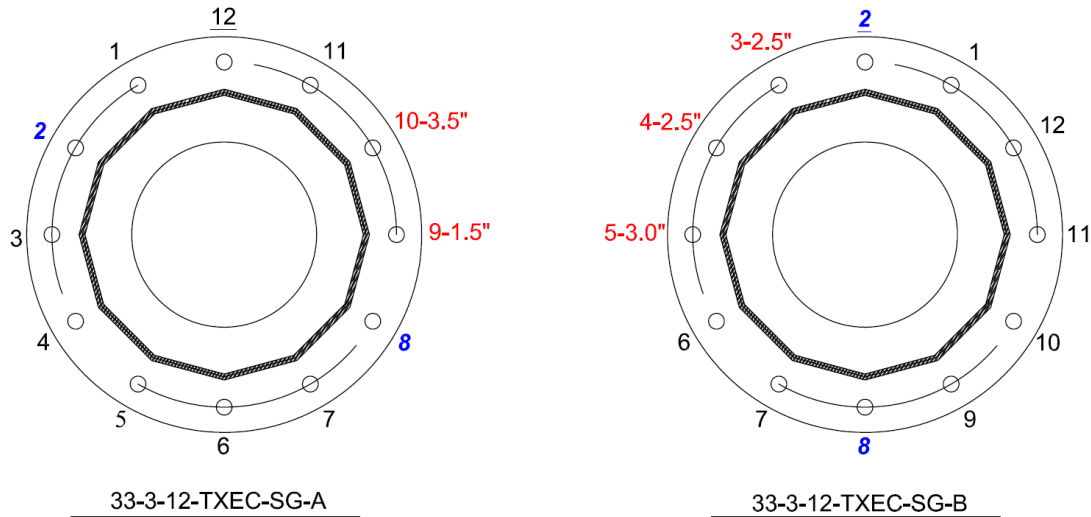
Figure 5-9: Initial crack locations after January 2010 galvanizing. Cracked bends and lengths marked in red.

Figure 5-9 shows the results from TxDOT ultrasonic testing after galvanizing. Again, underlined bends were up during galvanizing, italicized, blue bends denote the location of weld seams, and red bends followed by a dimension indicate a galvanizing crack of that length. This convention of presenting crack information is used throughout the rest of this thesis. The results indicate that adding a 3/8" thick external collar to a pole with a 5/16" shaft thickness reduces the number of occurrences of cracks relative to the specimen evaluated by Pool (2010) in Figure 2-8, which had no collar and a 5/16" thick shaft. Despite the decrease in the number of cracks, the lengths of the crack are much greater in the external collars than what was observed in previous specimens. The locations also seem to cluster in the same general area as well, cracking within 90 degrees of the top bend during dipping.

5.2.4 Tension Testing

The greatest advantage of the external collar design detail for TxDOT, is that the external collar adds a greater section at the location where the pole shaft is welded to the baseplate. By increasing the section, the hot spot stresses that occur at the toe of this weld are reduced and a

better design for fatigue is achieved. The problem when it comes to initial crack observations is that it is not currently possible to discern with ultrasonic testing whether or not cracks have penetrated through the external collar into the pole shaft. The same issue prompted destructive testing to determine whether or not initial cracks were concentrated solely within the external collar or existed in the pole shaft as well.

Figure 5-10: Suspected non-ductile cracks due to yielding during destructive testing

To open these specimens, bend sections were cut from the baseplate section of the high mast illumination tower and vertically sectioned near the ends of the crack. These sections were clamped to a strong table and bent away from the cracked face to expose the cracked surface. The section was bent back and forth to begin yielding and fracturing the remaining steel shaft wall material. This technique, when applied to the high mast sections with external collars not only became a much more physically challenging procedure, but also resulted in oddly brittle

behavior in the external collar and shaft steel as shown in Figure 5-10. Figure 5-10 shows typical external collar and shaft behavior after fracturing at the base. The large number of small horizontal cracks suggests brittle behavior unlike characteristic structural steel.

Figure 5-11: Tension coupon being tested in uniaxial tension with universal testing

Witnessing this behavior prompted verification of the material properties of the steel being used to fabricate the pole sections. Two inch gage length tensile coupons were cut from regions of the shaft and external collars of both 33-3-12-TXEC-SG-A and 33-3-12-TXEC-SG-B. From each high mast, five coupons were cut from the shaft: two transverse to the length of the shaft, and three in the longitudinal direction. Of the three longitudinal specimens, one was cut approximately one inch from the bend in the shaft to see if a significant difference was observed in the tensile strength near the radial position where cracks had been measured at the baseplate-shaft weld. The tensile coupon specimen naming convention details all the locational

considerations listed above: SG-A/B designates the high mast from which the coupon came, V/H/B designates whether cut in the vertical (longitudinal), horizontal (transverse), or vertical near a bend orientation, E/S designates coming from an external collar or shaft, and the last number is used to identify a tensile coupon from a region with multiple tests.

All twenty specimens were tested on the same universal testing machine shown in Figure 5-11. The closed loop hydraulic machine has a 22 kip capacity and is manufactured by MTS. Most of the specimens were tested at a strain rate of 0.01 in/min from initial loading to the ultimate strain. In the case of A-VE2, strains were increased to 0.05 in/min within the yield plateau, and later during strain hardening decreased back to 0.01 in/min, hence the apparent rise in strength. A few specimens were unintentionally initially loaded at a rate of 0.1 in/min. Specimen A-VS1 was loaded in this manner, and displayed characteristics of instantaneous load behavior and was therefore prematurely stopped. Specimen A-VS2 was also stopped early due to the accelerated loading; however, after reviewing the stress strain curve, no abnormalities were observed due to correction of the loading prior to reaching the yield load.

The results of the tensile testing are enumerated in Table 5, and specific stress vs. strain curves are presented in Appendix C. Dashes indicate an error in testing that inhibits the accurate presentation of that specific value. Based on these results, researchers have reached the following conclusions. First, the tested high mast shaft and external collars are not made from the same steel. The test results from 33-3-12-TXEC-SG-A and 33-3-12-TXEC-SG-B indicate yield and ultimate strengths that varied by as much as 17ksi to 20ksi. Second, no consistency of strength was observed between the shaft and external collar. In 33-3-12-TXEC-SG-A, the shaft strength was much greater than that of the external collar, whereas, in 33-3-12-TXEC-SG-B, the external collar was the stronger element. Lastly, the steel is compliant with the necessary ASTM A572 specification when tested at room temperature after being galvanized. Because of this, researchers assert that these mechanical properties are acceptable and not significantly impacted by the galvanizing process when tested at room temperature.

Table 5-1: Mechanical properties of galvanized steel

Material	σ_{uyield}	σ_{lyield}	ε_{yield}	σ_{ult}	ε_{ult}
SG-A-BE1	58.81	55.30	0.002	70.78	0.195
SG-A-HE1	57.07	55.35	0.002	70.85	0.172
SG-A-HE2	60.70	55.30	0.002	71.14	0.184
SG-A-VE1	59.48	54.70	0.002	70.87	0.197
*SG-A-VE2	58.11	55.15	0.002	71.11	0.186
SG-A-BS1	77.35	72.99	0.003	92.22	0.132
**SG-A-VS1	-	-	-	-	-
SG-A-VS2	76.48	73.22	0.003	-	-
SG-A-HS1	76.57	72.21	0.002	89.62	0.128
SG-A-HS2	77.61	73.41	0.003	90.65	0.135
SG-B-B1	85.79	80.13	0.003	89.99	0.123
SG-B-HE1	82.14	77.80	0.003	89.02	0.128
SG-B-HE2	83.24	78.44	0.003	89.21	0.129
SG-B-VE1	86.70	79.08	0.003	89.02	0.117
SG-B-VE2	87.05	79.52	0.003	89.59	0.115
SG-B-B2	74.75	69.62	0.003	81.46	0.134
SG-B-HS1	79.08	73.72	0.003	-	-
SG-B-HS2	76.65	73.66	0.003	83.43	0.135
SG-B-VS1	75.13	70.49	0.003	81.68	0.136
SG-B-VS2	76.25	70.38	0.003	81.56	0.135

*Initially loaded at 0.01 in/min and increased to 0.05 in/min during yield
plateau, then decreased back to 0.01 in/min

** Initially loaded at rate of 0.1 in/min

5.3   June 2010 Test

The second set of field tests sought to determine the effect of varying the root face opening in the full penetration weld between the external collar and pole shaft on the likelihood of initial crack formation in HMIP sections with external collars. A section with no external collar was also galvanized as a means to provide a control and to determine the relative benefit of adding an external collar to a HMIP section. To reduce the costs of the specimens, the sections that were used were smaller compared to the first round of tests and are referred to as "stub high mast illumination pole sections". The sections had full size base plates, but the shaft length was reduced, as shown in Figure 5-12. Three different HMIP specimens were fabricated and instrumented for thermal data acquisition, although only two specimens were monitored due to an error in data acquisition initiation at the start of one test. The failure to capture thermal data had

no bearing on the formation of galvanizing cracks, and therefore all three specimens were later evaluated for initial cracks.

Figure 5-12: All stub HMIP sections from June round of testing suspended from rigging after being removed from fluxing bath

5.3.1   Design Details

The stub sections were fabricated with a reduced shaft length from 14' 2-1/4" to 5'-0" to save money on fabrication costs and enable the evaluation of a greater number of galvanizing tests. The following section illustrates the design details that were used in the fabrication of the different specimen.

5.3.1.1   Pole Geometry

Each of the three pole sections that were tested in June 2010 were designed to emphasize a specific element of external collar construction. As a result, two high mast stub sections were fabricated with external collars as depicted in Figure 5-13, while the other specimen was fabricated without an external collar as depicted in Figure 5-15. As before stated, the stub specimen with no external collar was selected to provide a basis of comparison against the performance of the external collar specimens. Both of these designs reflect the typical TxDOT construction standards for 80 mph 150 ft. high mast pole design. Unlike previous 14' 2-1/4" specimens that were fabricated with twelve anchor rod holes to allow for compatibility with the fatigue testing set up from previous phases of the research project, these stub sections maintained the ten anchor rod hole pattern, as shown in Figure 5-14 and Figure 5-16.
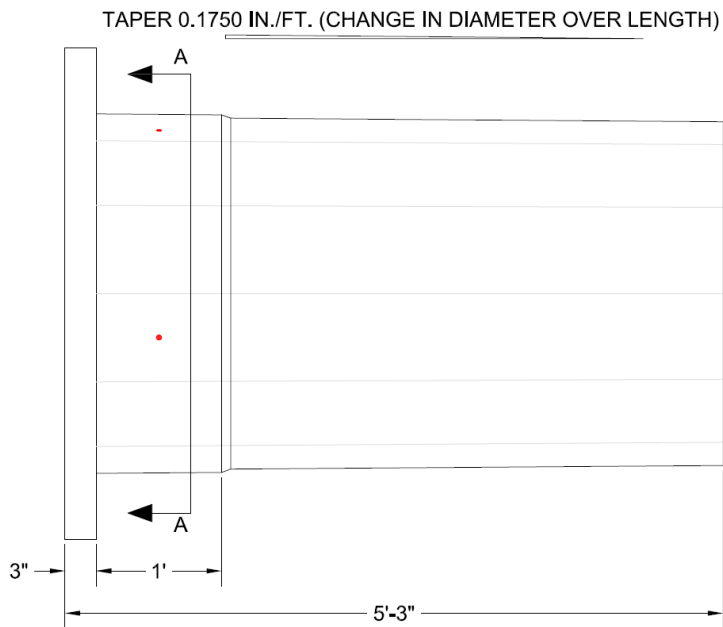
Figure 5-13: Profile of 33-3-12-TXEC-SG-SA and 33-3-12-TXEC-SG-SC

FRONT OF BASE ℄
47"
41"
10-2¾"Ø BOLT HOLES EQUALLY SPACED

5/16" Shaft +
3/8" Ground Sleeve

22"
32⅝"
Outside Ø of Shaft

¼" GALVANIZING VENT HOLES DRILLED EVERY 3 BENDS (4 TOTAL) AFTER ALL CLEANING AND FLUXING BATHS AND PRIOR TO GALVANIZING

1'

DETAIL 1

DETAIL 2
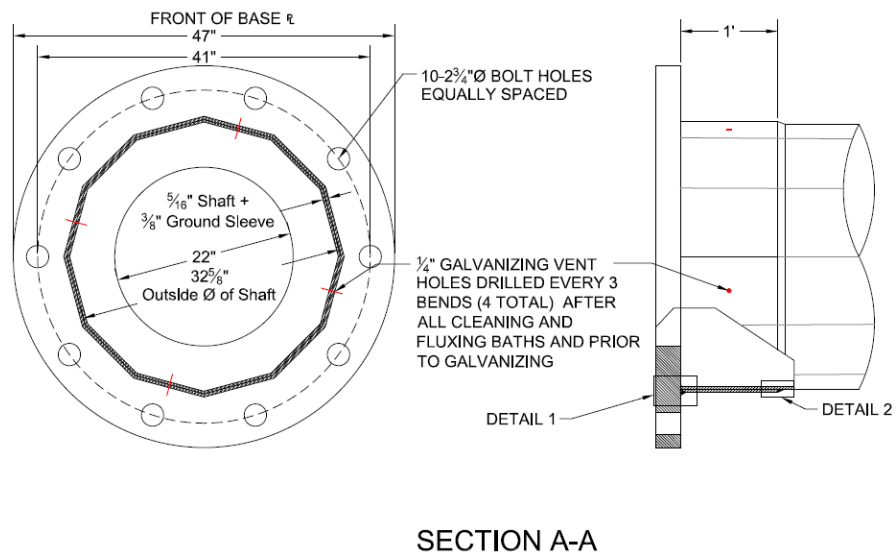
SECTION A-A

Figure 5-14: Section cut A-A from 33-3-12-TXEC-SG-SA/SC with dimensions as specified in Figure 5-13

TAPER 0.1750 IN./FT. (CHANGE IN DIAMETER OVER LENGTH)

A

A

3"

5'-3"
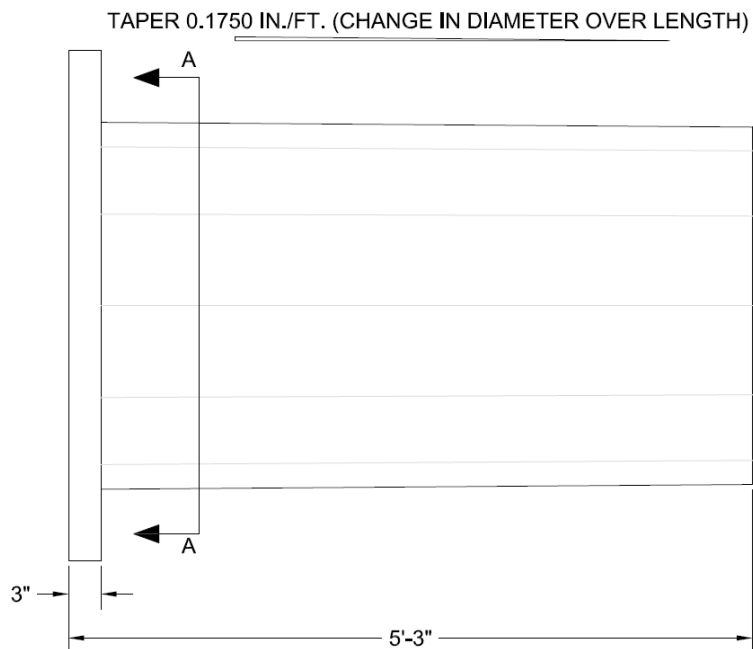
Figure 5-15: Profile of 33-3-12-TX-SG-SB

FRONT OF BASE ℄

47"

41"

5/16"

22"

32⅝"

10-2¾"Ø BOLT HOLES
EQUALLY SPACED

DETAIL 1
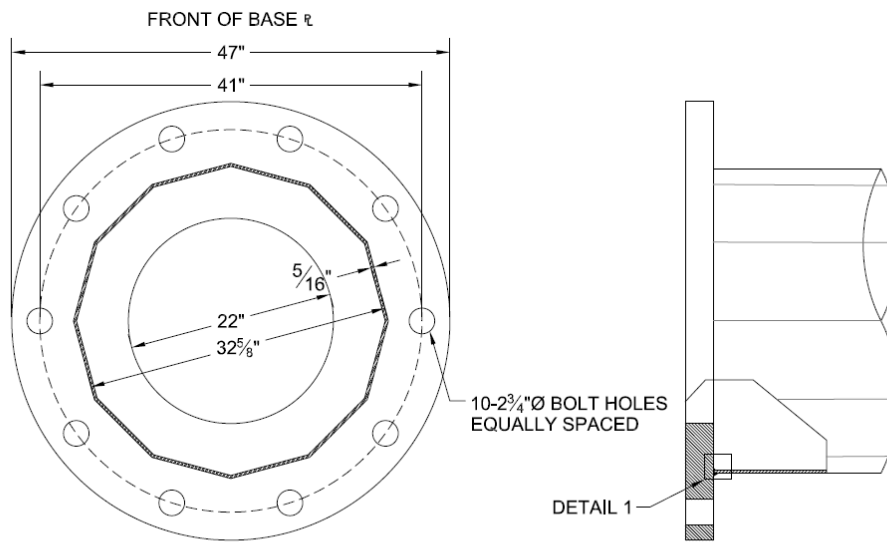
SECTION A-A

Figure 5-16: Section cut A-A from 33-3-12-TX-SG-SB, as specified in Figure 5-15

Drawing on the successful capture of thermal data from the previous galvanizing trip, additional thermocouples were placed on the June 2010 test specimens to better monitor the developing temperature gradients during hot dipping. Rather than placing thermocouples near the extremities of the base plate edge, thermocouples were relocated closer to the middle of the baseplate to afford a greater understanding of how temperatures vary directly across the weld. As shown in Figure 5-17, these tests placed thermocouples directly below the weld in the middle of the baseplate and also four inches out from that location. A shaft thermocouple was aligned with the radial position of the base plate thermocouples. Thermal data was only taken at three radial positions, set apart by 90 degrees.
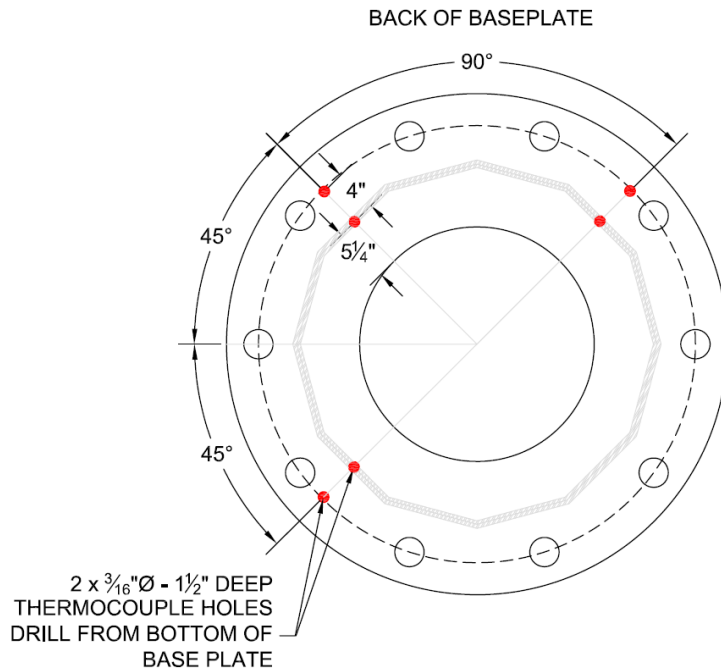
Figure 5-17: Thermocouple hole locations in the baseplate of all June 2010 specimens

5.3.1.2   Weld Geometry

The greatest concern for this round of testing was to determine whether the weld procedure used to secure the pole shaft and external collar to the baseplate would lead to additional cracking during the galvanizing process. Specifically, researchers hypothesized that by increasing or decreasing the root face opening between the external collar, or ground sleeve, and the baseplate, the concentration of stresses could change and potentially affect the likelihood of crack formation during hot dipping. It was chosen that specimen 33-3-12-TXEC-SG-SA would be detailed to have no root opening, as shown in Figure 5-18, and that specimen 33-3-12-TXEC-SG-SC would have a root opening of 5/16", as shown in Figure 5-19.

66
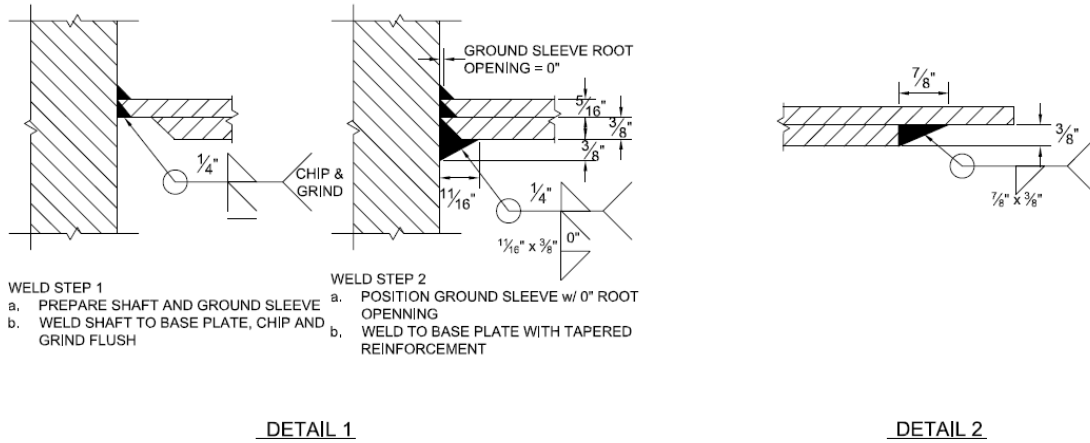
Figure 5-18: Weld details for 33-3-12-TXEC-SG-SA, as called out in Figure 5-14
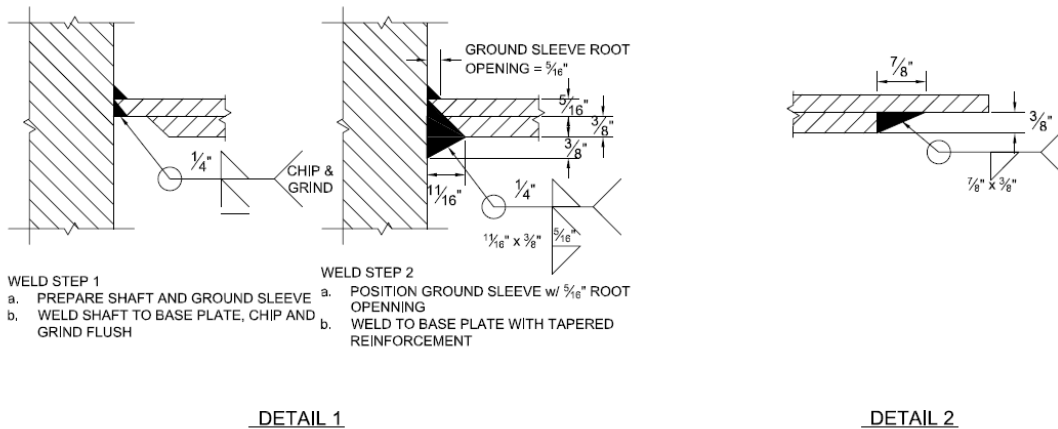
Figure 5-19: Weld details for 33-3-12-TXEC-SG-SA, as called out in Figure 5-14

Because 33-3-12-TX-SG-SB has no external collar, the weld detail is no different than those used in standard full penetration welds with no backing bar. Figure 5-20 shows the weld detail on this specimen.

67
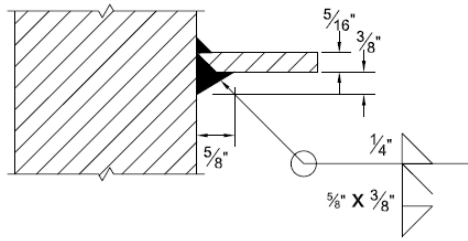
DETAIL 1

Figure 5-20: Weld detail for 33-3-12-TX-SG-SB, as called out in Figure 5-16

5.3.1.3   Instrumentation Locations

As stated before, the location of instrumentation in these sections varied from the previous round of testing in which thermocouples were placed at four radial positions with only two thermocouples at each radial position. Noting the similarity in test data taken at the radial positions near the horizontal, base plate thermocouples at one horizontal location were eliminated so that an additional thermocouple could be placed in the base plate at all other radial positions to further monitor radial thermal gradients without significantly prolonging the amount of time needed for instrumentation. The thermocouple locations selected for this round of testing are also used for the testing conducted in February of 2011. These instrumentation locations are depicted in Figure 5-21.

Connection details for Figure 5-21 are depicted in Figure 5-22. Since one of the stub poles had no external collar, researchers were afraid of attaching thermocouples at shaft locations using the adhesive since the 5/16" thick pole shaft would need a hole 5/32" deep in which to set. Originally, it was thought that not enough bond strength could be achieved through adhesive within these shallow holes (though the next round of testing would prove otherwise). To maintain consistency between tests, screws were implemented to hold the thermocouple to the pole shaft wall for all three stubs sections.
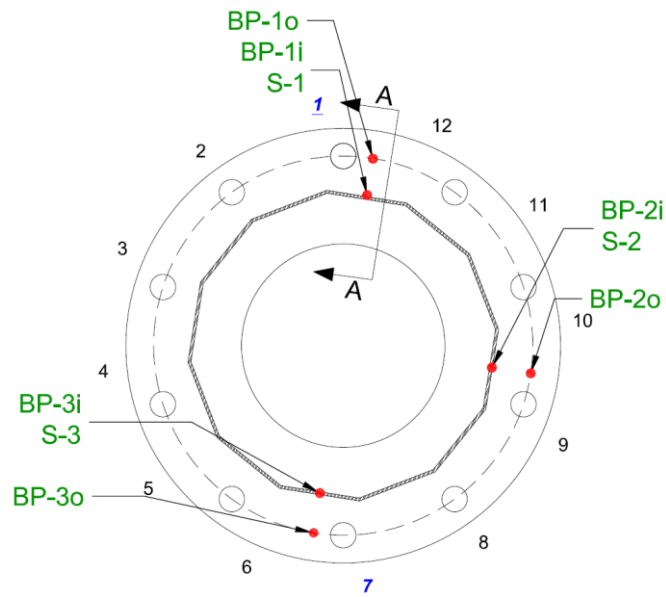
Figure 5-21: Typical thermocouple locations for galvanizing testing from June 2010 and February 2011
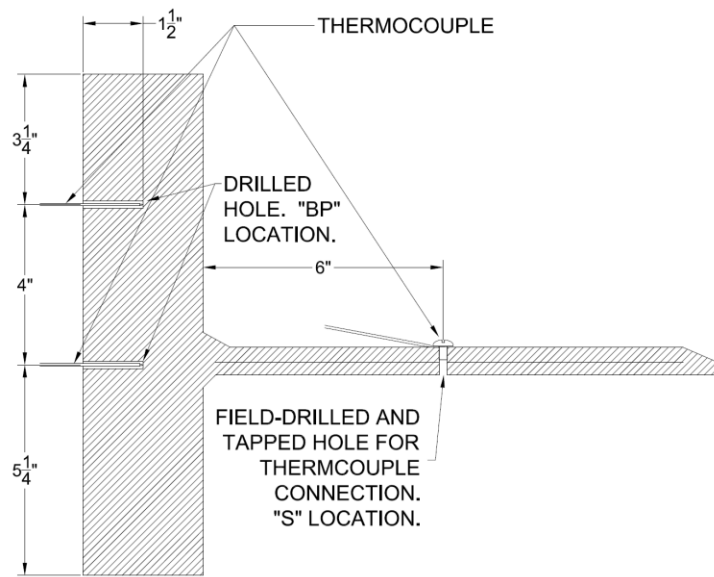
Figure 5-22: June 2010 typical thermocouple connection detail for 33-3-12-TXEC-SG-SA/SC specimens as in section A-A of Figure 5 19

69

5.3.2 Thermal Performance

High mast illumination pole stub sections were hot dipped in a similar manner as those in section 5.2.2. These poles were dipped with their baseplates entering the bath first, and the data sampling rate was 1Hz. Thermal data were only obtained for 33-3-12-TXEC-SG-SA and 33-3-12-TX-SG-SB due to an error that occurred while taking thermal data for 33-3-12-TXEC-SG-SC during hot dipping.

The June round of testing provided better insight into the thermal distribution due to the greater number of thermocouples placed in the baseplate. However, while a greater amount of useable data was gathered from base plate locations during this round of testing, the connection detail at the shaft locations only proved useful for determining when the sensor was exposed to zinc. As soon as the shaft sensor locations came into contact with the zinc, the sensors provided a reading of the temperature on the surface of the shaft and was not representative of the temperature in the middle of the shaft wall as desired. Because the thermocouples at the shaft locations were not sealed into place, the temperature of the liquid zinc skewed the recorded data. Typical results for these tests are shown in Figure 5-23. All temperature graphs taken during the June 2010 tests may be referenced in Appendix B. In Appendix B, each set of data is divided into graphs of data taken at specific locations to give perspective into the development of gradients within the base plate during galvanizing. Because poor results were gather from thermocouple shaft locations, information on gradient temperatures between shaft locations and base plate locations are not presented for this series of tests.

The data gathered through this round of research seems to correlate fairly well with that which was gathered during the January 2010 testing. This indicates that consistent data can be gathered by using the thermocouple instrumentation procedures identified in Chapter 4, and the results can be reliable, despite some newly discovered errors.
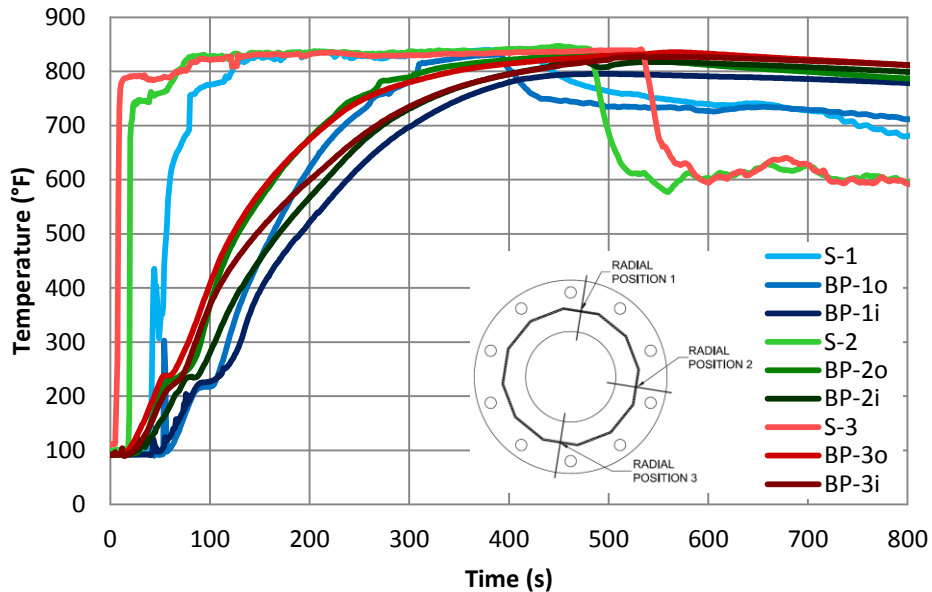
Figure 5-23: Typical thermal results from June 2010 galvanizing trip

5.3.3 Initial Cracks

After galvanizing, TxDOT inspected each bend on each high mast stub section before and after galvanizing to determine whether cracking had occurred in the galvanizing bath. The measured cracks from this round of testing are depicted in Figure 5-24.

The results from this round of testing were difficult to interpret since it appears that the worst performing specimen was SG-SA, which had a 0" root opening in the full penetration weld of the shaft to base plate weld. This is not, however, the preferred connection detail. When root openings are not specified on design drawings, the fabricator is able to choose how he would like to weld the base plate to the pole shaft. In the past, cracked poles have been delivered to the University of Texas in which the section would have the typical 5/16" root opening and still display greater cracking than indicated by these results, as evidenced by specimens 33-3-12-TXEC-SG-A and 33-3-12-TXEC-SG-B. Furthermore, from what has been observed throughout this research project, it is atypical for a section without an external collar, such as 33-3-12-TX-SG-SB, to exhibit worse performance than a comparable HMIP section with an external collar, such as 33-3-12-TXEC-SG-SA.
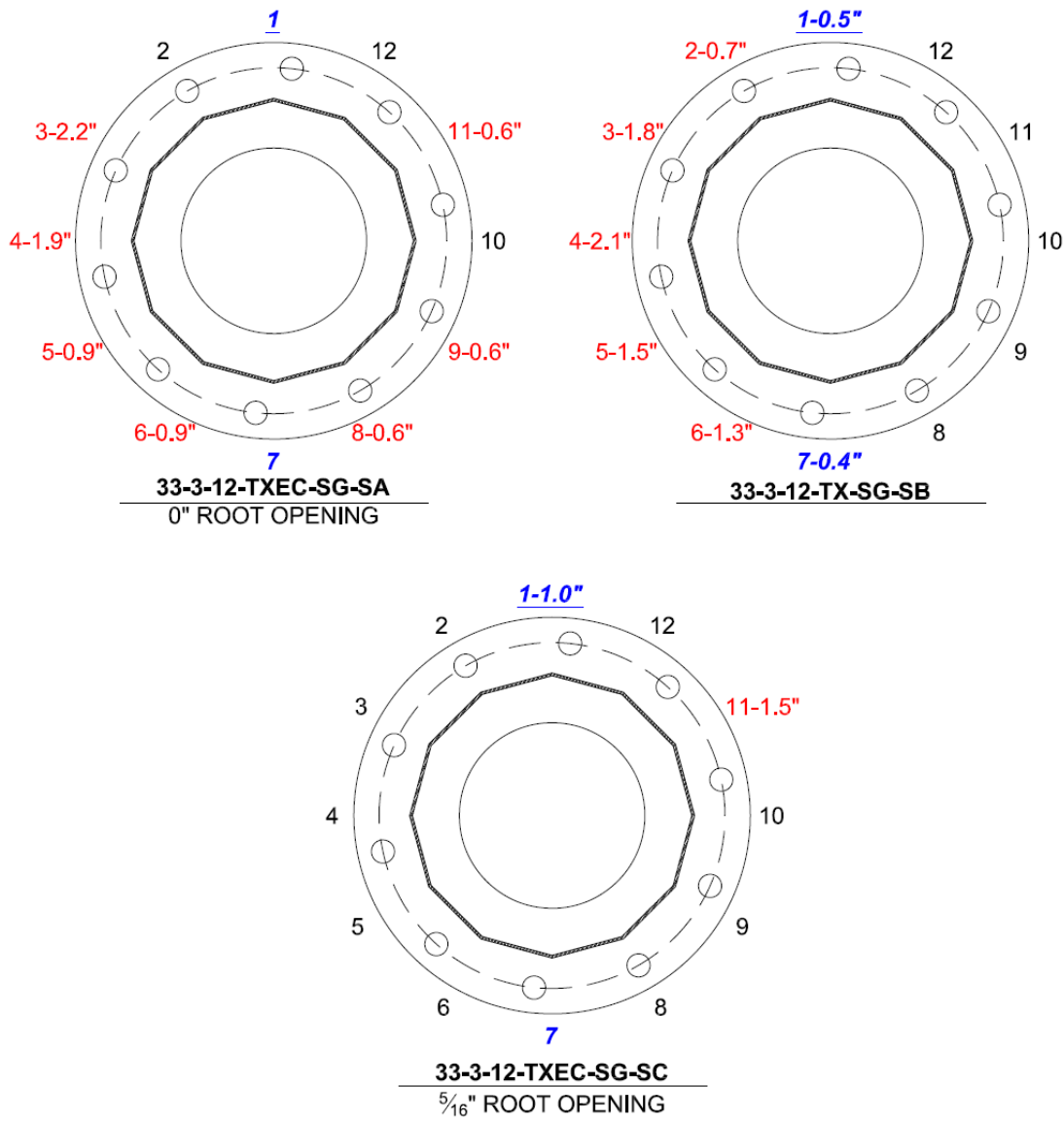
Figure 5-24: Initial crack locations after June 2010 galvanizing.   Cracked bend and lengths marked in red.

Also worthy of noting, the stub sections were galvanized in a manner that would not generally occur in practice. All three specimens were removed from the pickling process at the same time. Due to the time necessary to instrument the poles, significant flash rust appeared on the last two specimens. The research team originally assumed that such variables as flash rusting would not be an issue with regard to cracking; however the extent of cracking during galvanizing tracks

with the order in which these sections were hot dipped. The amount of flash rust was progressively worse in the order of dipping.

All of the poles were instrumented at the same time, and then dipped as soon as possible, but the amount of time that lapsed between the first and last pole being dipped was long outside of the range that is accepted to avoid flash rusting (which seems to occur faster when the ambient temperature is warmer, such as is the case in June). The pole section that cracked least was the first section hot dipped, and the section that cracked the most was the last section dipped. The extent to which this rusting affected the heat transfer between the pole and galvanizing bath, or the interface and interaction between the liquid zinc and base metal is unknown, but the results indicate that a correlation may exist linking the extent of flash rusting to the formation of initial cracks. More research is necessary to better understand if such a relationship exists.

Lastly, the results from the ultrasonic testing indicate that the severity of cracking may be related to the position around the pole. In each of these three tests, the longest initial cracks seem to cluster around the same location— at or just off the horizontal (nine o'clock) position. The longest cracks also seem to cluster on the same side of the high mast pole.

5.4   February 2011 Test

The final field galvanizing test took place in February of 2011. The galvanizing was conducted on three HMIP sections at one plant. Two of the HMIPs were stub sections and the third was a 14' 2-1/4" specimen that will be used in a fatigue-test with a cracked high mast that has been removed from service in the field. The purpose of this round of galvanizing testing was to determine the effectiveness of mitigating initial cracks by increasing the HMIP shaft thicknesses. Initial field observations indicated that if a specific ratio comparing pole shaft diameter to shaft thickness were met, the likelihood of crack detection in the field decreased substantially. Because HMIPs are erected in sections, it would be possible for designers to specify a thicker shaft on the bottom section of the high mast if increasing the shaft thickness proved to be a viable solution. The subsequent section addresses the effect of increasing shaft thickness of initial crack formation.

Figure 5-25: Fully instrumented HMIP 33-3-12-TX-SG-C prior to galvanizing

5.4.1   Design Details

All HMIPs tested in this round of galvanizing were held consistent in terms of base geometry and instrumentation. Despite the difference in shaft length, the weld details, baseplate geometry, and all thermocouple positions were kept the same.

5.4.1.1   Pole Geometry

As mentioned earlier, three different pole sections were fabricated to execute this round of hot dipping. The longest pole section, which was fabricated to be tested in the fatigue set up utilized by Pool (2010), Stam (2009), and Rios (2007), had a pole shaft thickness of 5/16" to match that of the pole being removed from service and tested in fatigue as depicted in Figure 5-26. Note that this pole's baseplate also has twelve holes for anchor rods, and these rods are of a smaller diameter—sized for the fatigue test set up.
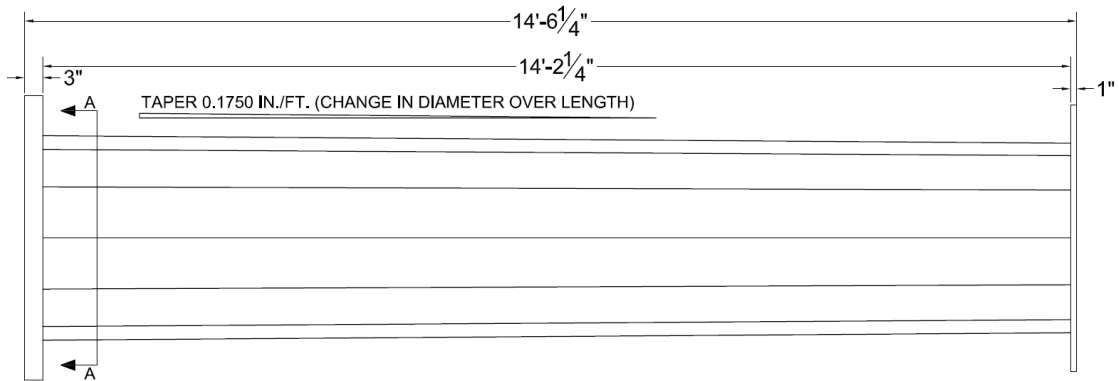
Figure 5-26: Profile of 33-3-12-TX-SG-C

Figure 5-27 depicts a section cut through the bottom portion of the high mast shaft, and Figure 5-28 depicts the weld detail between the pole shaft and the baseplate. These details are identical to 33-3-12-TX-SG-SB. This design has a shaft diameter to shaft thickness ratio of 104.4 which was expected to crack during galvanizing based on previous observations.
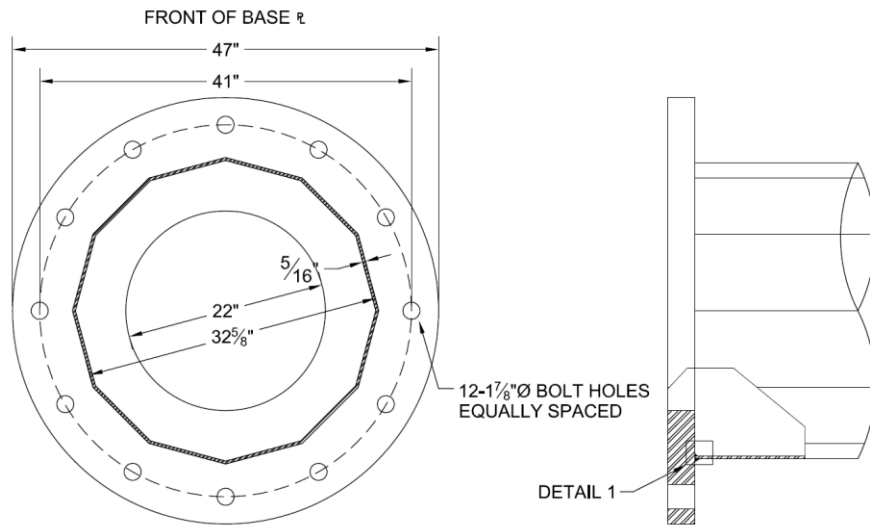
Figure 5-27: Section cut A-A of 33-3-12-TX-SG-C with dimensions as specified in Figure 5-26
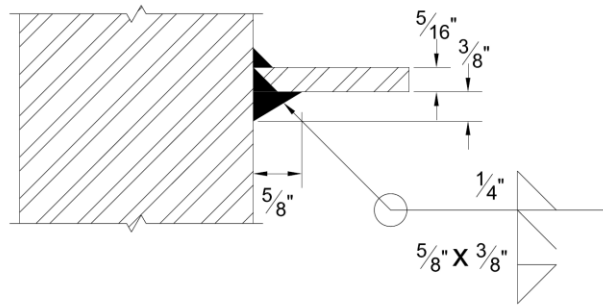
DETAIL 1

Figure 5-28: Weld detail for baseplate and shaft of 33-3-12-TX-SG-C, as called out in Figure 5-27

The primary differences between the other two specimens (33-3-12-TX-SG-SA and 33-3-12-TX-SG-SC) and 33-3-12-TX-SG-C were that these two poles were fabricated with the typical five foot shaft lengths, with only 10 anchor rod holes, and with larger shaft thicknesses. Respective shaft thickness values of 7/16" and 1/2" were chosen for specimen 33-3-12-TX-SG-SA and 33-3-12-TX-SG-SC to correlate to a shaft diameter to shaft thickness ratio of 74.57 and 65.25. Full design drawings for these specimens are provided in Appendix A. The diameter to shaft ratio for specimen 33-3-12-TX-SG-SA matches the level at which pole designs tend to show crack indications when tested by ultrasonic techniques. The ratio that was selected for the 33-3-12-TX-SG-SC specimen is below the cracking threshold that has been observed in previously galvanized poles. By selecting designs with these diameter to thickness ratios, researchers could make reasonable assessments regarding the viability of increasing the shaft thickness to potentially mitigate cracking damage.

5.4.1.2   Instrumentation Locations

Thermocouples were placed on the three high mast sections in a similar manner as those used in the tests conducted in June of 2010. Drilled thermocouple locations are depicted in Figure 5-29. In this phase of testing, half-depth holes were predrilled in all shaft thermocouple locations in order to provide a location where thermocouples could be embedded into the pole shaft to get more reliable data on shaft temperatures as a function of time during testing. It should be noted that the shaft thermocouple locations were moved up the pole shaft 6" relative to the June 2010 tests, 12" total off the baseplate. An additional through-shaft hole located nine inches off the

76

baseplate was also provided to help anchor the thermocouple wires during the volatile galvanizing process.
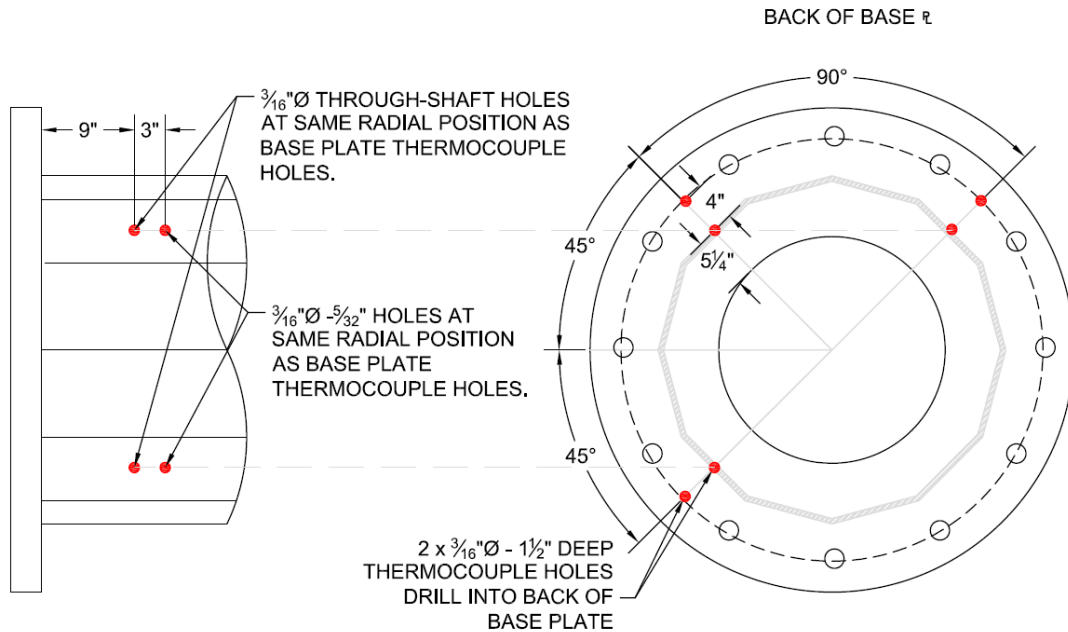
Figure 5-29: Drilled thermocouple locations for all tests from February 2011

The naming convention and locations depicted in Figure 5-21 also remain consistent with those used in this round of testing. While the names and locations did not change, poor results at shaft locations from the June 2010 round of testing prompted researchers to change the way thermocouple wires were connected. Rather than attempting to screw-clamp thermocouples to the pole shaft for recording exterior shaft temperatures, researchers embedded thermocouples into the pole shaft as shown in Figure 5-30. Embedding the thermocouples in the pole shaft provided more useful data, which could be later utilized to compare against ABAQUS output.
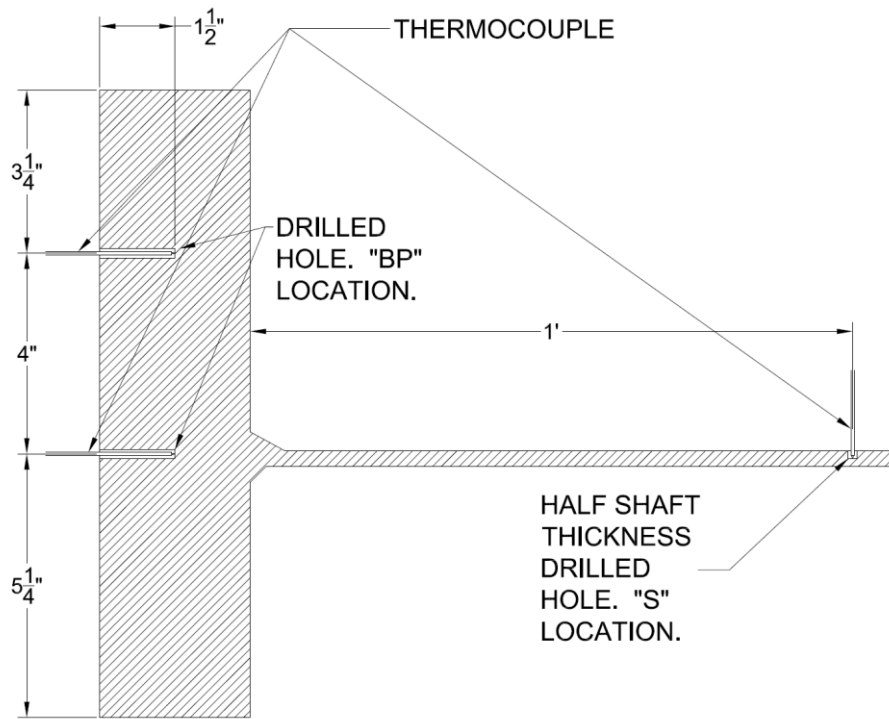
Figure 5-30: Thermocouple connections at section A-A from Figure 5 19 for all February 2011 thermal testing

In addition to the thermocouples, the high mast sections in the February 2011 tests were also instrumented with four foil strain gages to measure thermal strains prior to complete pole emersion. Strain gages were placed 3" off the base plate, and mid-way between bends in the pole shaft, and oriented to measure longitudinal strains in the pole shaft. A photograph of the a specimen instrumented with strain gages is shown in   These strain gages were designated "Top", "Mid-Top", "Mid-Bot", and "Bot" and align as shown in Figure 5-32.
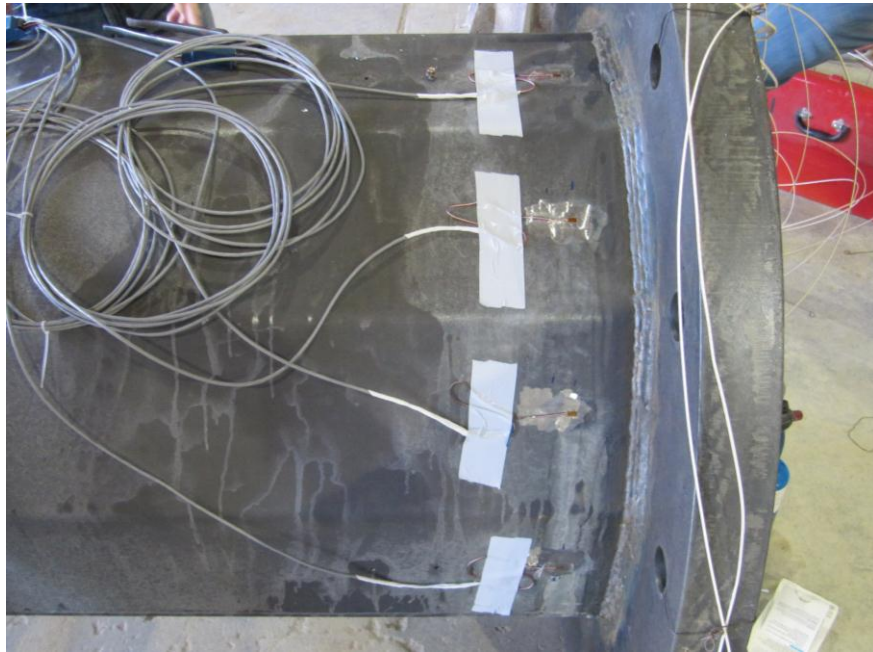
Figure 5-31: HMIP section with fully instrumented for strain data acquisition
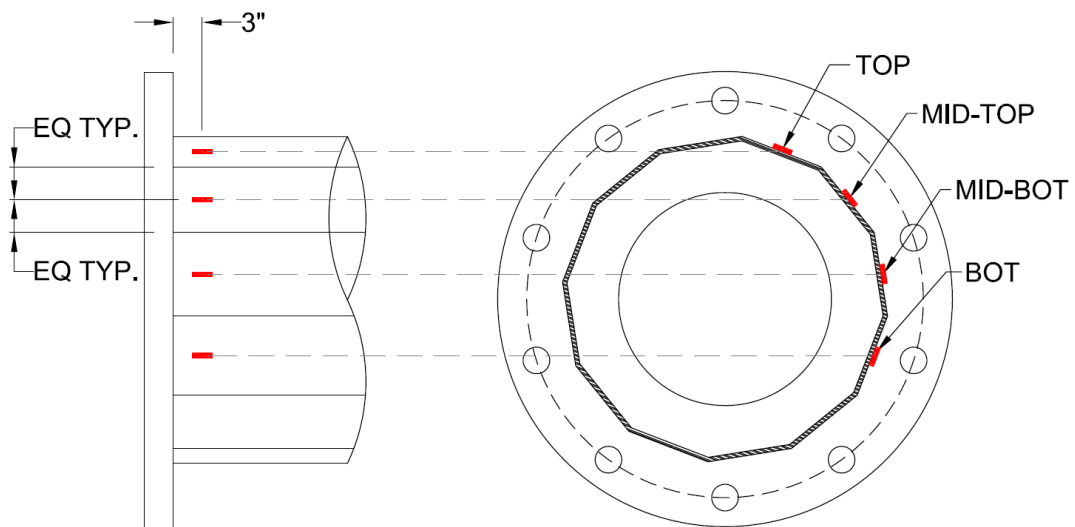
Figure 5-32: Typical strain gage locations on high mast sections

5.4.2 Thermal Performance

Based upon the experience gained in the first two sets of tests, the data gained in the final test provided the most complete set of data with the fewest errors. Typical results from this round of testing are depicted in Figure 5-33, which shows the thermal results from hot dipping 33-3-12-TX-SG-C. While the last two stub sections, 33-3-12-TX-SG-SA and 33-3-12-TX-SG-SC, were dipped at a different angle and a bit more quickly, the thermal output acquired through the DAQ remained relatively consistent. The rest of the thermal data gathered through this galvanizing test is presented in Appendix B.
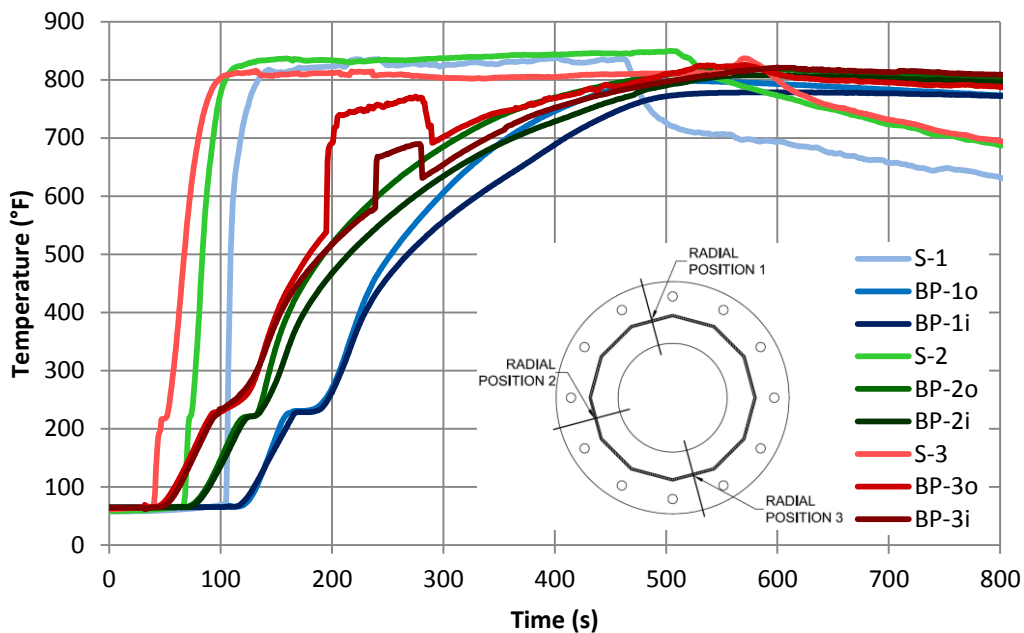
Figure 5-33: Typical thermal results from February 2011 testing

The data gathered during the final tests correlated well with the data taken during earlier rounds of testing at base plate locations. The curves are similar in shape and resultant temperature gradients from the earlier tests, despite differing dipping rates and variable dipping angels. Some thermocouple locations clearly heat up faster due to the faster dipping speed, and variable dipping angle. The effect of varying these parameters is addressed in Chapter 7. Base plate thermocouples located closer to the perimeter heat faster than those located directly below the full penetration weld, and the general order in which baseplate locations heat remained consistent.

Also, the general shape of each heating curve remained consistent from initial heating to reaching thermal equilibrium.

Compared to the data gained from the June 2010 tests in which the shaft thermocouples were fastened to the shaft using screws, the data gathered in the final round of testing seemed to be more representative of the actual shaft behavior. Rather than rapidly spiking, as was seen in the June 2010 round of testing, these curves display a changing slope and therefore show gradual heating, as would be expected at the mid-thickness of the shaft wall. This also seems to indicate that realistic data can be taken at the shaft locations of high masts by using the embedding procedure to fix thermocouple wires to steel.

5.4.3   Strain Data

Strains measured along the pole shaft were used to determine the structural response of the HMIP sections to heating. As anticipated, not much information was collected after the gages entered the galvanizing bath. However, the gages did provide a good indication of how the strains developed in portions of the pole outside of the bath as the section was gradually dipped into the bath. In all cases, the DAQ was able to record between 30 to 60 seconds of useful strain data. For clarity, the resultant curves are truncated at their respective times when they began to show erratic responses. The presentation of this strain data is shown in Figure 5-34, Figure 5-35, and Figure 5-36.
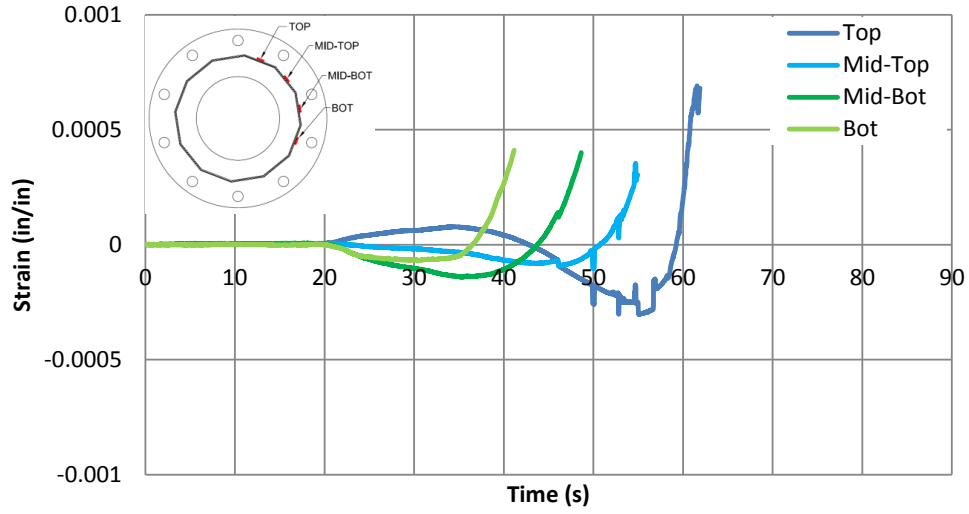
Figure 5-34: Strain data for 33-3-12-TX-SG-SA
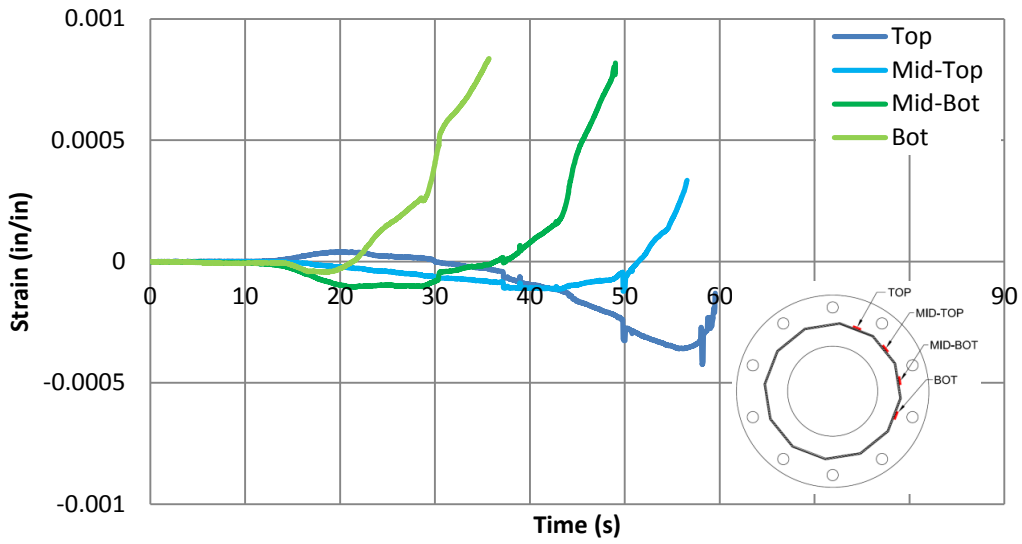
Figure 5-35: Strain data for 33-3-12-TX-SG-SC
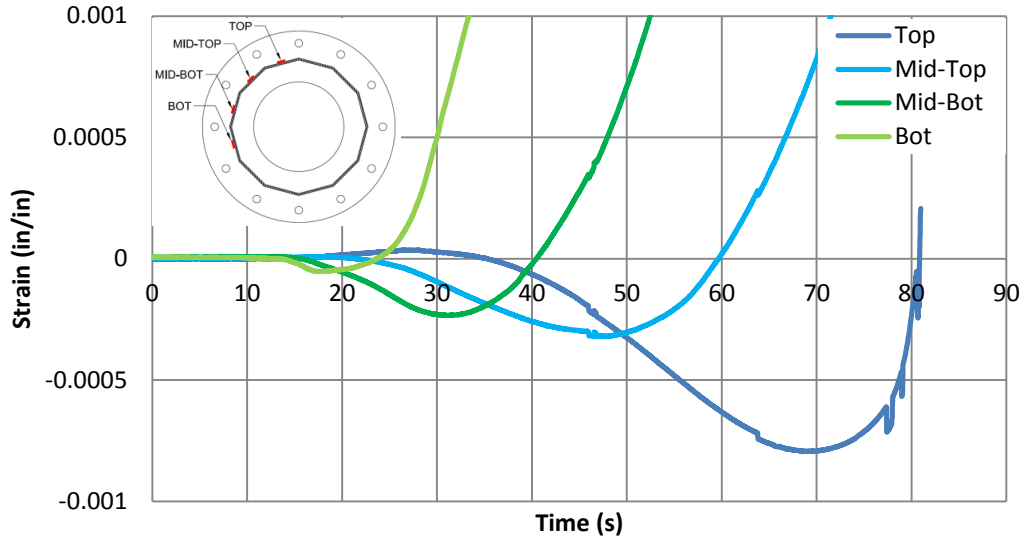
Figure 5-36: Strain data for 33-3-12-TX-SG-C

While the completeness of the strain data shown above is particularly lacking, a few key observations may be made regarding their trends. First, the data shown above was zeroed at time = 0 seconds to remove the influence from the self-weight of the sections. In zeroing the data, one finds that initially, many of the locations from which data is being taken initially go into compression. The portions of the high mast closer to the twelve o'clock position indicate the greatest initial compressive result on each high mast. The strains recorded on specimen 33-3-12-TX-SG-C also display, in some cases, a maximum compressive strain more than twice that of the other two stub sections. Section 33-3-12-TX-SG-C also had the thinnest shaft wall. While it is impractical to extrapolate this data to tensile strains as well and assume that higher tensile strains develop in the 5/16" pole shaft, the trend of greater strain magnitudes are worthy of note.

Along with the observations solely related to strain, these results also indicate the effect of the crane operator on the development of strains during galvanizing. Both of the stub sections were hot dipped by the night crew crane operator, as opposed to the day crew crane operator who hot dipped the longer fatigue specimen. The night crew operator dipped the stub sections at both a different angle and much faster, as is indicated by the lesser amount of time necessary for the strain gages to fail. The impact of the operator's performance cannot be easily understood by examining these results, but it is worthwhile to recognize that a link exists between operator

performance and strain response in the item being hot dipped. Finite element analyses are presented in Chapter 7 that demonstrate the impact of the rate and angle of dipping on the strains that develop.

5.4.4   Initial Cracks

The initial cracks information gathered from ultrasonic testing are displayed in Figure 5-37 according to the previously defined convention.   The most significant observation to be made from these results is the fact that no indication of cracking was found on the stub sections with thicker pole shafts. The pole section with 5/16" shaft thickness, on the other hand, had crack indications at nearly every bend. This is consistent with past results, such as those found in the identical high mast galvanized for the last portion of fatigue testing, 33-3-12-TX-SG-A (Pool, 2010). The results also correlate with the ultrasonic test data gathered by TxDOT showing that field HMIPs with pole shaft diameter to shaft thickness ratios lower than 75 tend not develop cracks.

A lesser observation to be made regarding the cracking pattern of 33-3-12-TX-SG-C is that this pole did not experience the same clustering of cracks as were found in the June 2010 round of testing. The cracks observed in the June 2010 tests seemed to indicate a greater likelihood of larger cracks to form within a quadrant above the horizontal axis of the base plate, whereas 33-3-12-TX-SG-C shows no such correlation. Because all the poles that were tested in the June 2010 tests had their weld seams oriented in the twelve and six o'clock positions, it is possible that some residual stresses exist that tended to cause the development of stresses related to fracture to cluster in a particular orientation. Perhaps in changing the location of the weld seam relative to the twelve o'clock bend changes the accumulation of stresses and leads to different cracking patterns. Additional testing should be conducted to verify this speculation.
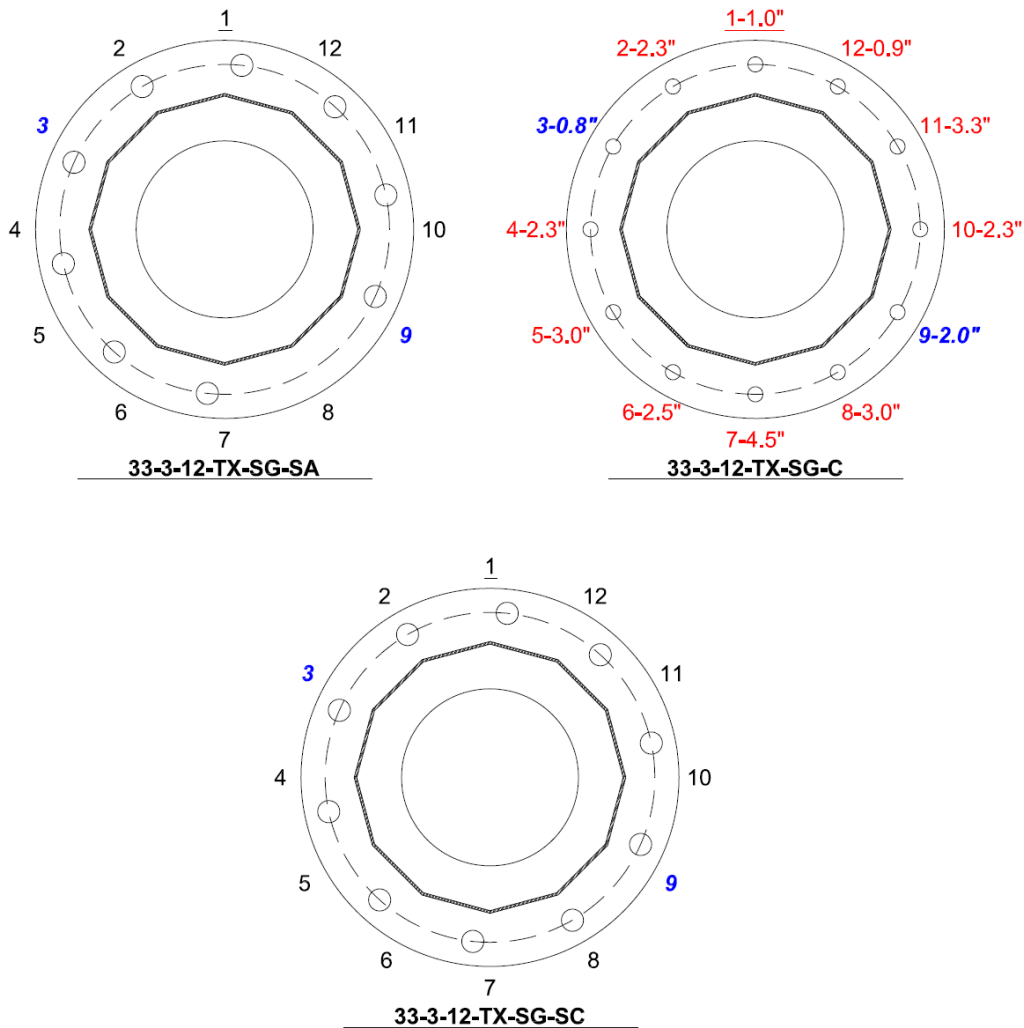
Figure 5-37: Initial crack locations after February 2011 galvanizing. Cracked bends and lengths are marked in red.

5.5   Thermal Data Errors

Figure 5-38 shows the data collected from the first galvanizing procedure. This data is indicative of poor test results, but is useful for better understanding weaknesses in the data collection methods and how researchers were able to correct for these faulty results. In particular, these results show errors on nearly every channel and are consistent with those observed during separate galvanizing instrumentation trips. The following sub-section provides a discussion of the major errors observed during data capture, what researchers believe to be the cause of these errors, and what impact these errors have on reading the temperature output.

85
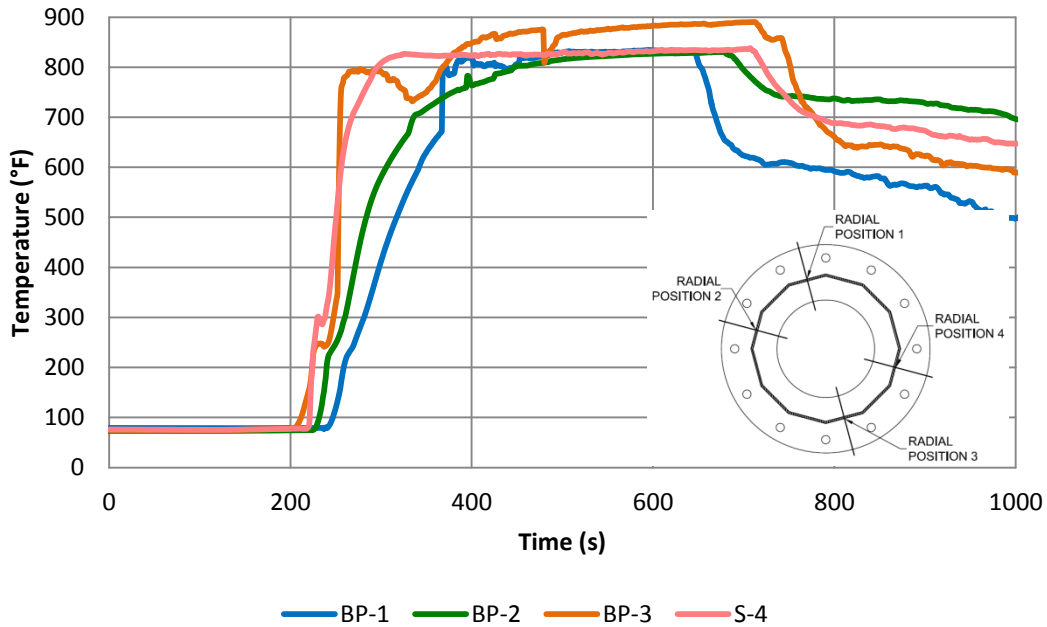
Figure 5-38: Temperatures as a function of time during galvanizing of 33-3-12-TXEC-

5.5.1   Adhesive Error

The first noticeable error is the change in curvature of the heating plots between 200°F and
300°F. This error was found to be an artifact of the bonding agent used to adhere the
thermocouple to the high mast illumination pole. In order to verify this assertion, small scale
galvanizing tests were run in the lab on two prismatic steel specimens measuring 2" by 2" by 4",
with two 3/16" diameter thermocouple holes drilled in the top located 1" from each specimen face
on either side of the specimen. The two specimens tested are shown in Figure 5-39 after being
galvanized. These specimens were both lowered into a small zinc bath horizontally such that
both thermocouple locations recorded roughly the same temperature data at the same time.

86
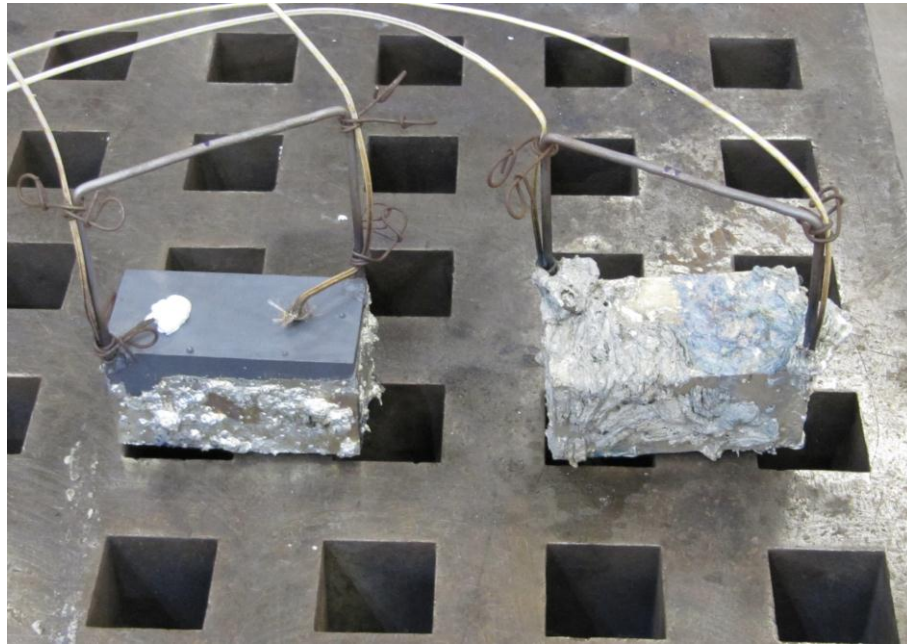
Figure 5-39: Thermocouple heating discontinuity test specimens after testing. Test 1 left, Test 2 right.

The two tests that were run on the specimens in Figure 5-39 were designed to verify that a thermocouple in the absence of adhesive will not produce the odd curvature discontinuity, and that the discontinuity can be related to the state of curing in the adhesive. In both specimens, one thermocouple location was attached with the adhesive the day before and allowed to air-cure, while the other thermocouple was either not attached with adhesive (Test 1), or was cured using a fast-curing technique. The fast curing technique consists of heating the adhesive with propane torches for five minutes (Test 2). The results from these heating curves are shown in Figure 5-40 and Figure 5-41.

The results of these two tests clearly indicate the link between the presence of adhesive and the appearance of the curvature discontinuity in the heating region of the temperature vs. time curves shown for Tests 1 and 2. In Test 1, the specimen, was hot dipped such that the specimen was completely covered with zinc on five sides, excluding the top to avoid thermocouple contact with molten zinc, and as can be seen in Figure 5-40, while the symmetry of the system remains and the heating is nearly constant, the thermal curvature discontinuity is non-existent at the location where the open thermocouple is taking data.
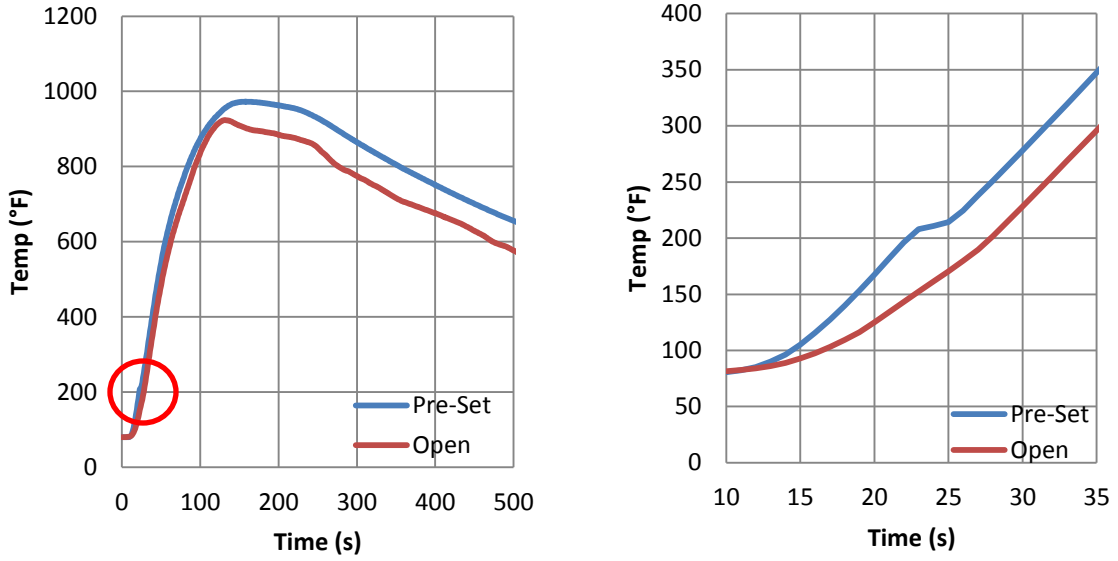
Figure 5-40: Test 1 heating results for a pre-set and open thermocouple attachment
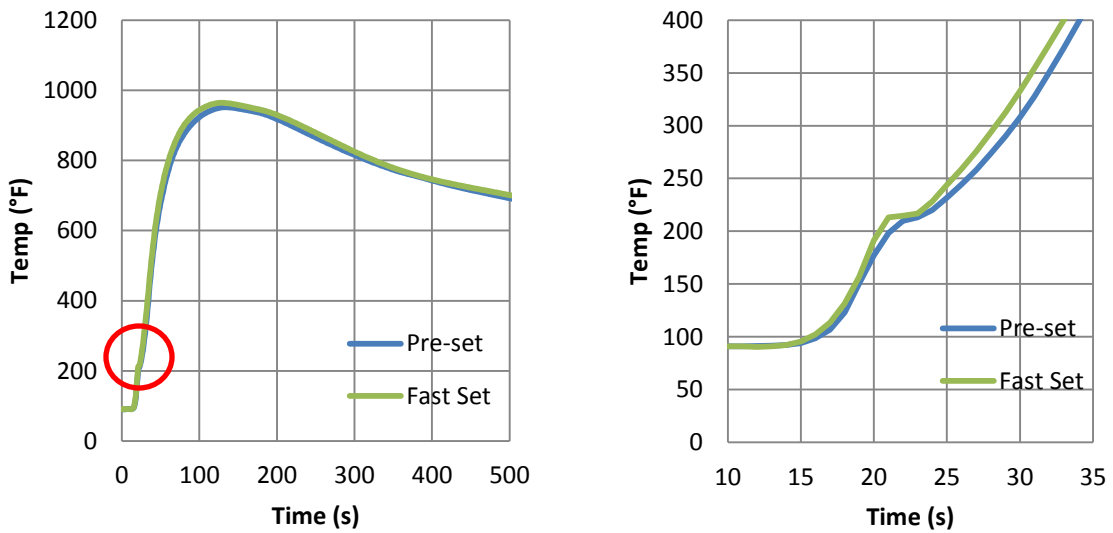
Figure 5-41: Test 2 heating results for a pre-set and fast-set thermocouple attachment

The results presented in Figure 5-41 show the difference obtained in the heating curves due to the different setting conditions when both thermocouple holes were prepared with adhesive. In this

test, the specimen was completely submerged in liquid zinc after both thermocouples had been prepared with adhesive. The designation "pre-set" indicates that the thermocouple adhesive at that location was applied the day before, and "fast-set" indicates the adhesive application procedure used in the field—applying the adhesive to the thermocouple location, and then heating for 5 minutes with a propane torch. While both curves from Test 2 seem to track fairly consistently, there seems to be a reduction in the curvature discontinuity for the pre-set case. While more extensive studies should be conducted to validate this claim, it appears as if the process of curing allows the adhesive to absorb energy to properly harden from a mostly liquid/paste consistency to its hard consistency. The pre-set case, having already had an opportunity to partially set up, would not need to absorb as much energy before completely hardening, and hence resulted in a slighter disruption to the curvature.

Regardless of the physical mechanism causing the discontinuity, these two tests clearly indicate that the cause of the discontinuity is linked to the presence of adhesive, and not an actual characteristic of the way that high masts are heated in the galvanizing bath. Because of this, observation of these discontinuities in the temperature readings presented from field measurements should not be considered as significant.

5.5.2   Thermal Spikes

Another typical abnormality encountered during testing is a temperature spike. These spikes, as documented in Figure 5-42, indicate a rapid jump in temperature at a specific location. Bearing in mind that in some cases these locations are embedded as much as 1-1/2" from the surface of a mass of steel, it seems unlikely and counterintuitive for such a temperature jump to occur. For the heat to make such a jump, a change in the heat flux would have to occur, and since the high mast is already submerged in the bath with no additional heating sources, no change in heat flux exists. This indicates that such spikes are the result of an error with data collection from the thermocouple junction.

Once the spike forms in the temperature vs. time graph at a specific location, the temperature reading usually behaves erratically for the next several seconds before returning to the expected temperature at that location. Researchers believe this fluctuation in temperature to be the result of liquid zinc penetrating into the thermocouple hole, and then solidifying. It appears that it takes a significant amount of time before the temperature equilibrates with the surrounding steel, but based on matching the trend of the heating curve prior to the thermal spike with data after the

spike, it appears that the spike has little effect on the overall temperature readings at a thermocouple location. After the spike occurs, the temperature readings look similar to other unaffected thermocouple locations.

For this reason, while thermal spikes distort local regions of the temperature vs. time curves, researchers do not believe the thermal spikes to be a significant cause for concern when evaluating the thermal performance at a specific location.
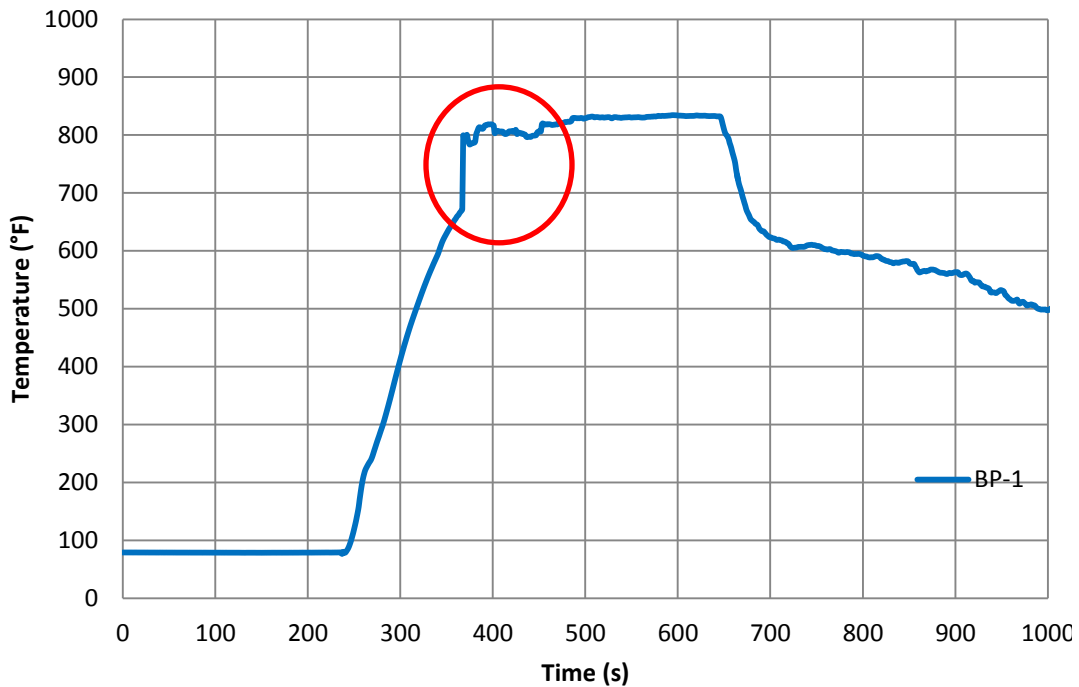
Figure 5-42: Temperature spike from temperature reading at BP-1 of 33-3-12-TXEC-SC-A

5.6   Galvanizer Observations

To test an adequate number of high masts for this study, researchers sought to get a fair representation of the different methods used during the galvanizing process. Two galvanizers were used during the study, and researchers found that substantial differences exist in dipping practices both between galvanizers, and even with different personnel at the same galvanizer. The main source of these differences stems from the lack of regulation on dipping practices. While the processes of cleaning, fluxing, and inspecting remains consistent, the manner in which

each of these processes are executed can change widely from galvanizer to galvanizer, and can substantially change the thermal implications on the article being dipped. The primary source of differences with thermal implications stem from the practices of the crane operator.

Figure 5-43: HMIP being lifted from the galvanizing bath

The crane operator is the individual responsible for lowering the HMIP into and lifting the HMIP from the molten bath. He can determine the speed as well as the angle at which the poles are submerged. He can also determine the length of time that the poles are left submerged, and the speed and angle at which the poles are removed from the bath. When desiring to better understand the thermal effects of the dipping process, each of these parameters can fundamentally change the time vs. temperature relationship of elements within pole sections.

Based upon conversations with galvanizing personnel, one may find that rules of thumb are utilized for controlling the dipping procedure. Not surprisingly, these rules of thumb do not ensure consistent practice from crane operator to operator. For example, each crane operator addressed by this study indicated that the proper way to dip high mast illumination poles with thick baseplates is to dip the pole baseplate first. Since all the observed baths were not deep enough to dip the pole vertically, the high masts were all dipped at some angle off the horizontal, which again varied from operator to operator, and then after lowering the baseplate side of the

pole into the bath, the shaft end of the pole was lowered into the bath at a faster rate. Essentially this created a variable dipping plane and dipping speed, all of which have an effect on the heat transfer within the pole, and all of which is left to the discretion of the crane operator.

Also, the duration of dipping is determined from qualitative observation. The standard length of time to leave poles submerged is "until the bath stops bubbling"—an indication of chemical reactions that facilitate the bonding of the zinc alloy to the steel. This length of submergence is determined solely with the quality of the galvanizing finish in mind, and does not recognize the potential thermal or mechanical implications. Once the bubbling stops, the article is removed with a speed and angle determined by the crane operator.

Finally, there are some galvanizers who use a quenching bath to aid in the cooling of the galvanized article after galvanizing to decrease handling time. Although no data was taken during this quenching process, a sharp decrease in temperature due to quenching could further aggravate cracks that had already formed during dipping, and would be an interesting topic for future research.

5.7 Summary

Through all tests, a number of significant observations have been made. First, thermal data was recorded during the galvanization process for HMIP sections, and indicate that significant thermal gradients develop during the galvanizing process. Second, the most reliable way of collecting thermal data is to use high temperature adhesive to embed thermal couples into HMIP sections. Third, while crack patterns do not seem to maintain consistency between galvanizing testing dates, the ratio of pole shaft diameter to shaft thickness seems to serve as a strong indicator of the likelihood of developing cracks. Finally, hot dipping variables such as dipping speed, angle of dipping, and duration of submergence vary from crane operator to crane operator. Other practices of hot dipping also vary between galvanizers as well, but these alone serve as a reminder that while the practice of galvanizing may be well established, well defined industry standards on dipping practices do not exist and are left to the discretion of the plant management. It would be worthwhile for research to be conducted to determine the effects of these dipping variables on the life of high masts in the field.

CHAPTER 6.   FINITE ELEMENT MODELING

6.1   Introduction

While field experiments are a capable method of discovering under which conditions HMIPs crack during galvanizing, they give little insight into the mechanisms that govern the cracking phenomenon unless extensive monitoring is possible. Due to the extreme conditions present in the galvanizing environment, finite element modeling was used to better understand the effects of hot dipping on HMIP sections. The creation and verification of a finite element model can be a complicated process. In order to match reality, dipping procedures, geometries, boundary conditions, material properties, and interactions need to be well understood and properly addressed. The following chapter details the creation of the finite element models used in the subsequent parametric study, and the verification of these models.

6.2   Base Model Development

Finite element modeling of HMIP sections was conducted with the commercial software ABAQUS 6.9EF-2. Development of the model began in two parts—by modeling the heat flow from the molten bath into the HMIP and the resultant thermal gradients, and then constructing a structural model to evaluate resultant stresses as they propagate through the HMIP. ABAQUS allows for this sort of analysis by using output from a heat transfer analysis as the loading condition for the subsequent static general analysis. The purpose of thermal and structural models is to evaluate the resultant concentration of stresses that accumulate within the HMIP as a result of the heating procedure. After finding these stresses and strains, output may be compared to other model runs to determine how different variables might change the formation of "hotspots", and whether this resultant concentration of stresses and strains correlate with the observed cracking phenomenon. The term "hotspots" refers to locations along the HMIP where significant stress or strain gradients are coincident with likely crack initiation locations.

6.2.1   Model Geometries

Three versions of the high mast model were created: one model of the fatigue specimen with the 14' long pole shaft and end plate, and two models of the steel specimen with a 5' long pole shaft. All of these fatigue pole specimens were modeled to be consistent with the design drawings presented in Appendix A.3. All three high mast pole sections which were fabricated in the February 2011 round of testing were modeled in ABAQUS.

The 14' model was created by merging together three independent parts that were formed from extruded and swept solid elements. Since these elements were all fabricated with the same material, ASTM A572 steel, merging the parts was the best way to analyze the assembly in that it allows for faster computation time (Stam, 2009). The individual parts were comprised of a base plate, a pole shaft, and a reaction plate. All bends for the high masts were assumed to have a 0" shaft bend radius for simplicity. The end plate was 1" thick and had no included anchor holes, as these holes would not greatly affect the heat flow or stresses near the interface between the base plate and pole shaft.

The 5' models were created by merging together two independent parts, a pole shaft and a base plate, also composed of extruded and swept solid elements. Like the 14' pole, these stub models also used a 0" shaft bend radius.

Due to a lack of information on residual stresses near weld regions, and the relatively small effect on cross section geometry, weld details were not modeled. While weld modeling inherently affects the way in which stresses develop, it is believed that in neglecting the weld, the flow of heat into the high mast will not be significantly affected. Also, since the formation of stresses is largely due to the global behavior of the structure, the exclusion of the weld is believed to not significantly alter the way in which stresses develop at critical regions. Not modeling the weld will, however, shift the critical region to the base plate-shaft interface. By maintaining similar geometries between parametric runs and making comparisons in which all models neglect the weld, a reasonable assessment of HMIP performance should be possible. If more precise behavior, such as the actual initiation of a crack due to galvanizing were to be modeled, researchers would need to model the weld.

6.2.2 Temperature-Sensitive Parameters

A significant consideration regarding the thermal and structural analysis of HMIP sections is how material properties change as a function of temperature. Most structural analyses are conducted at a uniform temperature, or within such a range of temperatures that the effects of temperature changes on material properties are negligible. But when temperatures fluctuate nearly 800°F, this same simplifying assumption is not valid.

The steel properties in need of definition for the completed analyses were the thermal conductivity, the coefficient of thermal expansion, the specific heat, the stress-strain relationship

before and after yielding, and the density. Density was the only property assumed to be independent of temperature change since external research indicates the temperature change fosters a change of less than 2% (Peil and Wichers, 2005) in this property through the temperature range being studied. Two different sources of thermal parameters were considered for the finite element analyses: research conducted by German researchers Peil and Wichers (2004) and information published in Eurocode 3 (2003). Ultimately, researchers did not notice a substantial effect by changing constants between Eurocode 3 and Peil and Wichers, especially when evaluating the effect relative to changing the convective heat transfer coefficient. Based on this observation, material properties from Eurocode 3 were used for all finite element analyses.

Eurocode 3 provides a convenient way of compiling properties for a finite element analysis of a steel system due to the easy application of equations that model temperature dependent parameters. This simplicity does come at a cost since the recommendations for using these properties assume a maximum heating rate of 4°F/min to 90 °F/min. Results from the previous rounds of full scale experimental work reveal that the actual rate of heating is much greater than the range given by Eurocode 3. As inadequate as it may be, no work was found defining properties of steel or stress-strain relationships when subjected to more rapid heating. Figure 6-1 shows examples of the stress-strain relationship defined for the purposes of finite element modeling.

As shown in Figure 6-1, the Eurocode 3 model allows for the benefit of capturing strain-hardening when steel temperatures remain below 752°F. Since a maximum temperature of approximately 830°F is reached during galvanizing, the stress-strain curves were modified by the recommendations in Appendix A of Eurocode 3 to account for strain hardening. Up until 572°F the strain hardening region reaches a maximum of $1.25f_y$. For the sake of these analyses, f_y was assumed to be 50 ksi and Young's modulus was assumed at 29,000 ksi at room temperature—typical values associated with ASTM A572 material. These properties provide a conservative lower bound with the tensile tests reported in Appendix C. After reaching 572°F, the ultimate strength begins to diminish until coinciding with yield. At this point, the stress-strain relationship essentially becomes a modified elastic-perfectly plastic model. While research contained in Kinstler (2006) seems to indicate that fracture strains diminish in the presence of molten zinc, researchers could not locate the actual research to supplement the ideas presented in Figure 2-11. Rather than changing the stress-strain relationship to account for this strain reduction, 0.2 was

universally chosen as the fracture strain to maintain consistency with Eurocode 3 (2003). The rest of the temperature dependent properties of steel were also derived from the equations listed in Eurocode 3. All stresses and strains were input into ABAQUS as true stresses and strains using the conversions identified by I. Scheider et al. (2004) as shown in Equation 6-1 and Equation 6-2.
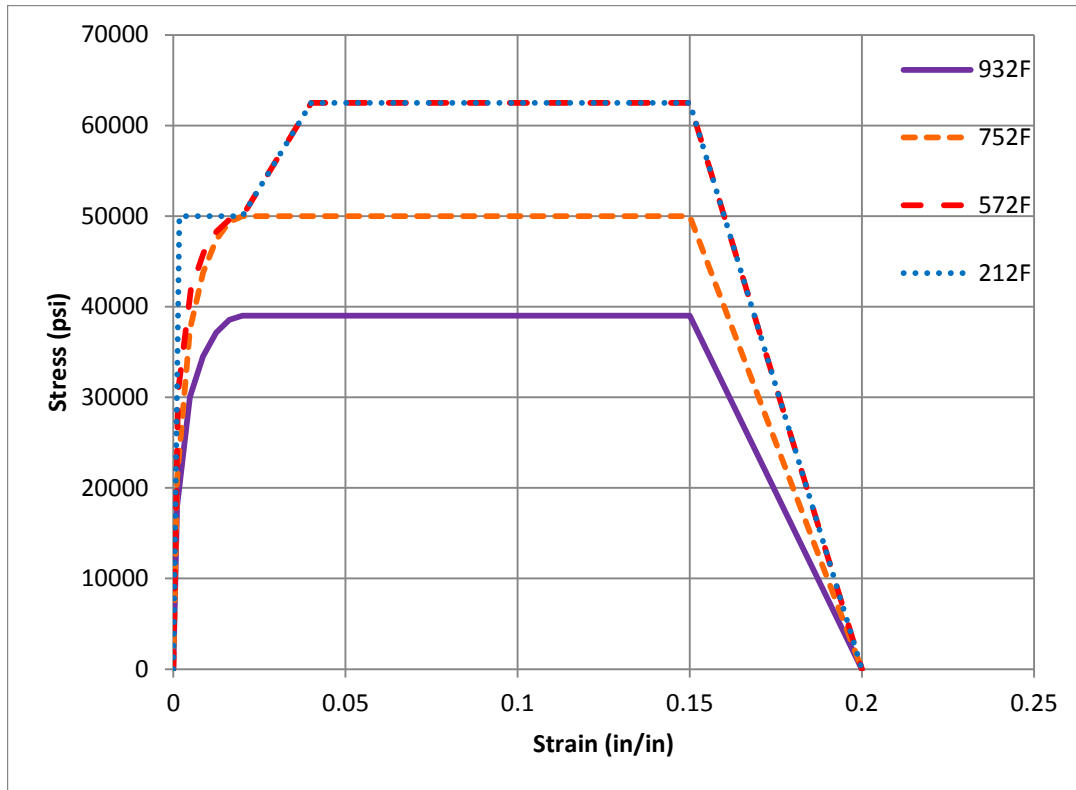
Figure 6-1: Temperature dependent stress vs strain relationship as defined by Eurocode 3

$$\dot{\sigma} = \frac{F}{A_0}; \quad \dot{\varepsilon} = \frac{\Delta L}{L} \tag{6-1}$$

$$\sigma = \dot{\sigma}\,(1 + \dot{\varepsilon}); \quad \varepsilon = \ln(1 + \dot{\varepsilon}) \tag{6-2}$$

6.2.3 Loading

As previously stated, the primary method of thermal loading on HMIPs is through heat transfer from the molten galvanizing bath. The only other external forces acting on the high mast are the

self-weight of the pole, the reactions that occur where the pole is lifted, and the buoyancy force from the molten bath. Relative to the forces necessary to cause cracking, and due to the fact that cracks are not oriented solely on the bottom half of the high mast, as shown in Sections 5.2.3, 5.3.3, and 5.4.4, it is reasonable to assume that the cracking is independent of the external forces acting on the HMIPs. Instead, it appears much more likely that thermal stresses and strains introduced during dipping are the primary contributors to the cause of cracking.

6.2.3.1   Heat Transfer

In every heat transfer analysis, the three mechanisms of heat transfer must be understood to precisely describe heat flow from one component to another. In the case of hot dip galvanizing, it is easy to isolate the primary heat transfer condition due to the nature of galvanizing. While some heat transfer occurs due to radiation during pre-heating, and conduction, the majority of heat transfer is understood to occur through convective heat transfer between the fluid in the molten bath and the steel HMIP sections. Analytically, convective heat transfer is understood to behave according to Newton's law of cooling. Newton's law of cooling states that the rate of heat transfer by convection is proportional to the temperature difference between the heated medium (T_s) and heating medium (T_∞), the exposed surface area (A_s), and the convective heat transfer coefficient (h), as shown in Equation 6-3. This equation has been adapted to ABAQUS by manipulating the formula to define convective heat flux through a surface as defined in Equation 6-4.

$$\dot{Q}_{conv} = h\,A_s\,(T_s - T_\infty) \qquad\qquad (6\text{-}3)$$

$$\dot{q}_{conv} = \frac{\dot{Q}_{conv}}{A_s} = h\,(T_s - T_\infty) \qquad\qquad (6\text{-}4)$$

Most of these parameters are fairly easy to define based on information from testing or from implicit model information. For example, ABAQUS can calculate the surface areas on each element, and temperatures of the steel prior to emersion and the bath temperature can be found by examining experimental results. The heat transfer coefficient, h, is much more complicated to properly capture. The property h is dependent on the properties of the heating medium, the flow conditions around the heated element, and the surface geometry over which the fluid moves

(Çengel et al. 2005). Because there are so many different conditions that affect *h*, values for this variable are typically derived experimentally.

Ultimately, the proper value for *h* was determined in this study by varying the parameter in the ABAQUS analyses, and comparing the output with the experimental data results discussed in Chapter 5. While attempting to correlate thermal data between experimental and ABAQUS results, researchers found that *h* did not always remain consistent between different tests, and potentially changed from location to location along the length of the HMIP. This is not surprising given the nature of the variable. It is important to emphasize that for the parametric work to be completed, a value of *h* needed to be selected for each ABAQUS run. To most accurately capture the value of *h*, it is necessary to perform experiments for each HMIP geometry, dipping angle, and dipping speed under consideration. In the case of these ABAQUS runs, a single value of *h* was selected that reasonably matched data captured in the field experiments for the whole pole. While this assumption is not necessarily the most accurate, it does provide a reasonable basis for comparing ABAQUS output between different analytical runs. Further experimental work should be conducted to validate the convective heat transfer coefficient being used for finite element analysis and parametric evaluation.

6.2.3.2   *Thermal Analysis*

To run this thermal analysis on the HMIPs, loading is applied in two steps. In the first step, an initial surface condition is applied with a temperature consistent with ambient air temperature. The second step is to apply the changing surface condition that defines a heat flux matching the environmental conditions at the galvanizing plant. In order to apply this condition, Equation 6-4 is applied with the necessary selected variables to reflect the convective heat transfer observed at the galvanizing plant. The flexibility of ABAQUS allows for calling a user-defined subroutine to specify the way in which a surface flux is applied to an assembly.

6.2.3.3   *User Defined Subroutine*

The subroutine DFLUX is used to simulate the dipping procedure. The dipping procedure subroutine was written in FORTRAN and developed using Equation 6-4. Given the appropriate convective heat transfer coefficient, speed of dipping, and angle with which the assembly is lowered into the molten bath, a convective heat flux is calculated and applied across the HMIP section as a function of time. The FORTRAN subroutine coincides with changes in the step increments. At each time increment, the program defines a reference plane, meant to model the

interface between the galvanizing bath and surrounding air, and moves the plane across the modeled HMIP at a user-defined angle and speed.

Figure 6-2 illustrates the way the bath-air interface is defined in ABAQUS. As the program moves the plane across the high mast section, nodes that fall above the plane are assigned a convective heat transfer coefficient consistent with that for typical values for air, $3.397 \cdot 10^{-5}$ Btu/s in^2 °F or 100 W/m^2 K, and the nodes falling below the plane are assigned the experimentally derived heat transfer coefficient for the molten bath. The angle of dipping, speed of dipping, and time of dipping were also programmed as variables that can be specified within the subroutine. These parameters were selected to correlate with observations made during experimental work at the galvanizing plants during the galvanizing of specimens 33-3-12-TX-SG-C, 33-3-12-TX-SG-SA, and 33-3-12-TX-SG-SC.

Figure 6-2: DFLUX subroutine schematic
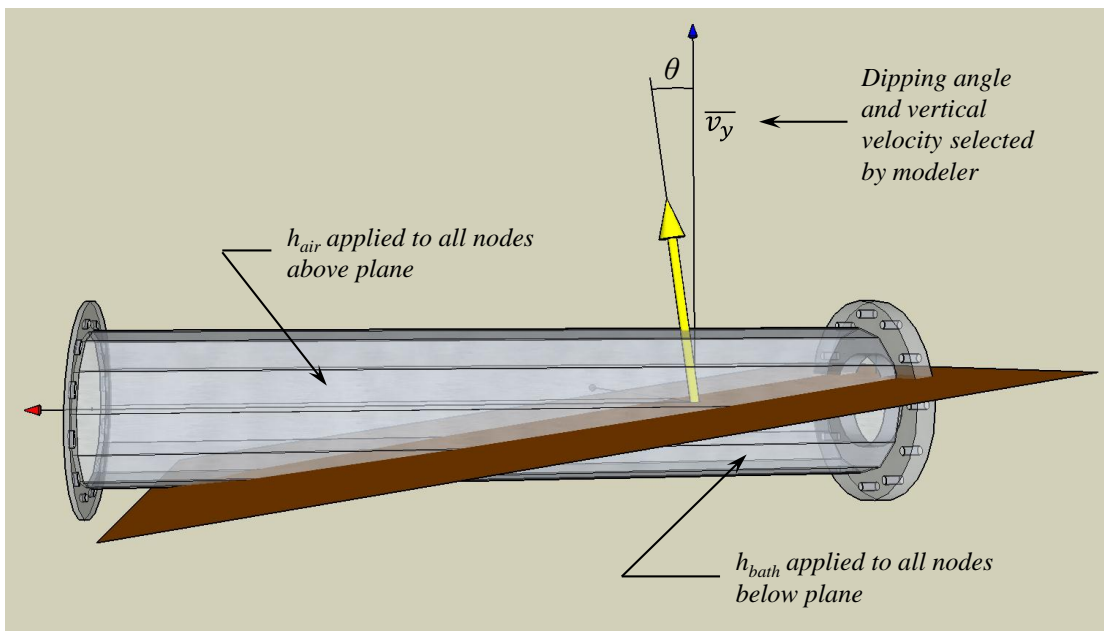
Due to the geometry of the HMIP and particularly the access hole in the base plate, at certain angles the model does not accurately model the flow of fluid into the inside of the high mast section. This is due the inability for the molten bath to flow into the inside of the high mast, similar to what happens when trying to submerge an empty bowl in a basin full of water, when

$90° > \theta > 0°$. But in practice, this effect of HMIP geometry does not hold back the zinc from flowing into the HMIP for long, and was therefore assumed negligible.

The thermal loading step lasted for 640 seconds to match the observed amount of time that the HMIPs remained submerged. Time increments were computed by ABAQUS as a means of selecting the most efficient and accurate time durations to achieve convergence.

6.2.3.4   Structural Analysis

Once an analysis is run that reflects the thermal gradients present during galvanizing, the next step is to apply the thermal gradient to the HMIP and subject the section to a stress analysis. To run the new analysis, a complete new model is created that considers the stresses, strains, and internal forces that result from the galvanizing process. A two-step loading procedure is used, to apply the thermal gradient from the earlier thermal analysis. The initial step applies the initial temperature as recorded from the database file recorded during the thermal analysis, and then the subsequent step modifies the temperatures as defined by the thermal analysis output database file. Time increments coincided with seconds during galvanizing and ran until reaching the 640 seconds defined in the previous analysis. Time increments are also computed by ABAQUS during the structural analysis as a means of selecting the most efficient and accurate time durations to achieve convergence.

6.2.4   Boundary Conditions

The boundary conditions selected for both the thermal and structural analyses are selected to have the least effect on the development of stresses at the base plate to shaft connection. To do this, pinned restraints are applied at the opposite end of each model to simulate a cantilever, as shown in Figure 6-3. In actuality, since the HMIPs are suspended at only two points, they are statically unstable. To run an anylsis, ABAQUS requires a model to be statically determinant. Therefore, all pinned connections were assumed at the side of the HMIP opposite of the base plate. This configuration is thought to most closely mirror the boundary conditions from the field. Boundary conditions were applied by pinning non-critical nodes on the side of the HMIP opposite the base plate for all models. A small study was performed to determine the influence of shifting the boundary conditions 30 degrees from the geometry shown in Figure 6-3, but a neglegible effect was observed.
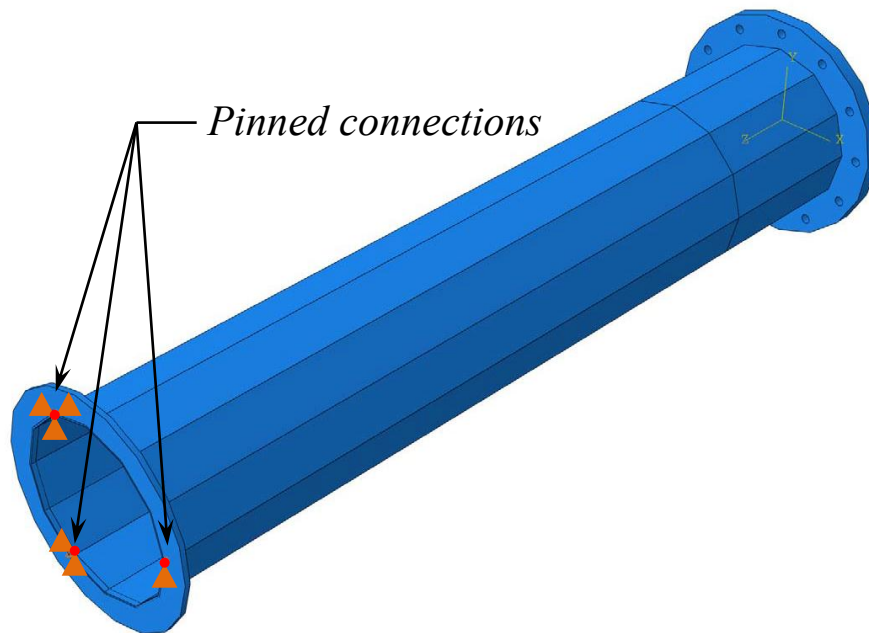
Pinned connections

Figure 6-3: Boundary conditions applied to finite element model

6.2.5 Meshing

After assembling the individual parts together, assigning material properties, and defining the loading conditions through the user defined subroutine, the high masts are meshed. The meshing procedure selected uses hex shaped elements that are formed by sweeping across the section. In the case of both the 14' fatigue specimen and the 5' stub specimens, two regions were defined by local seeds to control mesh size. Since the most critical region is considered to be near the shaft to base plate connection, the whole baseplate and the first 33" of the shaft was seeded at 1/2" for the thermal analysis, and after a meshing study, the region was re-seeded to match the thickness of the HMIP shaft. The rest of the shaft and the reaction plate were seeded at 5" for both analyses as shown in Figure 6-4.

Since the complete thermal stress analysis required two model analyses, two different element types are used. For the thermal analyses, 8-node linear heat transfer bricks are used, whereas for the stress runs an 8-node linear brick with reduced integration and stiffness hourglass control is used. To get the fewest errors a sweeping advancing front algorithm is used to mesh the base plate and a sweeping medial axis algorithm with minimized mesh transitions is used to mesh shaft and end plate locations.

Capturing the effects of local stresses at the shaft to baseplate connection requires a submodel consisting of 8-node linear bricks with reduced integration and stiffness hourglass control meshed in a similar fashion as the assemblies from the global model, but with elements sized at one fourth of the shaft thickness (t/4). Stam (2009) determined this size mesh to be adequate for using the DNV method to calculate hotspot stresses at regions of high stress concentrations caused by discontinuous geometry, such as that at the shaft to base plate connection. A sample image of a typical submodel is shown in Figure 6-5. The DNV method and calculations with the method will be presented in Chapter 7.
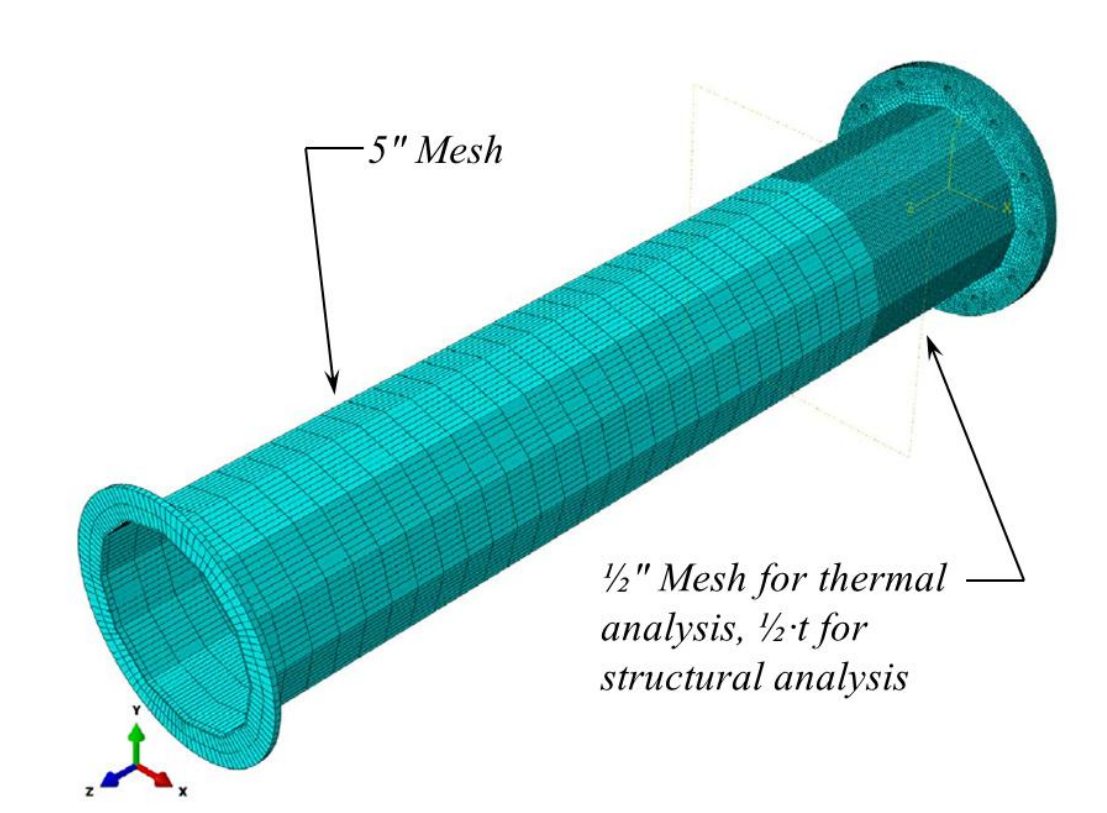

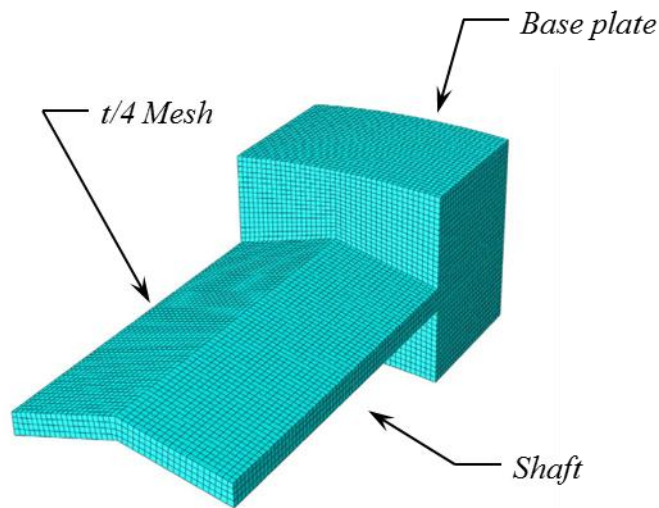**Figure 6-4: Meshed 14' fatigue specimen representing 33-3-12-TX-SG-C**

Figure 6-5: Typical meshed submodel of shaft to base plate joint at a bend

6.3 Model Verification

To ensure that the HMIP models that were run in ABAQUS produced accurate solutions, data from the galvanizing tests were used to validate the finite element models. The primary tests studied through finite element analysis coincided with the February 2011 testing. From the experimental work data, researchers were able to compare the thermal readings and corresponding strains with the results obtained from finite element analysis to determine the adequacy of the developed models and assumed parameters. The following sections discusses the results from the thermal and structural verification studies.

Each ABAQUS model was created to replicate the behavior of actual field tests. Specific temperatures from the thermal model were reported and compared against field data to ensure a reasonable representation of the behavior of each of the three HMIP sections during galvanizing. Since the method of heat transfer was believed to be understood well enough to be represented by convection, the greatest parameter considerations stemmed from the choice of constants to represent dipping speed, dipping angle, and the convective heat transfer coefficient. For each model, observations made while monitoring the galvanizing of the test specimens from Chapter 5 informed the initial selection of these constants, which are listed in Table 6 along with the

respective representative field test specimens. Figure 6-2 depicts how these parameters are applied to the HMIP thermal analysis.

Table 6-1: Thermal analysis parameters

Model Designation	Corresponding Field Test	t_{shaft} (in)	h_{bath} [Btu/(s in^2 °F)]	v (in/s)	θ (degrees)	T_{air} (°F)
SG-C	33-3-12-TX-SG-C	0.313	$5.095 \cdot 10^{-4}$	0.525	8	65
SG-SA	33-3-12-TX-SG-SA	0.438	$5.095 \cdot 10^{-4}$	0.609	4	79
SG-SC	33-3-12-TX-SG-SC	0.500	$5.095 \cdot 10^{-4}$	0.719	4	79

Once the thermal analysis was completed and temperature verses time curves had been generated, strains from the structural model were compared against the strain data taken during the dipping procedure as reported in Section 5.4.3. A total of three different models were assembled to reflect the formation of temperature gradients and the resultant stresses and strains which occur during galvanizing—one seeking to capture the behavior of specimen 33-3-12-TX-SG-C, one to capture the behavior of 33-3-12-TX-SG-SA, and one to capture the behavior of 33-3-12-TX-SG-SC.

6.3.1   Model SG-C

The model used to simulate the experimental data recorded from 33-3-12-TX-SG-C was model SG-C. This model used a heat transfer coefficient of $5.095 \cdot 10^{-4}$ Btu/s in^2 °F, or 1500 W/m^{2}K for applying Equation 6-4, which, bearing in mind the known errors discussed in Chapter 5, appears to match the behavior observed in Figure 6-6 fairly well. The standard convention for the graphs comparing ABAQUS output and experimental results in this thesis is to show ABAQUS results with a solid line, and experimental data with a dotted line. Both the general shape of the heating curve in the base plate and pole shaft seem to coincide rather closely. Likewise, for radial positions 2 and 3 the thermal data matches reasonably as well. The temperature difference between analytical and experimental data is no greater than about 85°F.
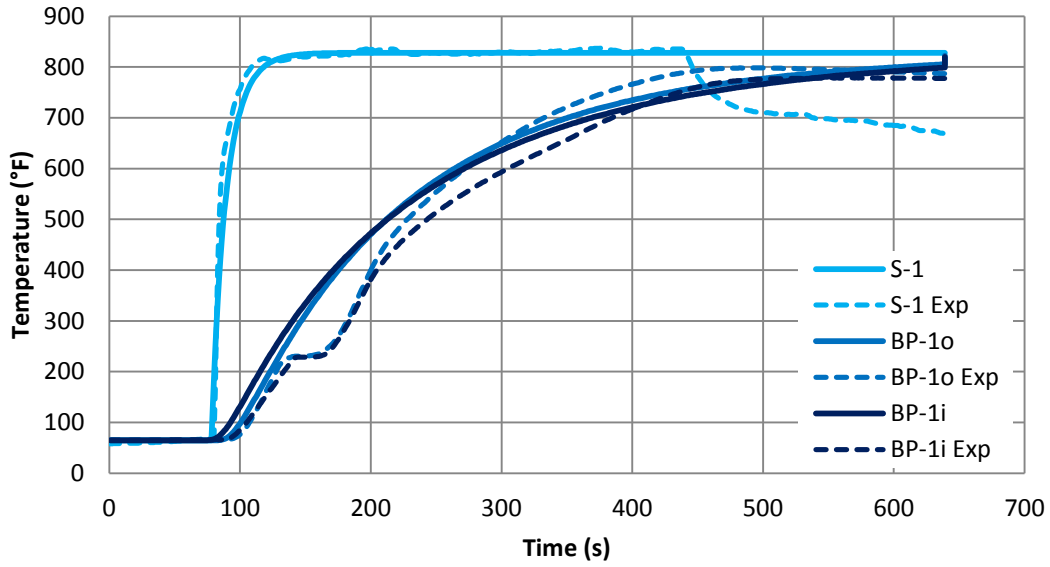
Figure 6-6: Experimental and analytical data for temperature vs. time relationship at radial position 1 of 33-3-12-TX-SG-C and SG-C
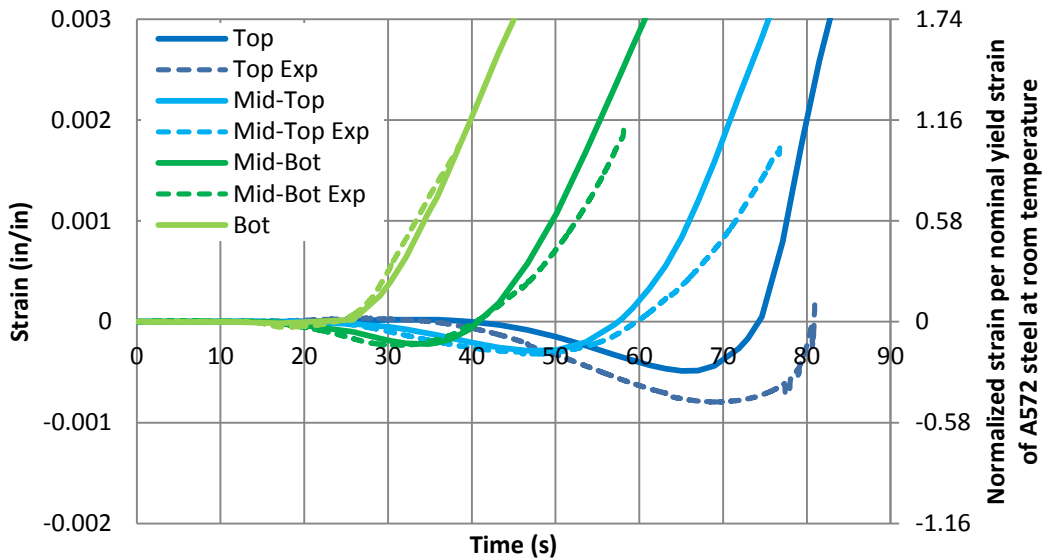

Figure 6-7: Experimental and analytical data for strain vs. time relationship at measured locations of 33-3-12-TX-SG-C and SG-C

Despite only having recorded about the first 60 seconds of strain data during the galvanizing process before the instrumentation melting, it is apparent that the strain model reasonably matches the experimental data. While the magnitude of compressive strain does not always quite match with that which was measured, the general shape and trend do seem to correlate rather well. Because of the freedom exercised by crane operators in executing the dipping procedures, deviation from the measured strains from 33-3-12-TX-SG-C could easily be a function of some discrepancy in the modeling of the dipping procedure: a variation in the dipping angle or speed by the crane operator could also force changes in thermal gradients and resultant strain development. Based on the observed trend, it is reasonable to conclude that the strain output given by model SG-C gives reasonable results that adequately reflect reality.

6.3.2 Model SG-SA

Similar to model SG-C, model SG-SA utilized a convective heat transfer coefficient of $5.095 \cdot 10^{-4}$ Btu/s in^2 °F for applying heat to the system. The resultant heating curves were compared against the experimental data recorded from specimen 33-3-12-TX-SG-SA as shown in Figure 6-8.
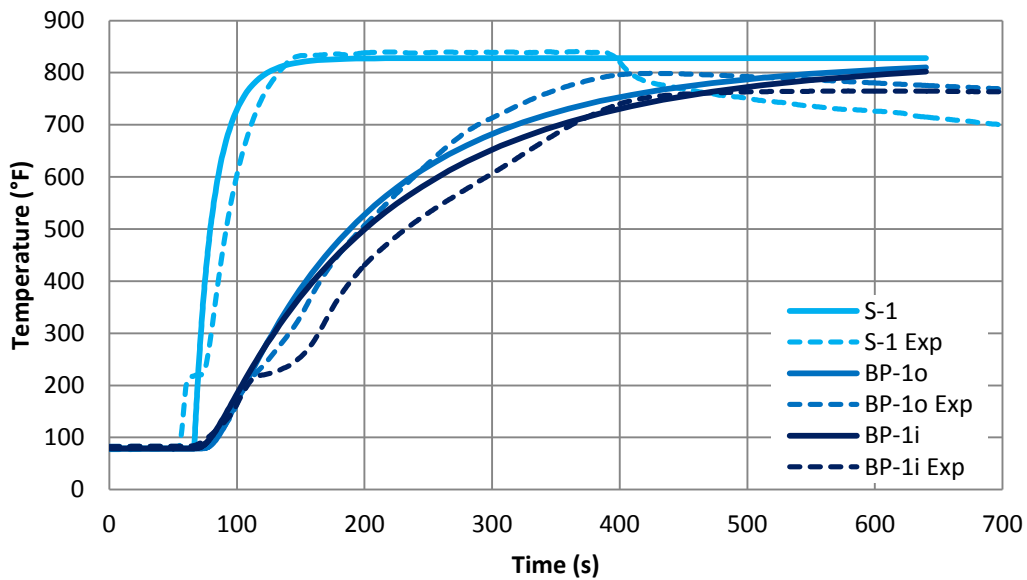

Figure 6-8: Experimental and analytical data for temperature vs. time relationship at radial position 1 of 33-3-12-TX-SG-SA and SG-SA

The comparison between analytical and experimental data was not exact, but the baseplate temperatures that were modeled in ABAQUS track fairly closely with the experimental data, as does the shape of the shaft heating curve. While the experimental test curves the temperatures indicates that heat moves slower through the structure, as evidenced by the greater time between heating curves at the same temperature, the analytical models still do a reasonable job of replicating the behavior of the high mast specimen and capturing the average heating of the base plate, and the pole shaft. The difference in time of where the shaft positions begin to heat can be attributed to the crane operator using a non-constant dipping angle. This analysis idealizes the dipping angle as a constant in the analytical model. A comparison of recorded strains at measured shaft locations due to heating is presented in Figure 6-9.

The most notable point of divergence in Figure 6-9 is that while the general trends of the measured strain curves seem consistent between analytical and theoretical models, the timing is off. The experimental strain values tend to cluster closer together as a function of time than is reflected by the structural model. This again, may also be a reflection of a changing dipping angle or speed. The temperature discrepancy between the analytical model and theoretical model at any radial location during the heating cycle is no more than 75°F.

Despite the difference in times during which these strains develop, the model displays reasonable enough agreement to gain greater insight into the formation of stresses and strains for this particular pole geometry. While the angle of dipping may differ from field conditions, no typical standard requires the crane operator to dip a specimen in a specifically defined manner. As such, the model provides a reasonably accurate portrayal of realistic straining which can occur during the galvanizing process.
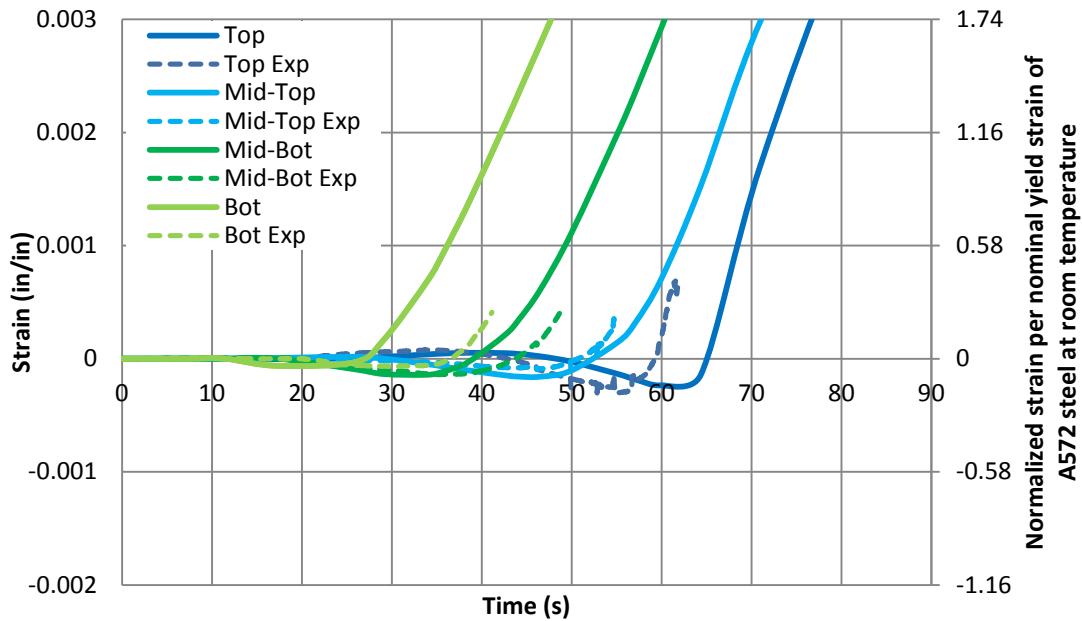
Figure 6-9: Experimental and analytical data for strain vs. time relationship at measured locations of 33-3-12-TX-SG-SA and SG-SA

6.3.3   Model SG-SC

Both 33-3-12-TX-SG-SA and 33-3-12-TX-SG-SC were hot dipped by the same crane operator and in a similar fashion during the February 2011 round of testing. This fact is reflected in the similarity of thermal analysis parameters chosen to coincide with these tests. The primary difference between model SG-SC and model SG-SA is the thickness in pole shaft and a faster dipping speed selected for model SG-SC. The resultant comparative heating curves between SG-SC and 33-3-12-TX-SG-SC at radial location 1 are shown in Figure 6-10.
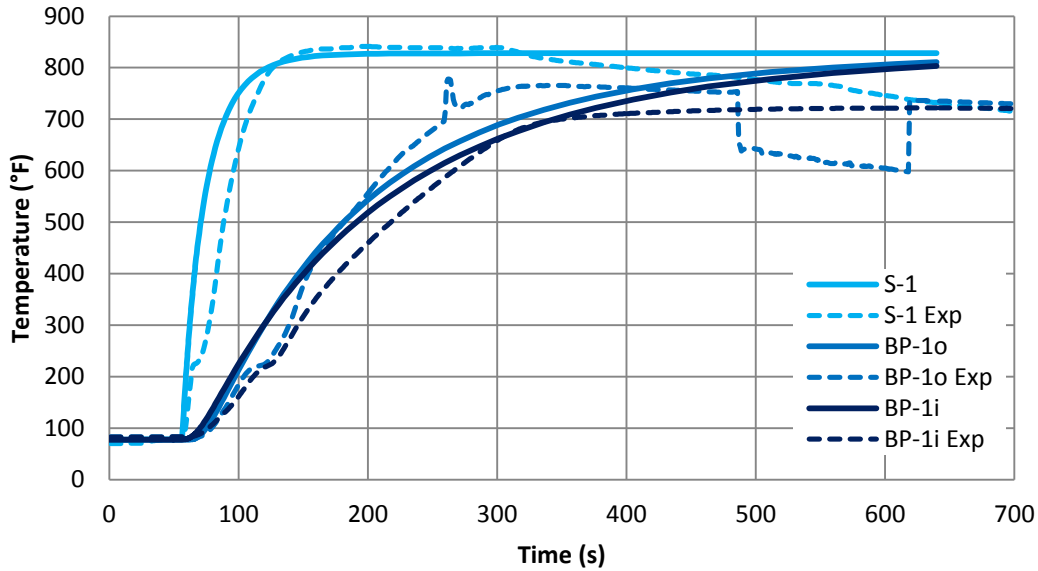
Figure 6-10: Experimental and analytical data for temperature vs. time relationship at radial position 1 of 33-3-12-TX-SG-SC and SG-SC

As observed in the comparison of 33-3-12-TX-SG-SA and SG-SA, the temperature differences between 33-3-12-TX-SG-SC and SG-SC shows that the analytical model does not reflect the larger temperature gradients that appear in the experimental results. However, the analytical model trends consistently with the experimental data, and in general, the shape of the heating curves appear to be consistent. Especially at the shaft position, the heating of the analytical model seems to capture the behavior observed in the field rather precisely when considering the thermocouple errors discussed in Chapter 5. The greatest temperature discrepancy between the analytical model and the experimental model at any radial location does not seem to exceed 75°F.

The resultant thermal strains from this heating condition are depicted in Figure 6-11. The analytical strains match well from a trending perspective. While the magnitudes of the maximum negative strain, particularly at the top location, do not perfectly align, the shapes of the strain vs. time curves seem to correlate between analytical and experimental data well enough to assume the analytical model is a reasonable approximation of reality.
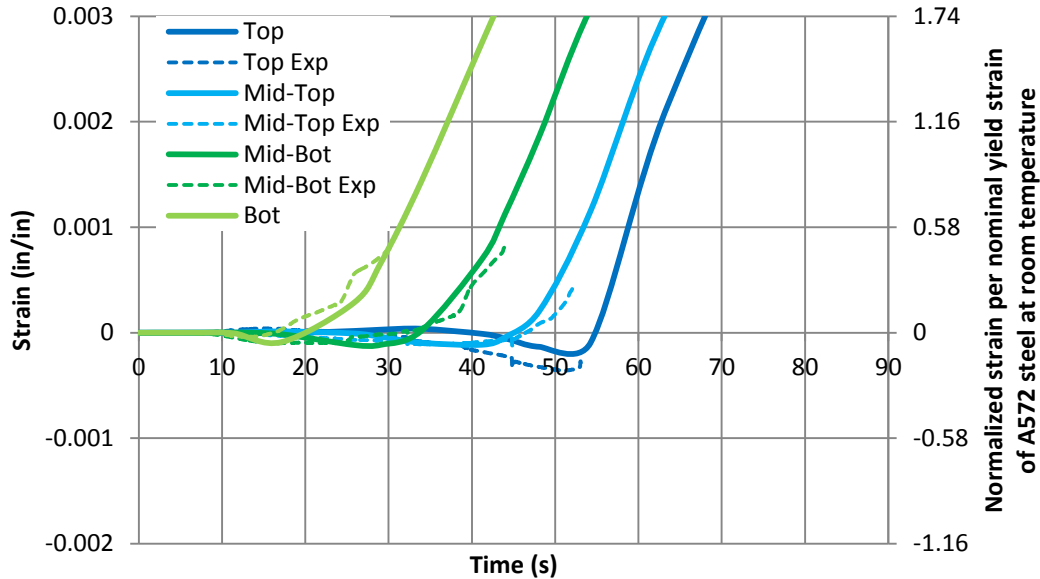
Figure 6-11: Experimental and analytical data for strain vs. time relationship at measured locations of 33-3-12-TX-SG-SC and SG-SC

6.4   Summary

Based on the comparisons between analytical results relative to those recorded in the field, the finite element model had reasonable agreement with field measurements of the hot dip galvanizing procedures observed in the February 2011 round of tests. The model assumes a constant convective heat transfer coefficient over the whole HMIP and requires a specified value of the speed and angle of dipping. In the next chapter, the results from the models developed in this chapter are used to isolate locations of large strains between the pole shaft and base plate to determine whether or not the cracks observed in Chapter 5 might be related to the results derived by finite element modeling.

CHAPTER 7.   FINITE ELEMENT RESULTS

7.1   Introduction

The models developed in Chapter 6 were analyzed to predict the extent of straining at the HMIP shaft to base plate connection during the galvanizing process. Strains were evaluated at a total of four different shaft bend locations along the perimeter of the shaft to conceptualize the strain distribution at critical regions along the cross section of the HMIP as a function of time during dipping. Taking these strain values from each of the models and comparing their maximum values provides insight into the development of galvanizing cracks. The results from this comparison are discussed in this chapter along with observations made during the modeling process.

7.2   Performance Evaluation Technique

When comparing the performance of HMIPs, or any structural member, engineers attempt to select a metric which is easily understood and for which they have a physical feel. Generally, the easiest metric to select is stress. Unfortunately, because the galvanizing process exposes steel to temperatures that result in a degradation of the stress-strain properties, stress becomes a poor reference point for evaluating performance. Evaluating the performance of structures by using stress necessitates the yield and ultimate stresses for a given material at the temperature being considered. In the case of elevated temperature studies, these yield and ultimate stresses are not constant, especially as the HMIP approaches the 830°F temperature of a galvanizing bath. Selecting maximum strain as the performance criteria eliminates this problem by mitigating the effects of variable yield and ultimate stress with temperature. Furthermore, as discussed in Chapter 2, research tends to indicate that galvanizing may reduce the ultimate strain capacity of a steel member. Ideally, by analyzing a steel section with respect to the development of ultimate strains, predicting cracking may be eventually possible as the implications of liquid metal embrittlement on steel straining is better understood.

Maximum strains needed to be evaluated at the HMIP shaft to base plate connection. The critical strain component to be considered is the longitudinal, or E33, component of nodal strain since galvanizing cracks always form perpendicularly to the longitudinal axis of HMIPs. Therefore, all strain discussed in this chapter are in terms of strains acting in the E33 nodal strain component.

The global geometry of the HMIPs also made the calculation of hotspot strains a difficult quantity to predict at critical nodes since the maximum hotspot strains occur at locations coincident with large geometric discontinuities. This means that stresses and strains at nodes right at the junction of the shaft and base plate will show an artificially large value. Stam (2009) resolved this issue by using a means of linear interpolation to calculate stresses at geometric discontinuities which he referred to as as the DNV Extrapolation Technique.

The DNV Extrapolation Technique was introduced by a maritime classification agency called Det Norske Veritas in its publication "Recommended Practice" for "Fatigue Design of Offshore Steel Structures" (DNV, 2008). This reference recommends that for three dimensional elements with a modeled weld, surface hotspot stresses due to fatigue can be measured by linearly interpolating the maximum principle surface stress at locations ½ of a plate thickness, and 1 ½ plate thicknesses away from the weld locations to project a stress at the weld toe. Despite that researchers did not simulate a weld in the HMIP model, success in implementing this technique by Stam (2009) led to its selection as the means of predicting localized maximum principle strains at critical regions at discontinuous surfaces. Slightly modified from a stress based interpolation, researchers used Equation 7-1 to calculate maximum longitudinal nodal strains at the baseplate to shaft connection.

$$\varepsilon_{HS} = 1.5 \cdot \varepsilon_{0.5t} - 0.5 \cdot \varepsilon_{1.5t} \tag{7-1}$$

Following the recommendation of Stam (2009), this technique informed the choice of submodel mesh size as a means to allow the selection of nominal strains at the ½ shaft thickness and 1 ½ shaft thickness locations from the base plate to shaft connection.

7.3   Qualitative Analytical Model Results

By completing the thermal, structural, and submodel analyses, several observations can be made about the flow of heat and internal forces within HMIPs. Ultimately, through better understanding these patterns, better designs of HMIPs can be created to reduce the likelihood of galvanizing crack formation due to thermal loading.

7.3.1 Global Thermal Analysis

Understanding the heating of HMIPs gives better insight into the load conditions to which HMIPs are exposed, and the effect of their response to these conditions. First and foremost, the effect of differential heating is very significant in HMIPs during galvanizing. As shown in Figure 7-1, despite the excellent heat conducting characteristics of steel, thinner elements such as pole shafts heat up significantly faster than base plates. In fact, Figure 7-1 indicates that by the time the entire HMIP is submerged, the internal temperature of the base plate is potentially on the order of 700°F cooler than the pole shaft just inches away.
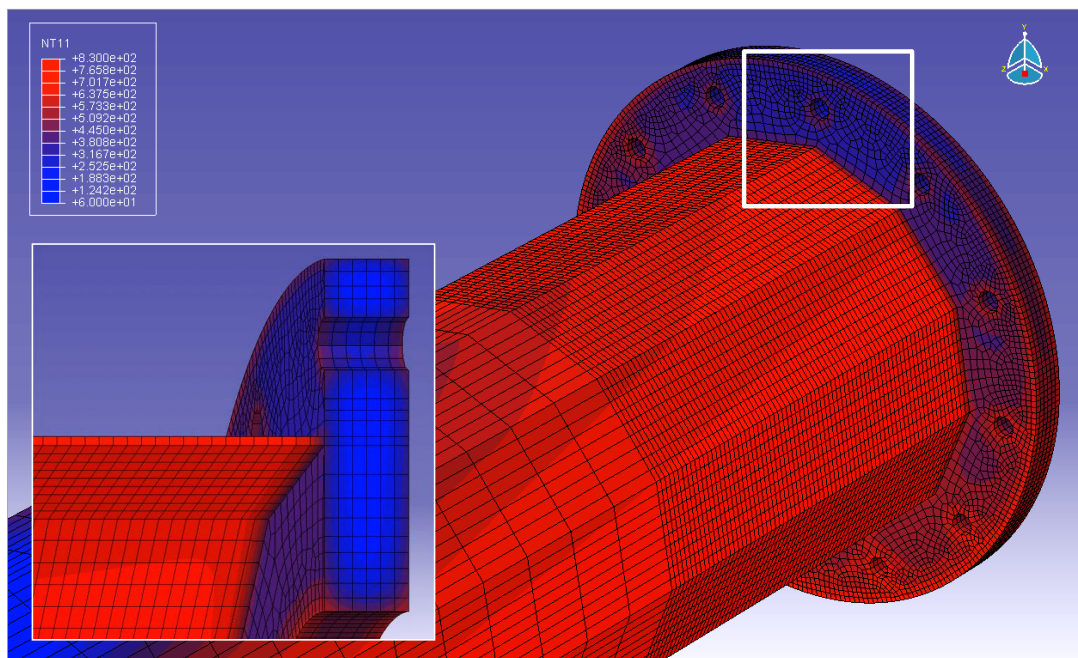
Figure 7-1: Thermal response of HMIP during galvanizing

The significance of the temperature gradient stems from the resultant formation of internal forces. Typically, engineers conceptualize structures loaded by heat as a free-expansion sort of problem. Since the HMIP is not even statically determinant while being suspended at two points during dipping, it is reasonable to think that as the HMIP heats it will simply expand without affecting the rest of the structure. The problem with this idea is that it fails to recognize the extreme differential heating that occurs. As the HMIP is submerged in the bath, the shaft regions below the surface of the bath heat very quickly, whereas the temperatures at base plate regions below

the surface of the bath lag behind the respective shaft locations by several seconds. The impact of this differential heating is best understood by examining the resultant strains.

7.3.2 Global Structural Analysis

The hot dipping process exposes elements of HMIPs to different heating conditions. For elements below the surface of the zinc, large heat fluxes are fostered by the molten bath, whereas elements above the surface are exposed to smaller magnitude fluxes due to convection from air and internal conduction. Differential heating forces elements exposed to the galvanizing bath to rapidly expand, whereas non-exposed elements then experience compression as these regions attempt to restrain the deformation, as can be seen in Figure 7-2. Thus, differential heating can also form both stress and strain gradients across HMIPs during galvanizing.
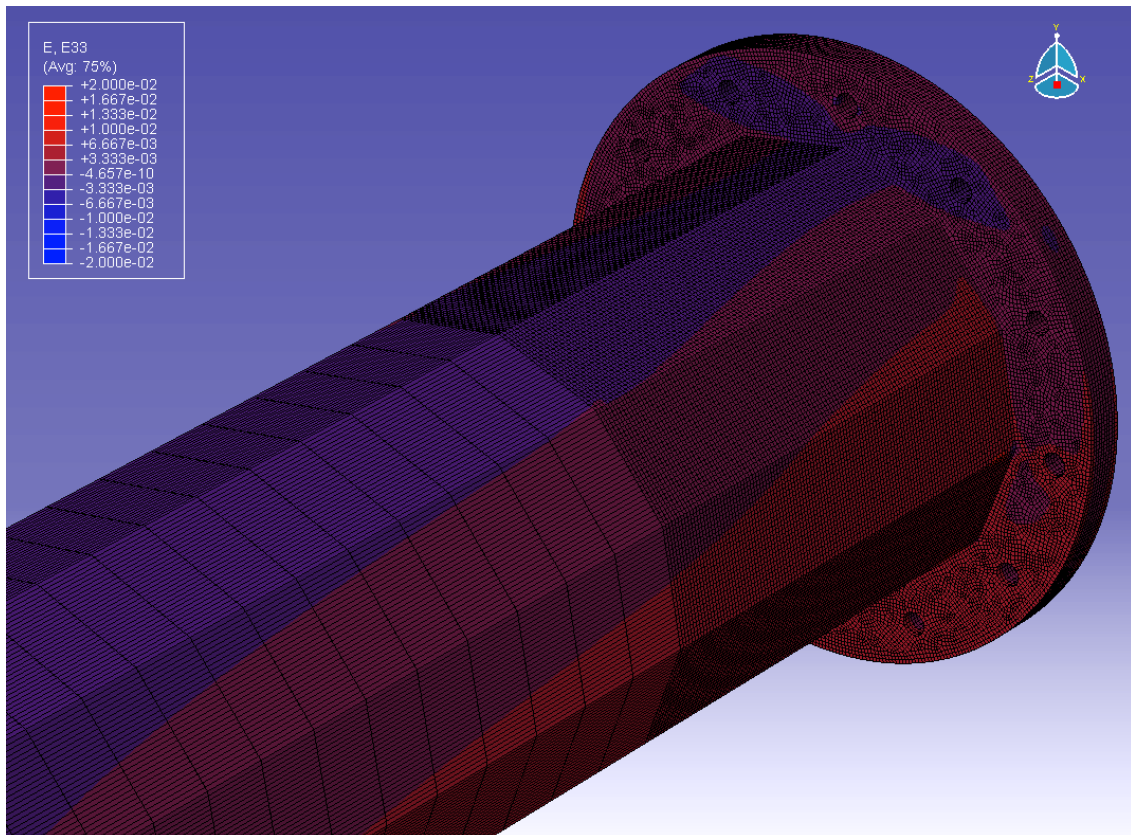
Figure 7-2: Development of longitudinal strains as the HMIP is dipped into the galvanizing bath

Figure 7-2 shows how the strain gradient lines run parallel with the bath surface and the concentration of resultant compressive strains balance the expanding elements below the bath surface. It is easy to understand how in order to maintain equilibrium, compressive forces gather at the top of the section as the high mast is being dipped. However, what is more difficult to see from Figure 7-2 is that even bend locations in high global tensile straining regions remain in compression. But in order to have a better understanding of this behavior, researchers analyzed submodels at these bend regions.

Researchers found that using these load cases and the meshing elements described in Chapter 6 resulted in hourglassing as shown in Figure 7-3. The deformations showing hourglassing have been scaled up 50 times to become recognizable. Hourglassing is a phenomenon which occurs when to reduced integration elements deform excessively because reduced integration elements are idealized as a single element and do not record strain (Hovell, 2007). Stiffness hourglassing controls were implemented on the structure; however hourglassing still occurred at locations where submodels were used to analyze local strains. Due to time constraints, a new model could not be implemented by the time this was discovered. Future research into this problem should recognize the possibility of this effect at shaft to base plate connections and consider using regular noded elements to mitigate issues from this sort of occurrence.
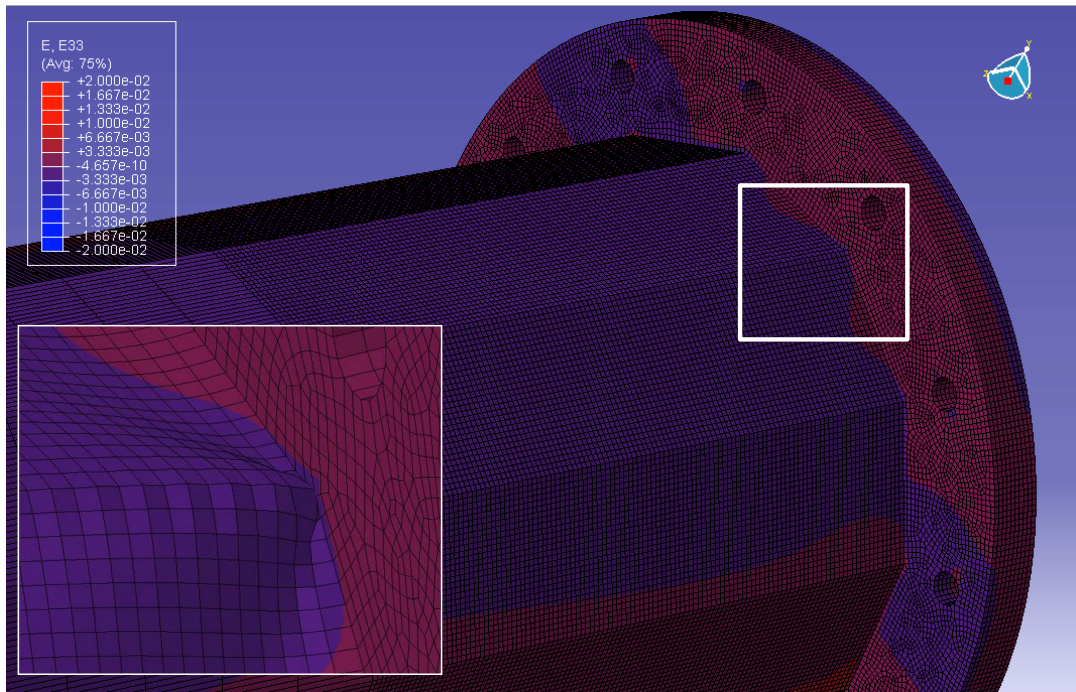
Figure 7-3: Hourglassing in global structural model

7.3.3   Submodel Structural Analysis

Submodels were created at the bend locations depicted in Figure 7-4. The purpose of the submodeling was to evaluate the performance of HMIPs along bends around the perimeter of the section to see if a correlation could be determined between what is observed in ABAQUS, and the cracks observed in practice. An image of a typical submodel output taken from bend 12 of model SG-C, the model matching the geometry of specimen 33-3-12-TX-SG-C, is presented in Figure 7-5. Figure 7-5 clearly shows the development of compressive hotspot strains at the shaft to base plate connection.
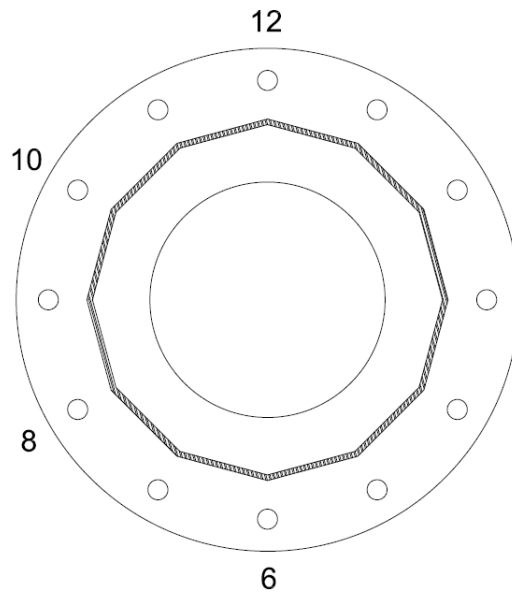
Figure 7-4: Submodel bend locations on each HMIP. Bend 12 is up during simulated dipping.
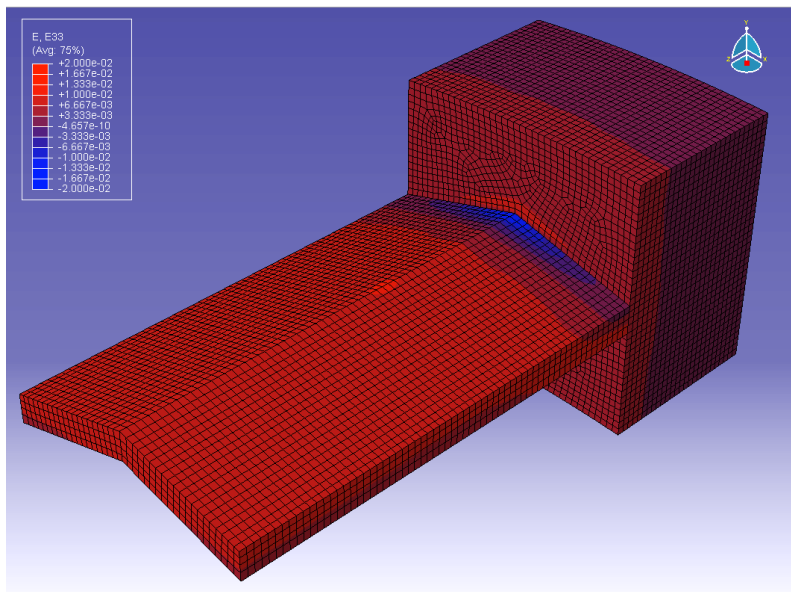
Figure 7-5: Submodel of bend 12 from SG-C showing concentration of forces at shaft to base plate connection

117

Typical of all models, the concentration of straining that accumulates at the shaft to base plate connection is particularly noticeable in Figure 7-5. In this case, nearly the whole submodel is expanding except for the region of the shaft abutting the base plate which shows very significant compressive strains. From a qualitative stand point, it is interesting that region of the shaft subjected to these large compressive strains coincides with the region where galvanizing cracks have been witnessed. Even the length of the compressive strain region seems to correspond to the same lengths of cracks witnessed from UT inspection. Though this does not necessarily indicate that compressive straining is the cause of the measured galvanizing cracks, there may be some sort of correlation between compressive strain locations and crack locations particularly when considering residual stresses due to welding in these regions.

7.4   Quantitative Analytical Model Results

By using the submodel analyses to evaluate straining at the pole shaft to base plate connections, hot spot strains have been calculated for models SG-C, SG-SA, and SG-SC. The primary differences between these structures are the shaft walls, ranging from 5/16" to 1/2", the dipping angle, and the dipping speed. The major differentiating parameters between these models are shown in Table 7. For each of these submodels, the strain profiles have been plotted against each other as a function of time during galvanizing as a means of evaluating the comparative performance. Plots have been assembled for submodel output at the bend locations designated in Figure 7-4.

Table 7-1: Differentiating parameters between HMIP finite element models

Model Designation	Corresponding Field Test	Shaft Thickness (in)	d/t ratio	v (in/s)	θ_{dip} (degrees)	θ_{long} (degrees)
SG-C	33-3-12-TX-SG-C	0.313	104	0.525	8	0
SG-SA	33-3-12-TX-SG-SA	0.438	75	0.609	4	6
SG-SC	33-3-12-TX-SG-SC	0.500	65	0.719	4	6

The plots depicted in Figure 7-6, Figure 7-7, Figure 7-8, and Figure 7-9 show the differences in performance of HMIP models SG-C, SG-SA, and SG-SC. These plots show that model SG-C consistently has higher maximum strains developing in tension and compression at the base plate to shaft connections than the other models. In fact, compressive strains at two bend locations in model SG-C exceeded the strains in models SG-SA, and SG-SC by more than a factor of two, as

shown in Figure 7-10. At some bends, such as bend 10 and bend 8, model SG-C also reports comparatively large tensile straining, far exceeding those measured at the corresponding locations from models SG-SA and SG-SC. The general shapes of heating curves align fairly well and tend to follow similar trends, though the amplitudes of trending regions differ substantially.
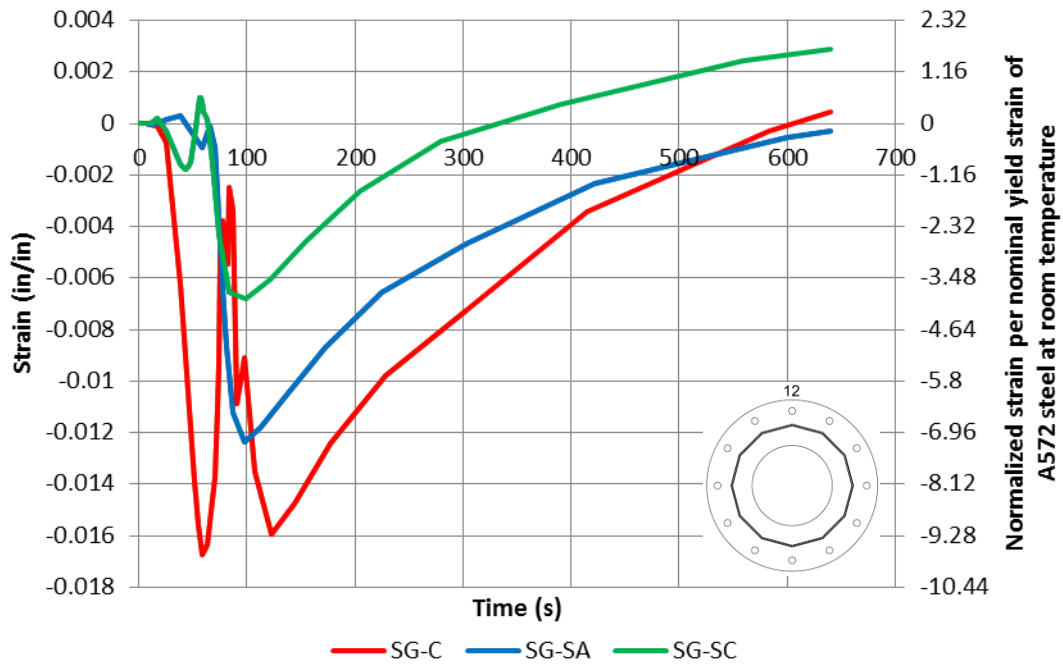

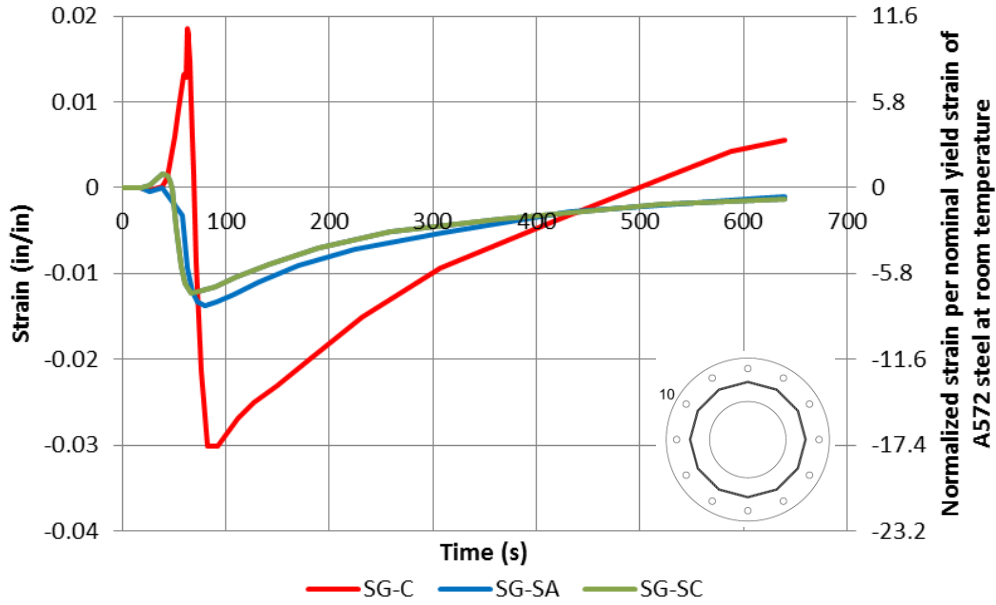**Figure 7-6: Comparative strains at pole shaft to base plate connection at bend 12**

Figure 7-7: Comparative strains at pole shaft to base plate connection at bend 10
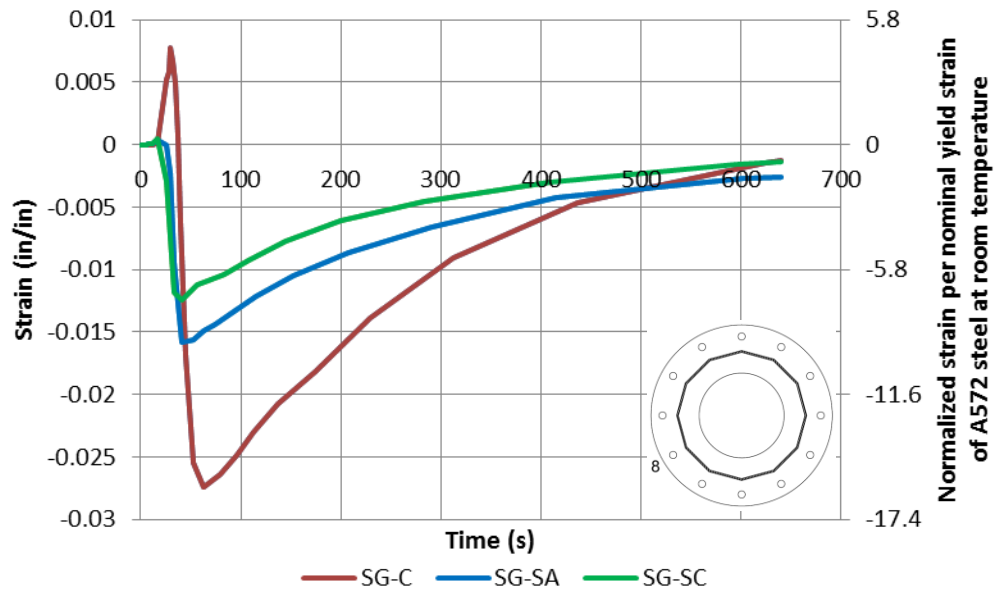
Figure 7-8: Comparative strains at pole shaft to base plate connection at bend 8

120
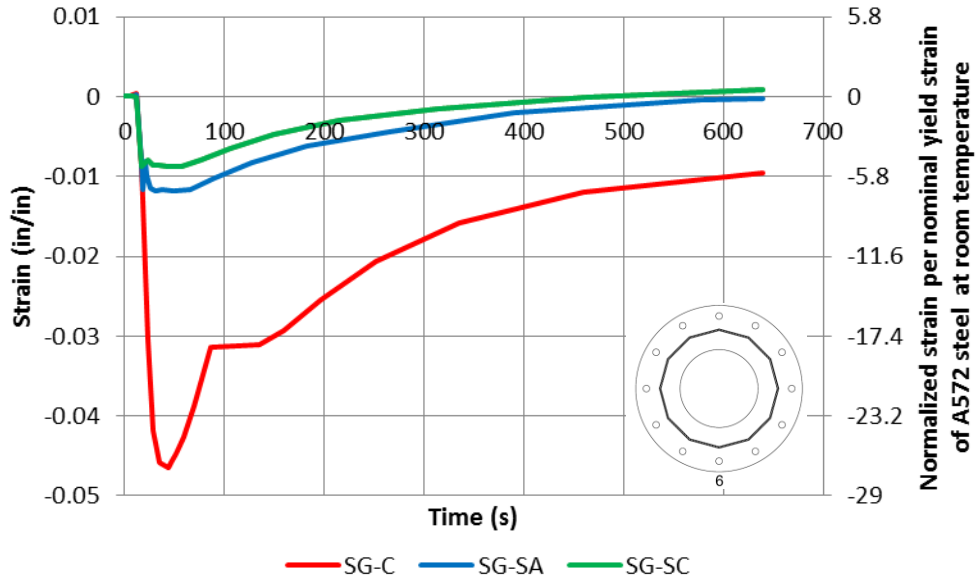
Figure 7-9: Comparative strains at pole shaft to base plate connection at bend 6
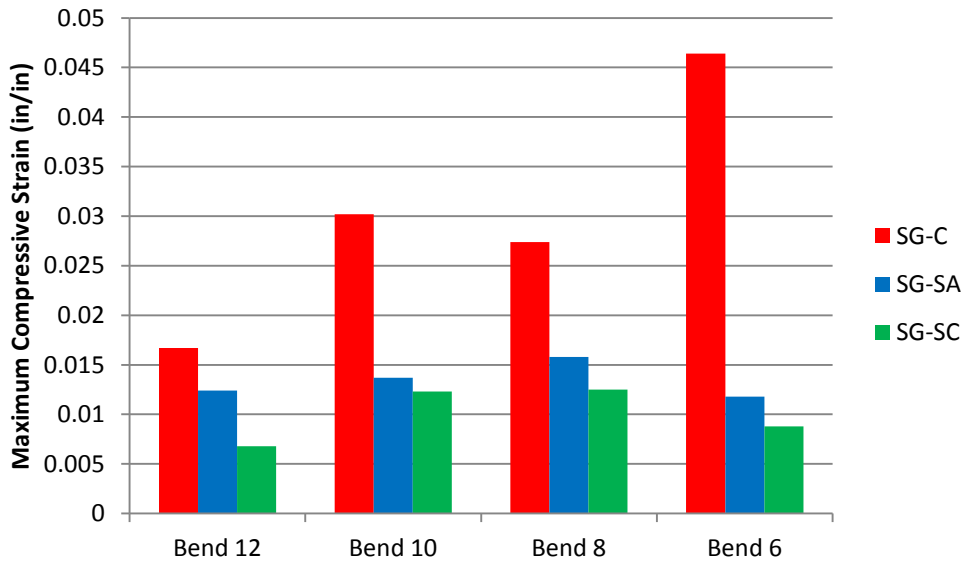
Figure 7-10: Maximum straining condition for each submodeled bend

7.5   Parametric Study

Validating conclusions from the results plotted in Figure 7-6 through Figure 7-9 necessitates special model runs to verify that the shaft thickness to shaft diameter ration governs the cracking phenomenon. Models SG-C, SG-SA, and SG-SC were all different originally because their galvanizing parameters were chosen to match those of the actual experimental HMIP sections discussed in Chapter 5. While apparent that the performance of model SG-C lacked behind SG-SA and SG-SC, it is still yet to be proven that the primary contributor to this difference in performance hinges on simply the d/t ratio. As mentioned in Chapter 6, the output from these analyses is dependent not only on the shaft thickness, but also the speed of submergence and dipping angle.

Performing additional runs where parameters such as dipping rate and angle are changed inherently changes flow characteristics of the molten bath over the HMIP and should, in reality, change the convective heat transfer coefficient used for running the assumed thermal analyses. For the sake of simplicity, the heat transfer coefficients used in this parametric study remained constant with those verified in Chapter 6. All parametric studies also evaluate performance only at bend 10. Experimentally, bend 10 is a likely site of galvanizing cracks and analytically, bend 10 is a location showing very large tensile and compressive strains in SG-C relative to the other models. Because of these characteristics, bend 10 serves as a good benchmark for how the performance of a pole changes due to parameter changes.

7.5.1   Model SG-SA

Parametric analyses were conducted on the SG-SA model with a dipping angle of 8° (θ_{dip}) to match SG-C, and a twist about the longitudinal axis of 6° (θ_{long}) to match the bend orientation of SG-C. Results from these comparisons were used to identify whether these parameter significantly impact the strain distribution in a way that might indicate performance more closely matching SG-C.

The results from this parametric study are shown in Figure 7-11 plotted with the results from the original model runs. Model run SG-SA-R is the resultant heating curve for the model rotated 6° about the longitudinal axis, and SG-SA-DA is the resultant heating curve for the model with an 8° dipping angle.
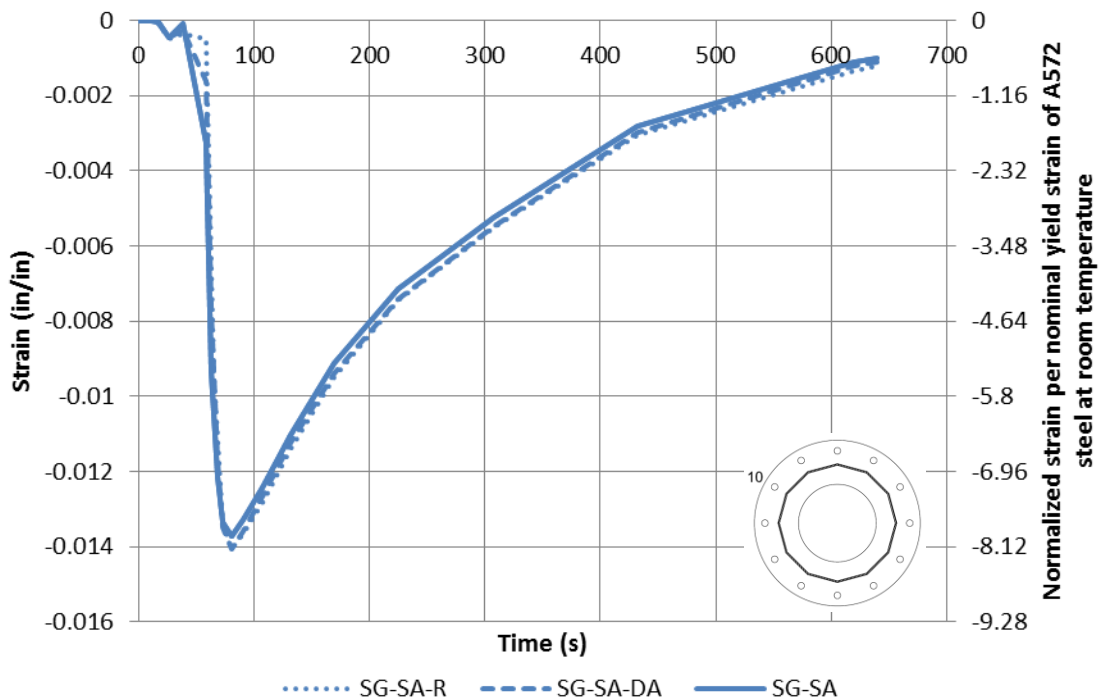
Figure 7-11: Parametric study on model SG-SA at bend 10

Figure 7-11 clearly shows that the small effect from changing the dipping angle, and rotating the bends of SG-SA to match those of SG-C. At least for the thicker shaft geometry, these parameters do not significantly impact the strain response forming at bend 10. These results indicate that the strain response to dipping may be far more dependent on the shaft geometry, at least for analyses completed on HMIPs with 7/16" pole shafts.

7.5.2   Model SG-C

Once it became apparent that changing the dipping parameters of SG-SA did not significantly affect the development of strains at bend 10, further analyses was conducted to determine whether or not these dipping parameters could have a larger effect on a thinner pole shaft. Analyses were run to better understand the effects of changing the dipping angle, and dipping speed on the development of strains at bend 10 in a HMIP with a 5/16" shaft thickness.
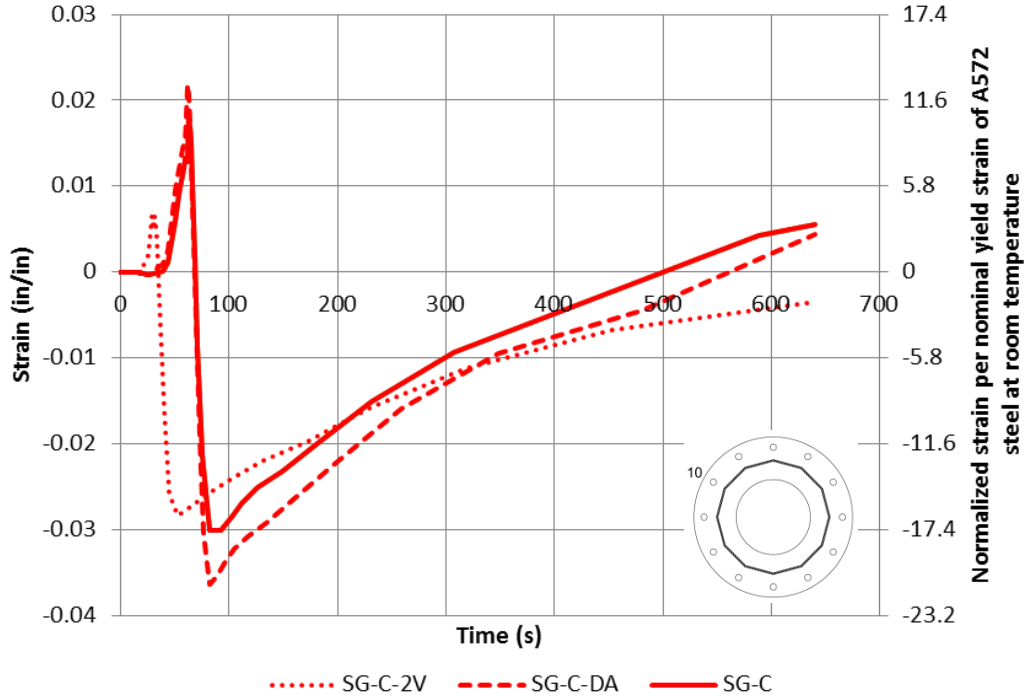
Figure 7-12: Parametric study results for SG-C

The results from the parametric study on SG-C at bend 10 are shown in Figure 7-12. Model run
SG-C-2V shows the effect of doubling the rate of dipping from SG-C to 1.05 in/s, and model run
SG-C-DA changes the dipping angle from 8° to 4° off the horizontal.

Figure 7-12 shows the effects of increasing the dipping rate and decreasing the dipping angle.
Both of these variables seem to have an inverse effect on strain development. Decreasing the
dipping angle results in higher maximum strains in tension and compression, while increasing the
dipping rate decreases maximum tension and compression strains. Of these two parameters, the
rate of dipping has a greater impact on the development of strains as a function of time during
dipping.

Despite the reduction in strain by increasing the dipping rate to 1.05 in/s, the tensile strains are
still significant (nearly 3.8 times nominal yield strain). And furthermore, the fastest any model
pole was hot dipped was SG-SC at 0.719 in/s, a value substantially less than the 1.05 in/s shown
above. This difference in dipping rates indicates that even if SG-C were hot dipped at the same

rate as SG-SC, bend 10 would still develop significant tensile strains at the base plate to shaft connection. Despite the smaller impact that increased dipping rate has on strain development, the reduction in tensile straining is worthy of notation. Should additional research be conducted on this topic, the effect of rapid dipping on strain gradient development should be explored.

Most importantly, this study emphasizes the significant impact HMIP wall thickness has on the development of strains at the base plate to shaft connection. No other parameter influenced the strain profile at bend 10 as severely as the reduction in shaft thickness when compared to models SG-SA and SG-SC.

7.6   Summary

Performing finite element analyses after observing the galvanization of 33-3-12-TX-SG-C, 33-3-12-TX-SG-SA, and 33-3-12-TX-SG-SC has given greater insight into what mechanisms may have a significant role in crack formation. Observing localized strains at shaft bends from finite element analysis verifies that a great difference in thermal strains develops during dipping as a function of HMIP shaft thickness. While the greatest strains observed were in compression, significant tensile strains were observed in the 5/16" HMIP model, SG-C. This finding coincides with typical crack locations observed in Chapter 5. Since cracks also have been found in bends which do not exhibit substantial straining from thermal loads, it is possible that other sources such as residual stresses from welding also play a key part in the failure mechanisms that lead to cracking as well. In either case, the results of this finite element analysis verify the importance of decreasing the nominal d/t ratio to reduce strain concentrations at shaft bends, and to reduce the likelihood of formation of cracks during galvanizing.

CHAPTER 8.   CONCLUSIONS AND RECOMMENDATIONS

The research presented in this thesis included an overview of field monitoring of HMIP sections as well as parametric finite element analyses of pole sections during the galvanizing process. The goal of the study was to determine the cause of cracking between the shaft and base plate connection and to propose design modifications that can help mitigate the cracking problem. This chapter provides a summary of the resulting conclusions from the study. Conclusions presented in this chapter are divided into four sections: Experimental Conclusions, Analytical Conclusions, Fabrication Recommendations, and Research Recommendations.

8.1   Experimental Conclusions

- Formation of galvanizing cracks in HMIPs can occur regardless of "non-reactive" bath chemistry and shaft bend diameters. Galvanized coatings do not change the mechanical properties of steel after application.

- Monitoring HMIP temperatures using embedded thermocouples can be successfully achieved even in shallow plate elements by using an adequate amount of high-temperature adhesive. Using high temperature adhesive was the most effective way of connecting thermocouples and recording temperatures during galvanizing.

- No formally codified galvanizing procedure is currently implemented for hot dipping HMIPs.

- Significant thermal gradients develop within HMIPs near the pole shaft to base plate weld during galvanizing primarily due to the difference in plate thicknesses used for pole shafts and base plates.

- Stub HMIP sections adequately model the behavior of full length HMIP tests specimens and may be effectively used for galvanizing crack tests.

- Galvanizing cracks form on HMIPs with and without external collars (or ground sleeves).

- When galvanizing cracks form on HMIPs, they usually form at the toe of the base plate to shaft weld, and typically concentrate near each other. The exception is that these cracks do not form in seam welds, though they might form beside a seam weld.

- The HMIP specimen tested with an external collar and 0" full penetration weld root opening exhibited the worst performance compared to sections with larger root openings. The section with 0" root opening cracked at every bend after galvanizing. More tests should be conducted to validate that 0" root openings should be avoided: it appears likely that this condition exacerbates conditions necessary to form galvanizing cracks.

8.2   Analytical Conclusions

- The convective heat transfer coefficient has a large effect on the flow of heat into a system and, therefore, also has a large bearing on the development of thermal strains.

- The strain gradients that develop across the cross section of the HMIP vary along the perimeter of the pole. Particularly near the base plate to shaft connections, hotspots develop at shaft bends that exhibit very different straining than the adjacent flat shaft sections. The formation of these hotspot stresses coincide with the formation of galvanizing cracks in HMIPs with high shaft diameter to shaft thickness ratios.

- The base plate section of HMIPs fabricated using the TxDOT 80 mph 150' design with a 5/16" shaft thickness performs many times worse than HMIPs of the same design with a 7/16" or 8/16" shaft thickness during galvanization. The reduction in shaft thickness exacerbates localized straining at shaft bends near base plate to shaft connections. In some bends this can lead to substantial tensile strains.

- Slight variations in dipping angle do not seem to have a dramatic effect on the thermal loading of a system, nor the development in strains; however, as the shaft becomes thinner, the effects of changing dipping parameters become greater. In the case of the finite element model HMIP with a shaft thickness of 5/16", the reduction of the dipping

127

angle from 8° to 4° resulted in larger tensile and compressive strains.

- Increasing the velocity of dipping seems to reduce the formation of tensile strains in bends with characteristically high tensile strains, such as bend 10 on model SG-C.

- The most effective means of decreasing the magnitude of tensile and compressive strains at base plate to shaft connections is to increase the thickness of the shaft. In all tested submodels, an increase in shaft thickness mitigated the formation of tensile strains and reduced compressive strains between 25% and 400%.

8.3 Design Recommendations

- After running the analyses, the most straight forward way to minimize the possibility of galvanizing crack development is to keep d/t ratios to a lower value. The nominal ratio experimentally proven not to develop cracks is approximately 75. To be safe, researchers recommend not exceeding a d/t ratio of 70 to mitigate the formation of galvanizing cracks at base plate to shaft connections in HMIPs.

- Conducting thermal and structural analyses on HMIPs gives credence to controlling the sources of thermal loading in these systems. Parametric studies conducted by the author indicate that dipping parameters such as speed and angle of dipping may have a significant impact on the development of strains at critical regions. It is the opinion of the author that purchasers of HMIPs and professional organizations such as American Galvanizers Association should consider adopting policies and standards of practice whereby galvanizing plant crane operators dip specimens in ways that seek to reduce the formation of large strains at critical regions consistent with current research. Professional organizations and private entities should also consider funding additional research to determine the most effective way to dip HMIPs so that these strains are reduced.

8.4 Research Recommendations

- As this project sought to provide a basis for understanding the implications of thermal strains during the galvanizing process, assumptions needed to be made with regards to

many key variables—many of which could have entire research projects dedicated to their exploration.

- o The convective heat transfer coefficient should be better understood with relation to different locations along the length of the HMIP. Also, galvanizing is a violent process that results in turbulent flow characteristics around the HMIP when the bath comes in contact with flux. After a short period of time, the turbulent bubbling around the HMIP subsides, but such a change in contact characteristics between the molten bath and HMIP have a local effect on the heat flux into the HMIP system. All of these thermodynamic considerations should be better understood.

- o Eurocode 3 (2003) parameters were used to provide all structural properties for HMIPs. These parameters were derived for fire-loading conditions and therefore do not account for the rapid temperature gains observed during galvanizing. Material properties for steel should be researched under these heating conditions to determine how an increased rate of heat absorption affects thermal and structural properties.

- o The effect of residual stresses in full penetration welds at base plate to shaft connections should be analyzed, in light of the research discussed within this thesis, to better determine the effect of straining in the galvanizing crack phenomenon.

- Future research should also focus on sensitivity of dipping parameters on HMIPs with different values of the shaft thickness. Particularly, research should be applied to examining the effect of severely increasing the dipping angle, and altering the dipping speed as a means for determining the relationship between what is done on the galvanizing plant floor and the effect these practices have on the final product. Hopefully such research could inform industry standards which could be used to govern the dipping of HMIPs.

- Additional research should pursue a greater understanding of the development of strains in HMIPs during the whole galvanizing process. This thesis only focuses on what

happens during the dipping phase. Additional research should explore the behavior of HMIPs during air cooling of galvanized specimens and/or quenching.

This page intentionally left blank.

APPENDIX A. HIGH MAST POLE DESIGN DRAWINGS

A.1   January 2010 Test Specimen Drawing

A.1.1   Specimens 33-3-12-TXEC-SG-A and 33-3-12-TXEC-SG-B

Figure A-1: Design drawing for specimens 33-3-12-TXEC-SG-A and 33-3-12-TXEC-SG-B

A.2 June 2010 Test Specimen Drawings

A.2.1 33-3-12-TXEC-SG-SA

Figure A-2: Design drawing for specimen 33-3-12-TXEC-SG-SA

133

A.2.2 Specimen 33-3-12-TXEC-SG-SC
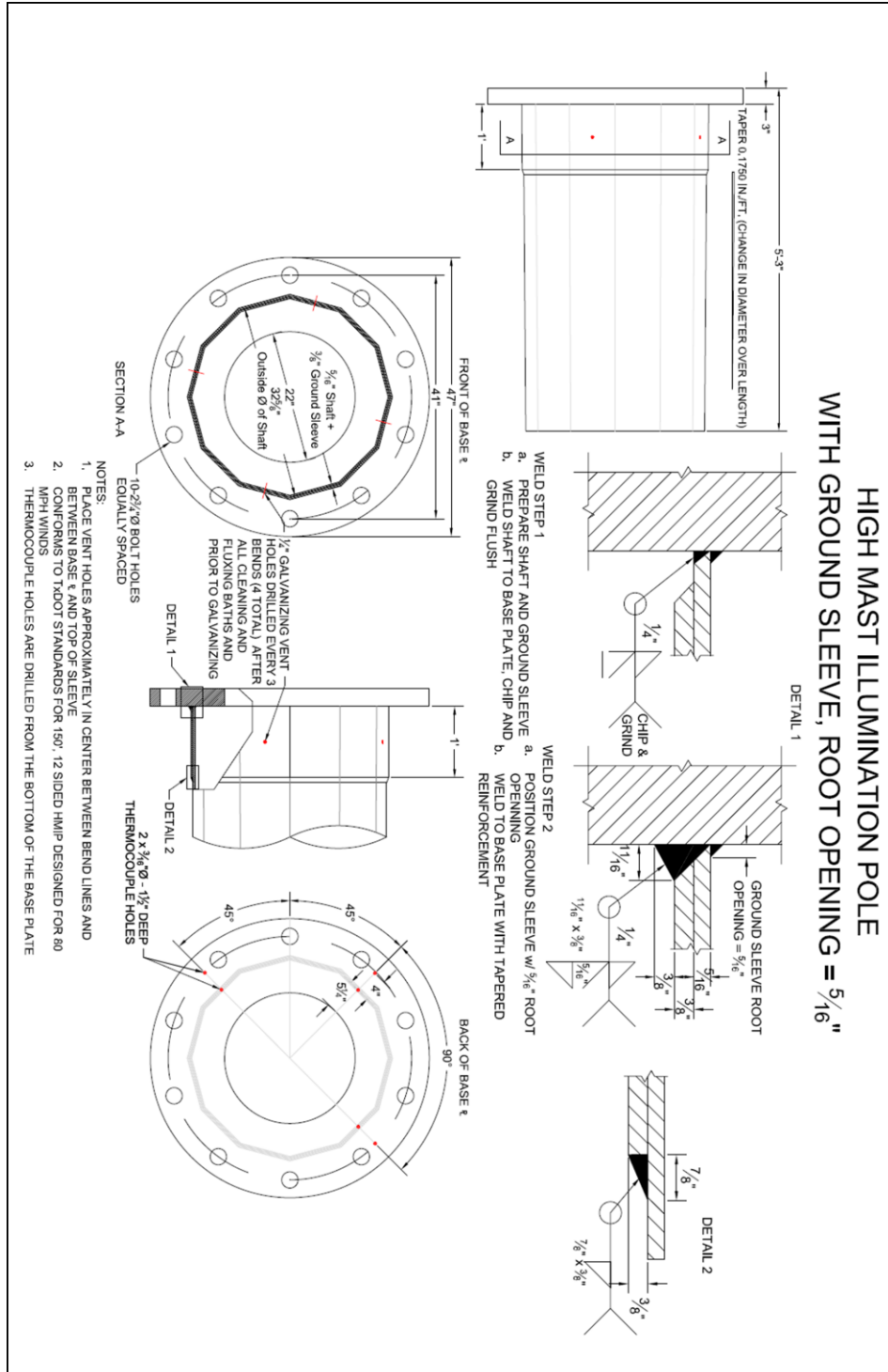
Figure A-3: Design drawing for specimen 33-3-12-TXEC-SG-SC

A.2.3 Specimen 33-3-12-TX-SG-SB
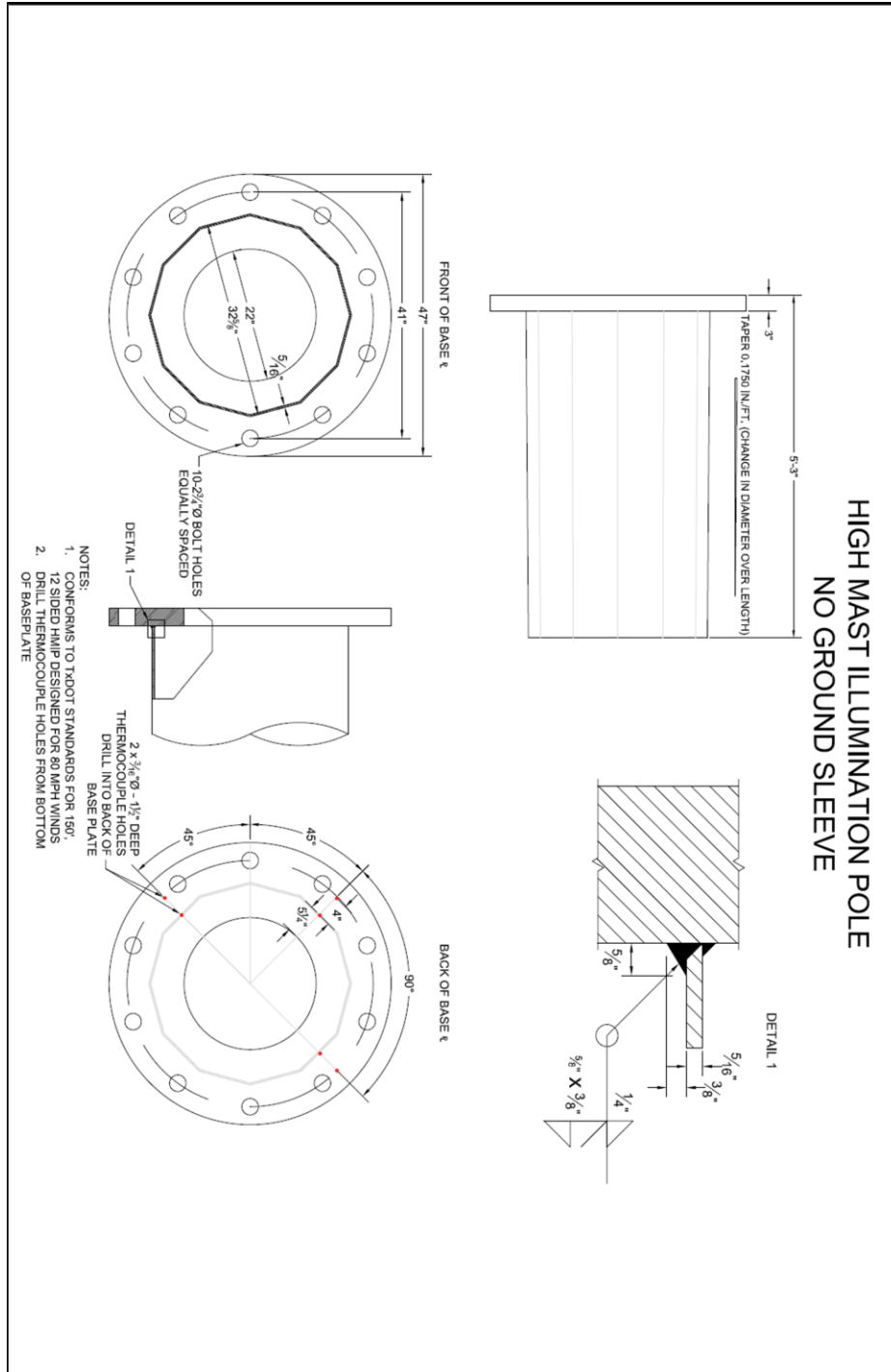
Figure A-4: Design drawing for specimen 33-3-12-TX-SG-SB

A.3   February 2011 Test Specimen Drawings

A.3.1   Specimen 33-3-12-TX-SG-C
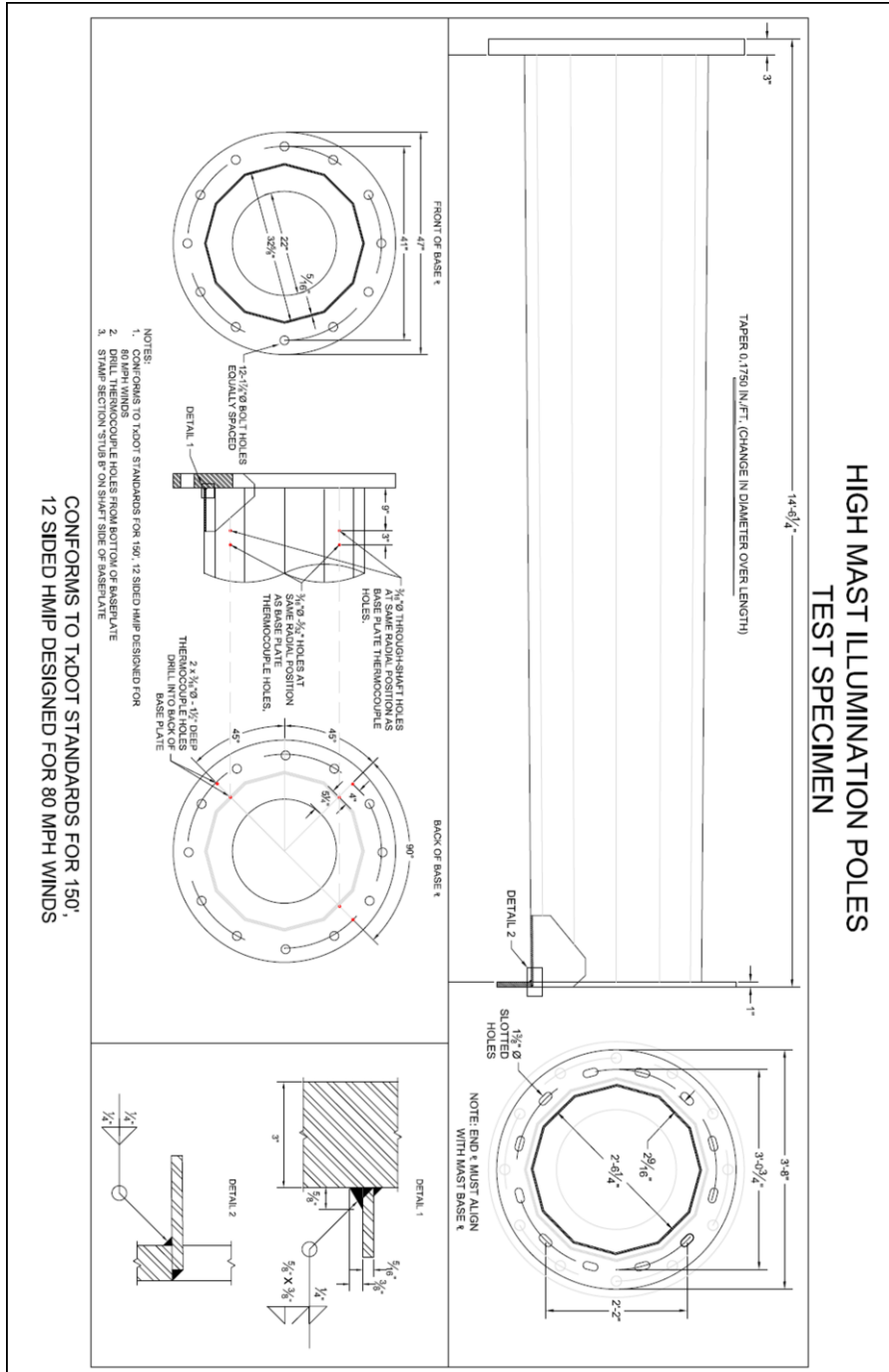
Figure A-5: Design drawing for specimen 33-3-12-TX-SG-C

A.3.2 Specimen 33-3-12-TX-SG-SA
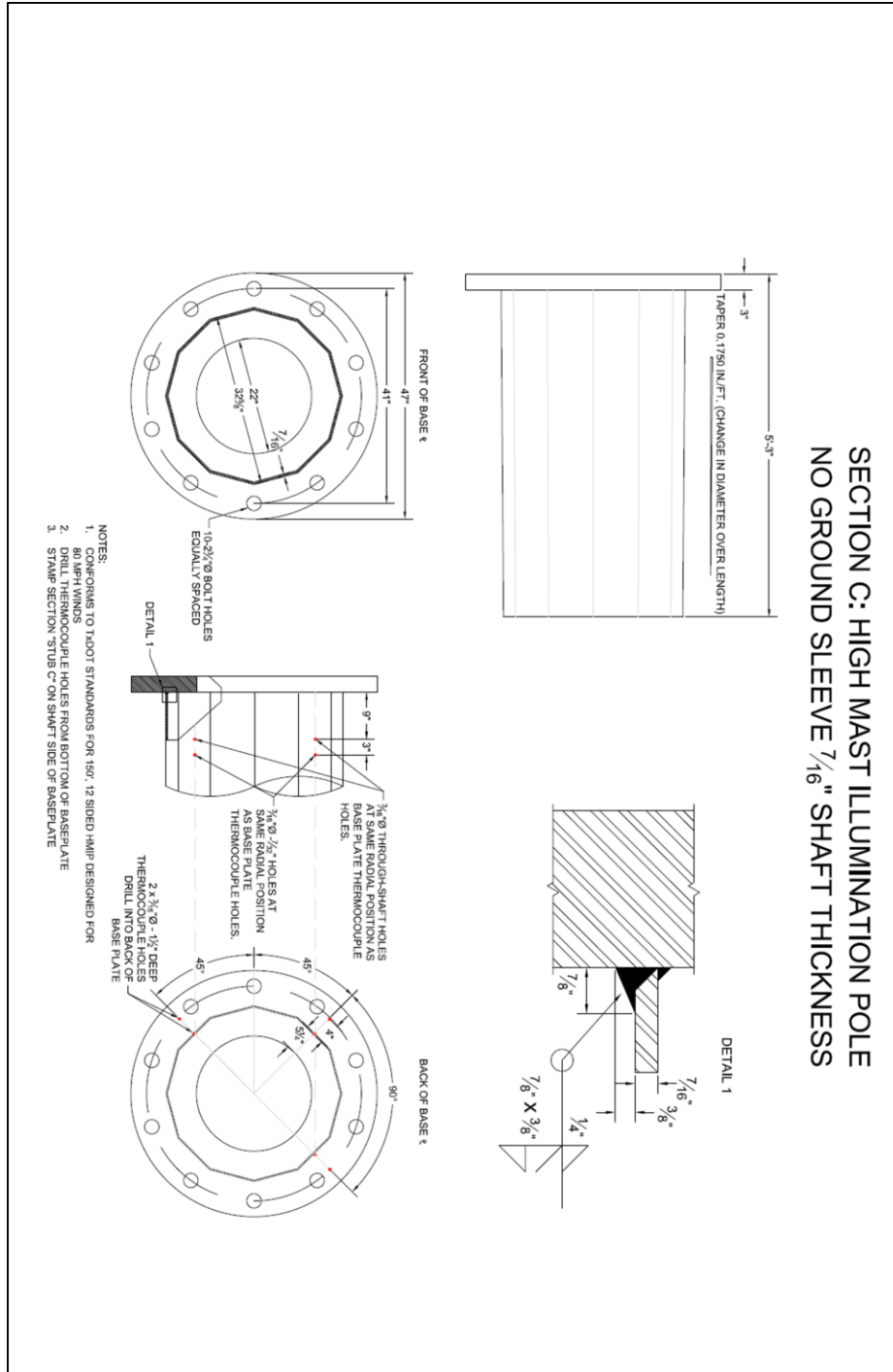
Figure A-6: Design drawing for specimen 33-3-12-TX-SG-SA

A.3.3 Specimen 33-3-12-TX-SG-SC
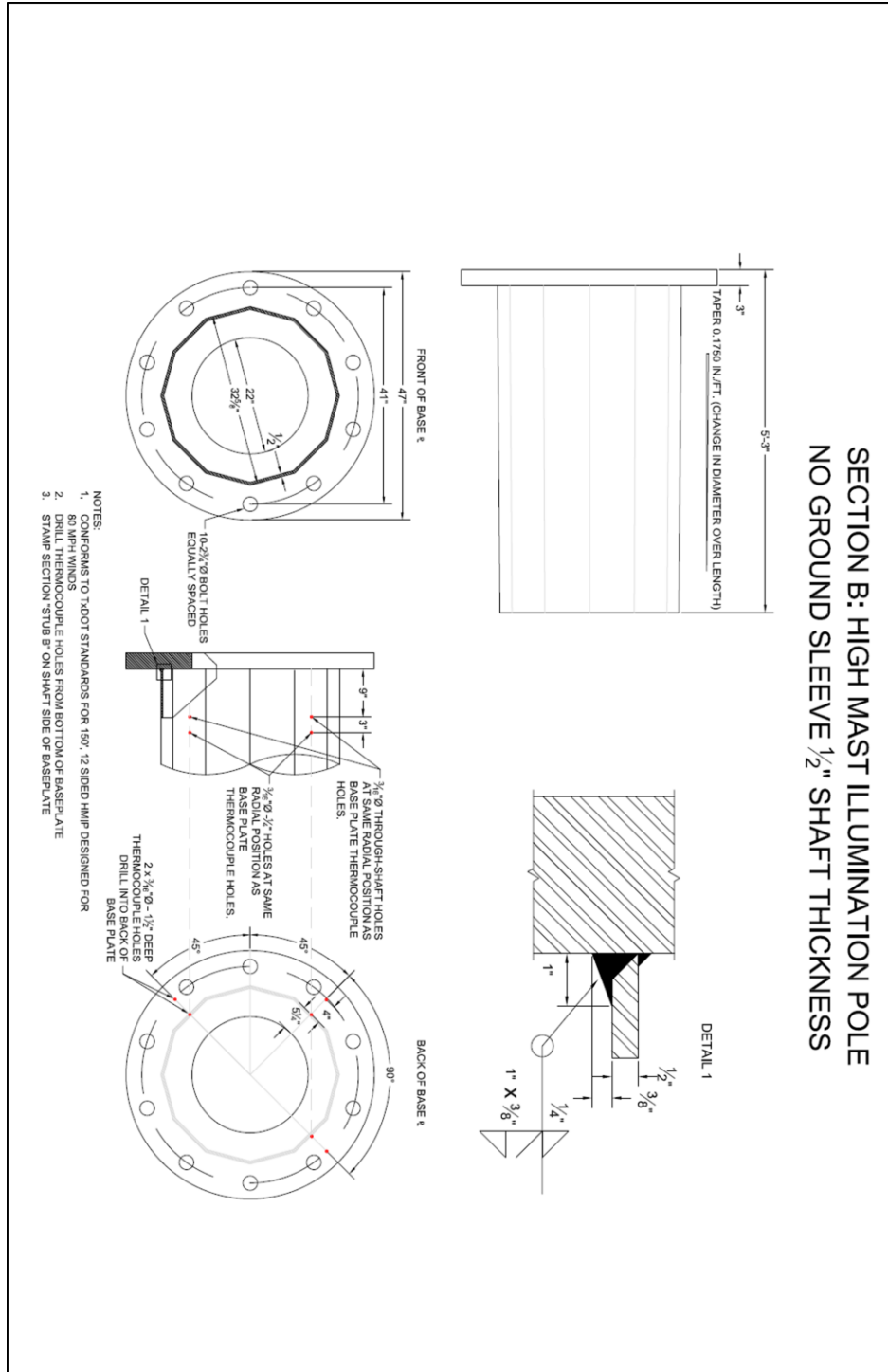
Figure A-7: Design drawing for specimen 33-3-12-TX-SG-SC

APPENDIX B. THERMAL TEST RESULTS

B.1   January 2010 Test Results

B.1.1   Specimen 33-3-12-TXEC-SG-A
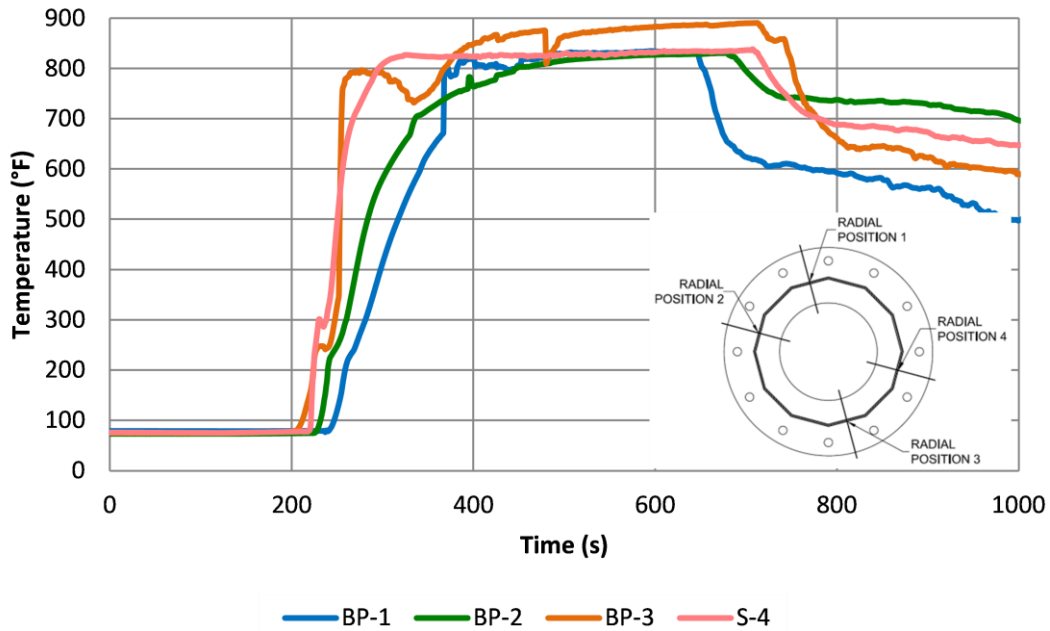
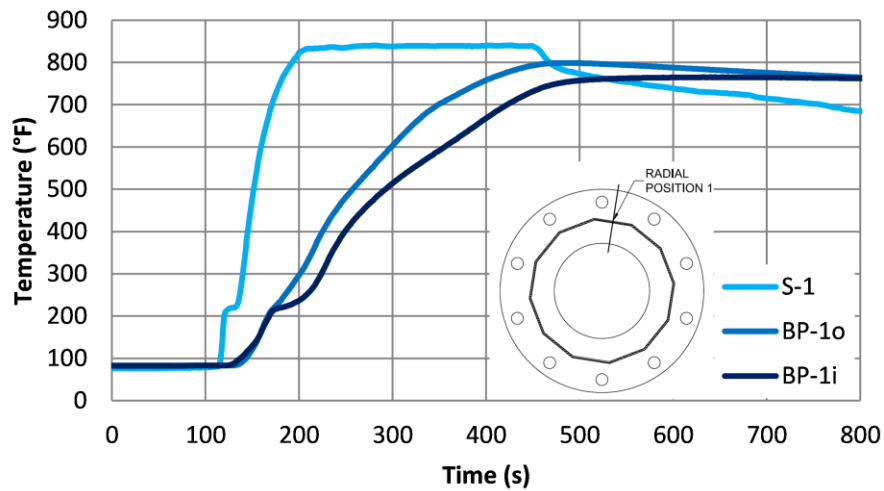**Figure B-1: Temperature vs. time graph of specimen 33-3-12-TXEC-SG-A during galvanizing**

B.1.2   Specimen 33-3-12-TXEC-SG-B
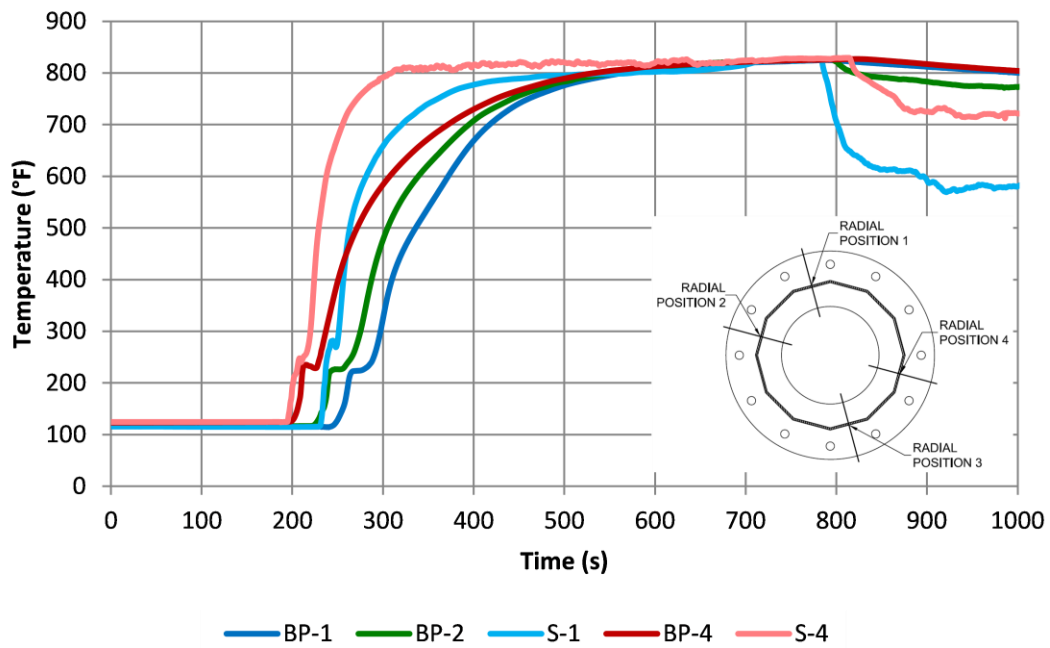
Figure B-2: Temperature vs. time graph of specimen 33-3-12-TXEC-SG-B during galvanizing
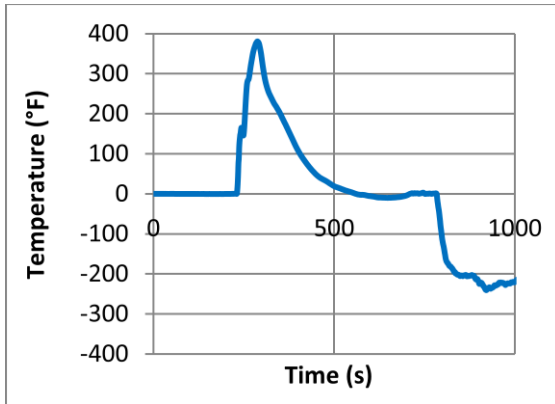
Figure B-3: Temperature difference between S-1 and BP-1 of 33-3-12-TXEC-SG-B
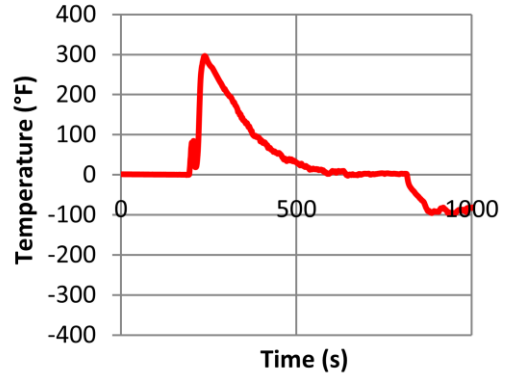
**Figure B-4: Temperature difference between S-4 and BP-4 of 33-3-12-TXEC-SG-B**
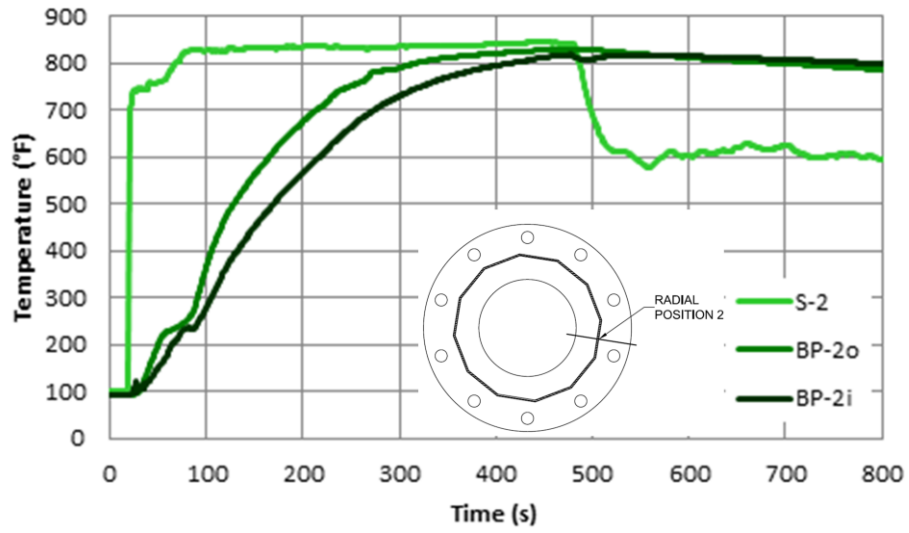
Figure B-7: Temperature vs. time graph of specimen 33-3-12-TXEC-SG-SA during galvanizing at radial position 2
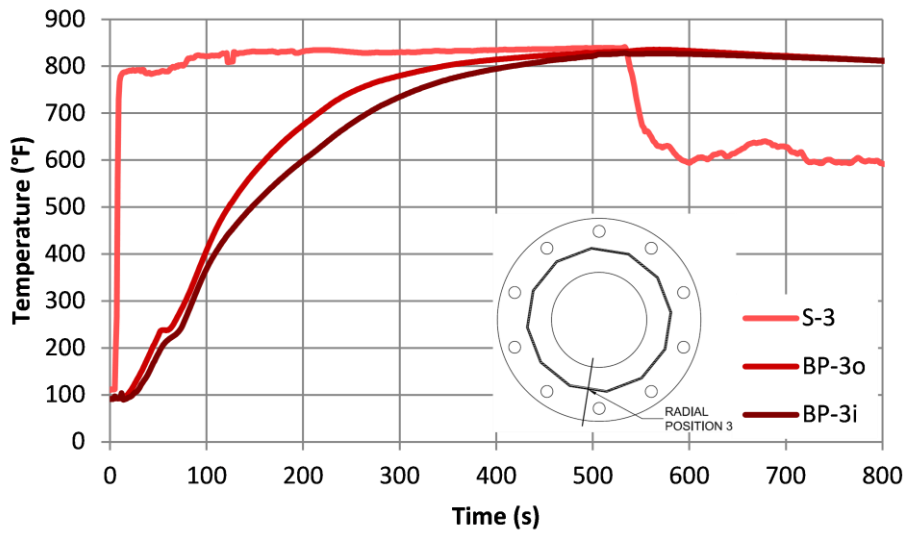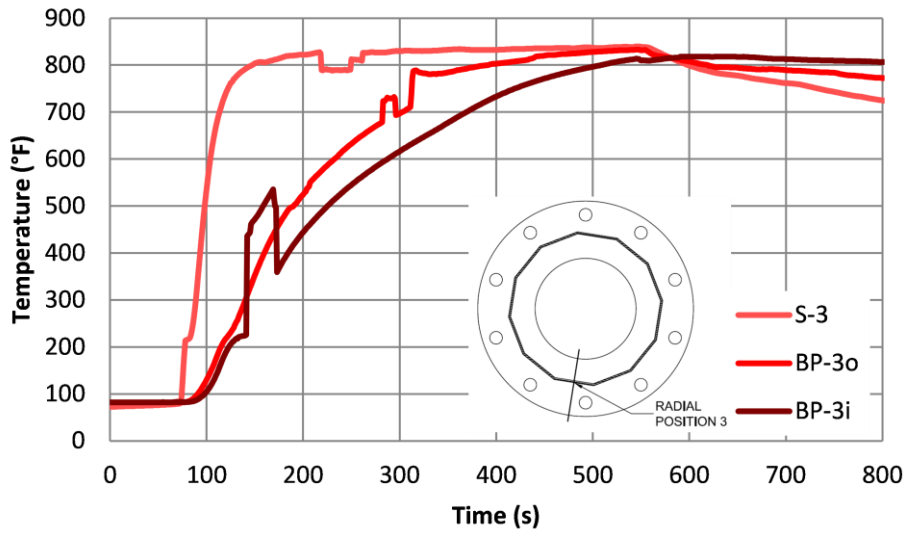

Figure B-8: Temperature vs. time graph of specimen 33-3-12-TXEC-SG-SA during galvanizing at radial position 3
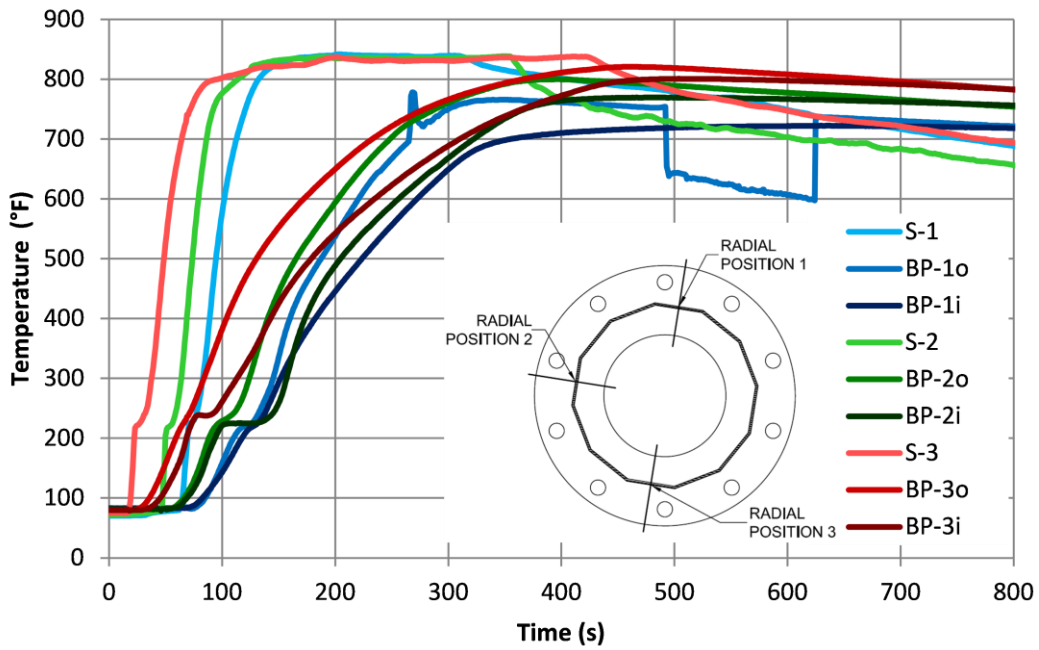
B.2.2   Specimen 33-3-12-TX-SG-SB
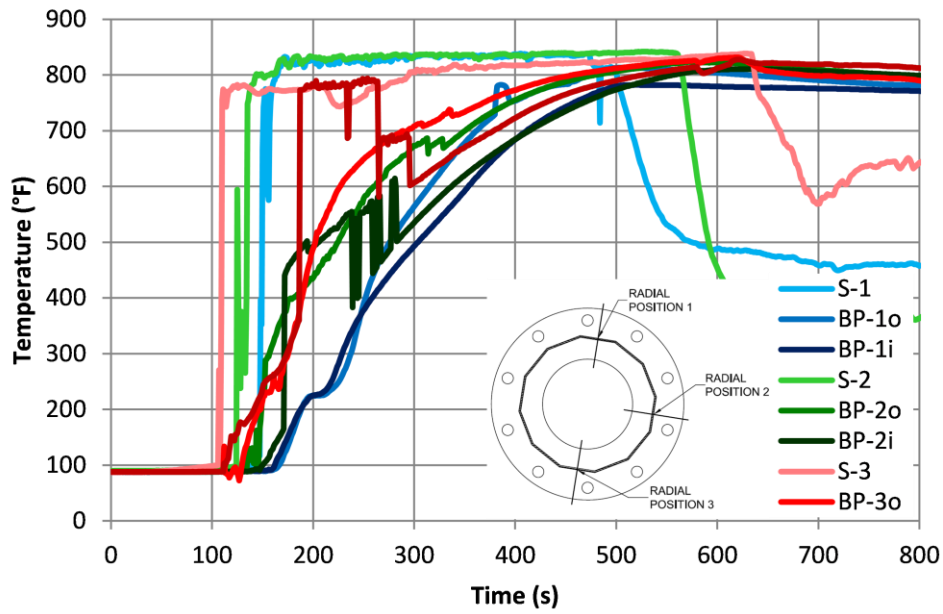
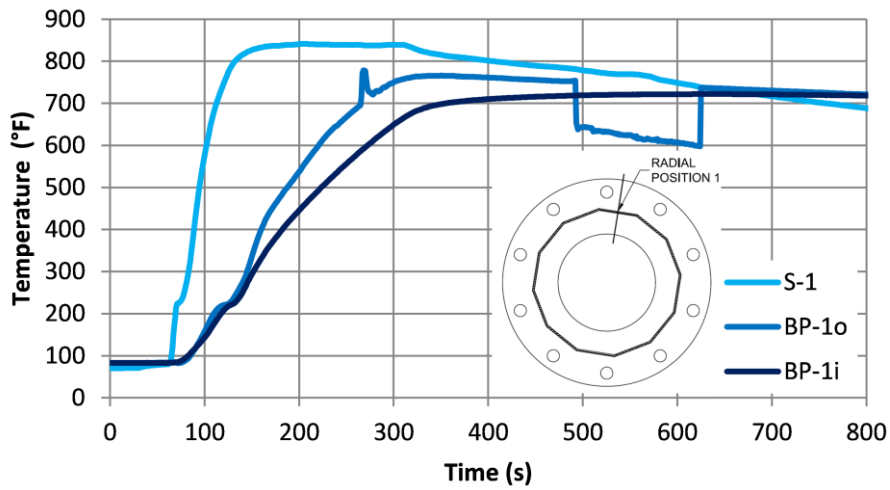Figure B-9: Temperature vs. time graph of specimen 33-3-12-TX-SG-SB during galvanizing
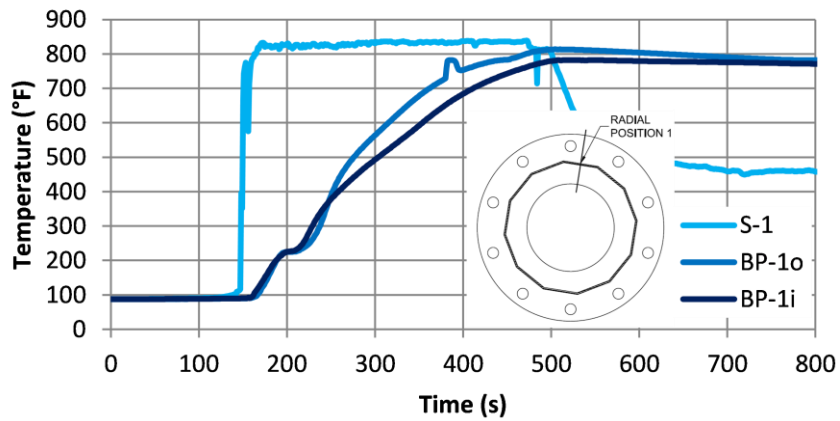
Figure B-10: Temperature vs. time graph of specimen 33-3-12-TX-SG-SB during galvanizing at radial location 1
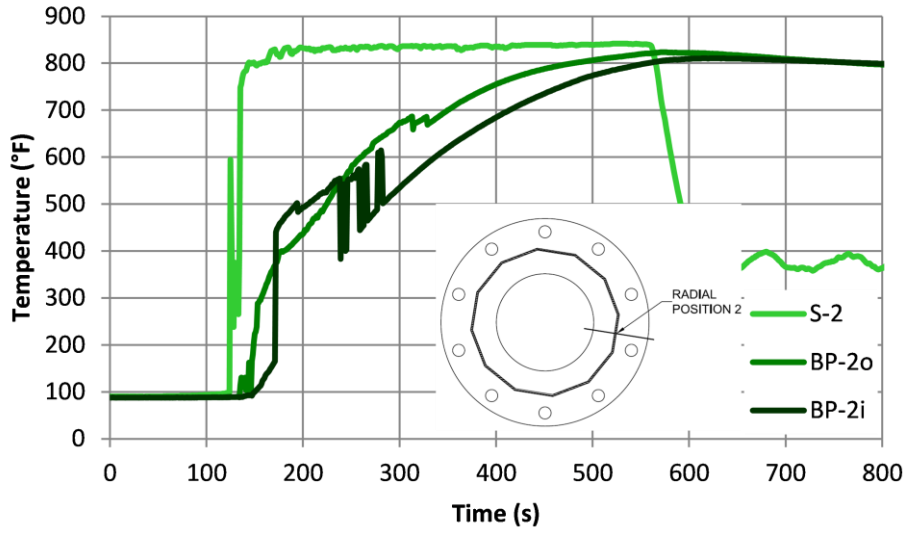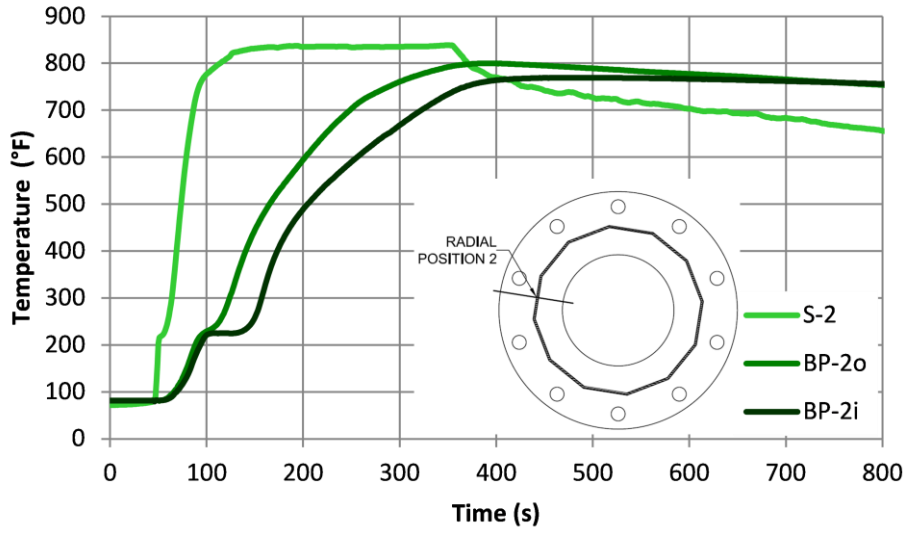
Figure B-11: Temperature vs. time graph of specimen 33-3-12-TX-SG-SB during galvanizing at radial location 2
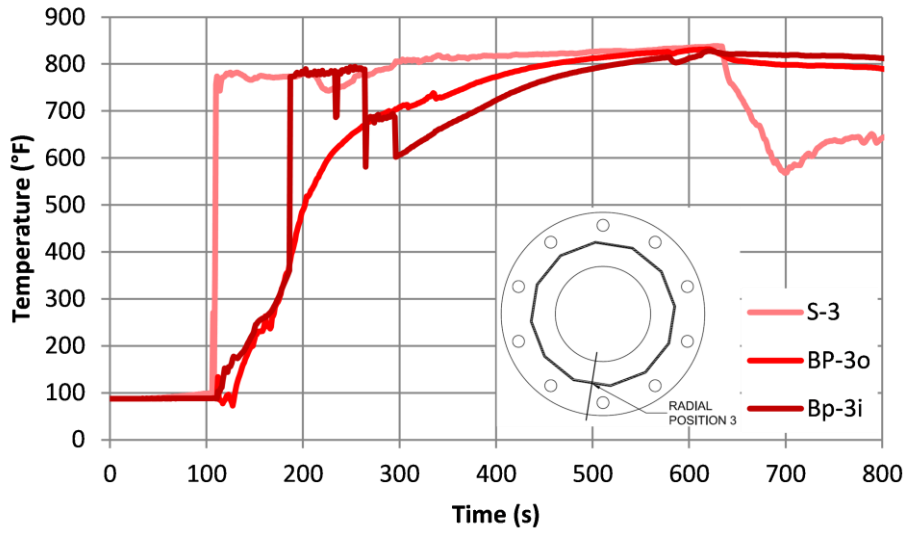
Figure B-12: Temperature vs. time graph of specimen 33-3-12-TX-SG-SB during galvanizing at radial location 3

B.3   February 2011 Test Results

B.3.1   Specimen 33-3-12-TX-SG-SA
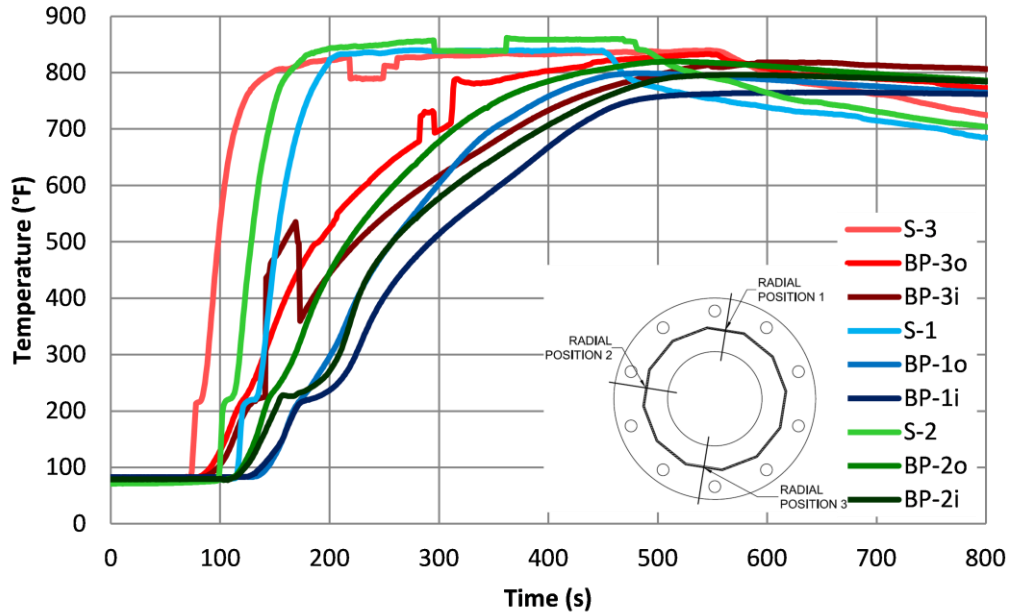
Figure B-13: Temperature vs. time graph of specimen 33-3-12-TX-SG-SA during galvanizing

Figure B-14: Temperature vs. time graph of specimen 33-3-12-TX-SG-SA during galvanizing at radial location 1
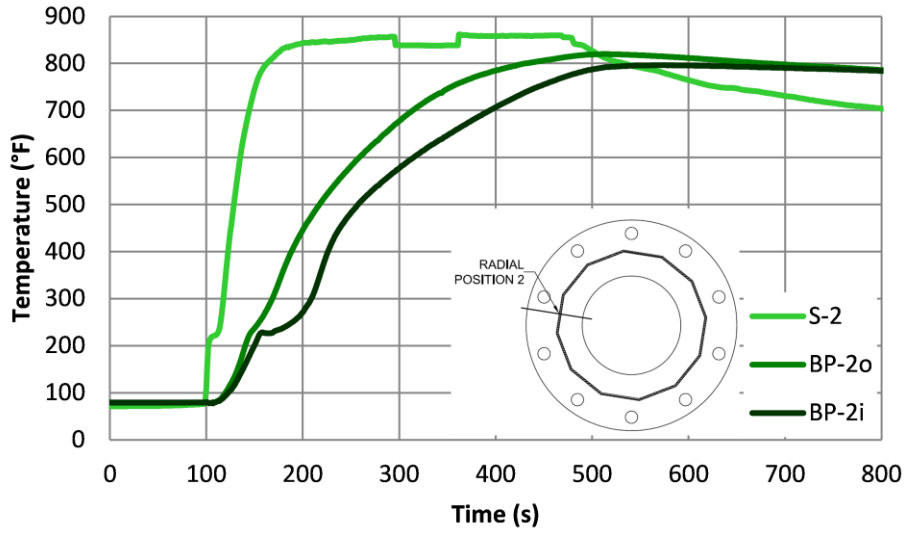
Figure B-15: Temperature vs. time graph of specimen 33-3-12-TX-SG-SA during galvanizing at radial location 2
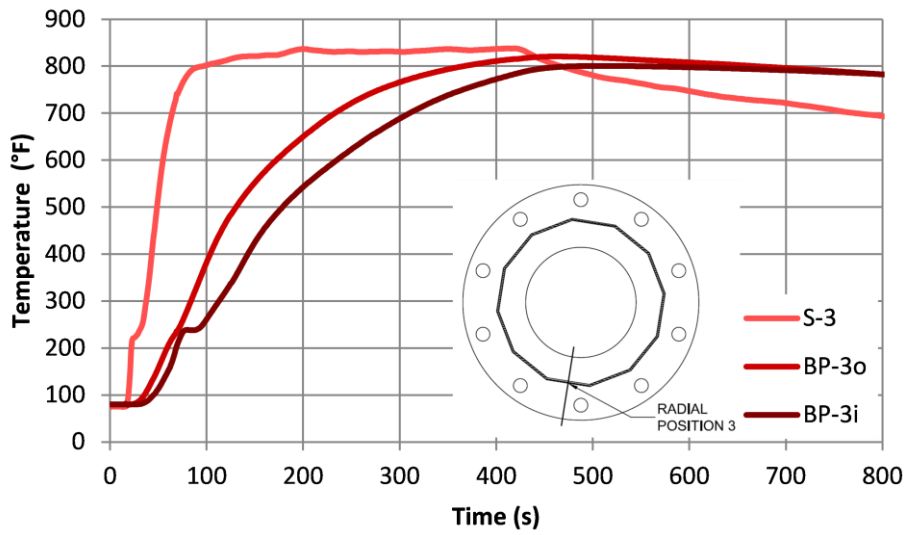

Figure B-16: Temperature vs. time graph of specimen 33-3-12-TX-SG-SA during galvanizing at radial location 3

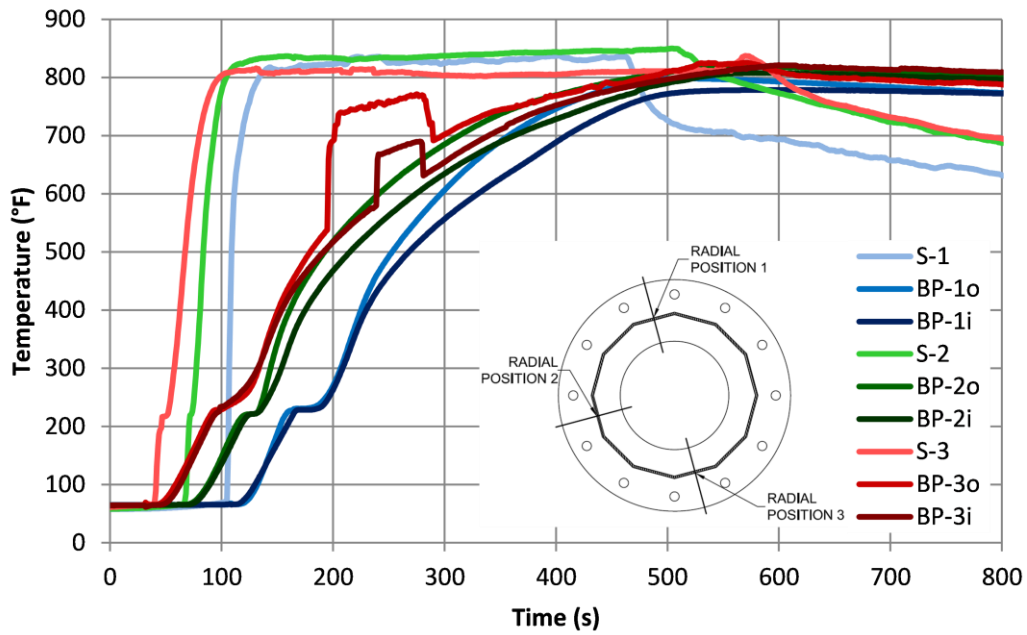**B.3.2   Specimen 33-3-12-TX-SG-SC**

Figure B-17: Temperature vs. time graph of specimen 33-3-12-TX-SG-SC during galvanizing
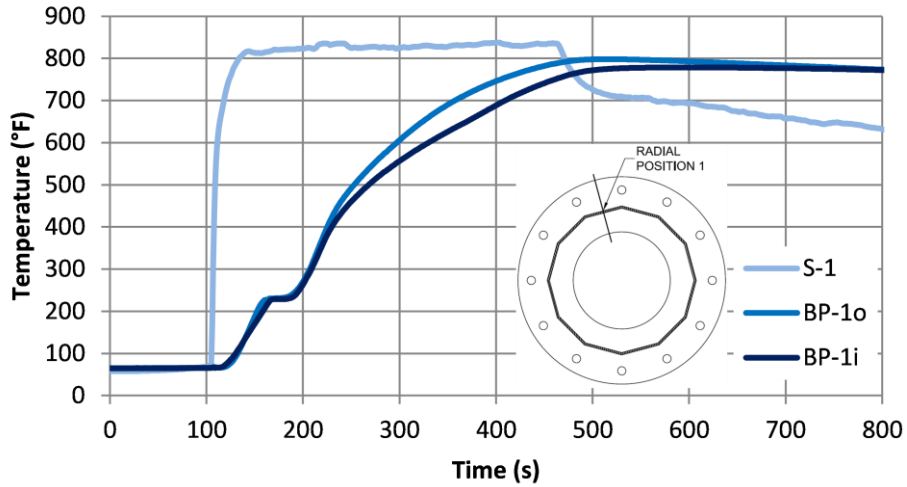

Figure B-18: Temperature vs. time graph of specimen 33-3-12-TX-SG-SC during galvanizing at radial location 1
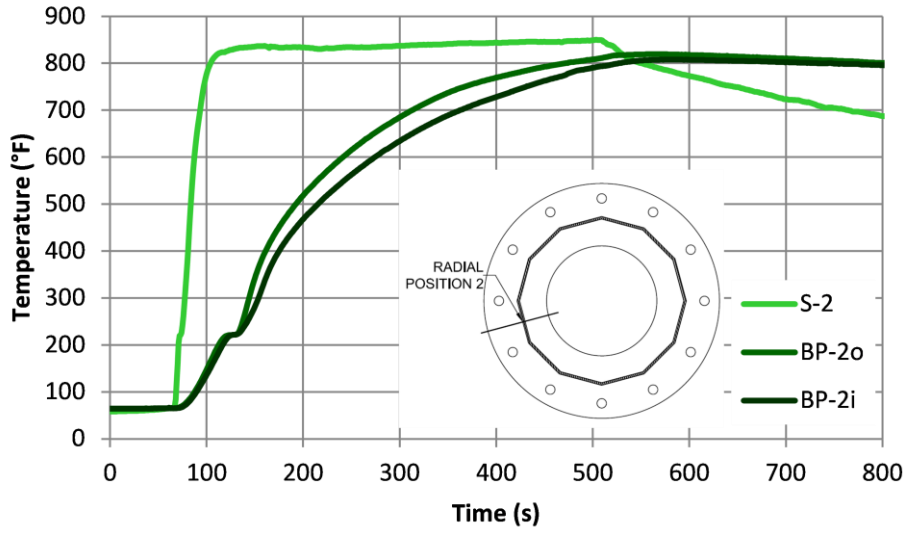
Figure B-19: Temperature vs. time graph of specimen 33-3-12-TX-SG-SC during galvanizing at radial location 2

Figure B-20: Temperature vs. time graph of specimen 33-3-12-TX-SG-SC during galvanizing at radial location 3

B.3.3   Specimen 33-3-12-TX-SG-C

Figure B-21: Temperature vs. time graph of specimen 33-3-12-TX-SG-C during galvanizing

Figure B-22: Temperature vs. time graph of specimen 33-3-12-TX-SG-C during galvanizing at radial location 1

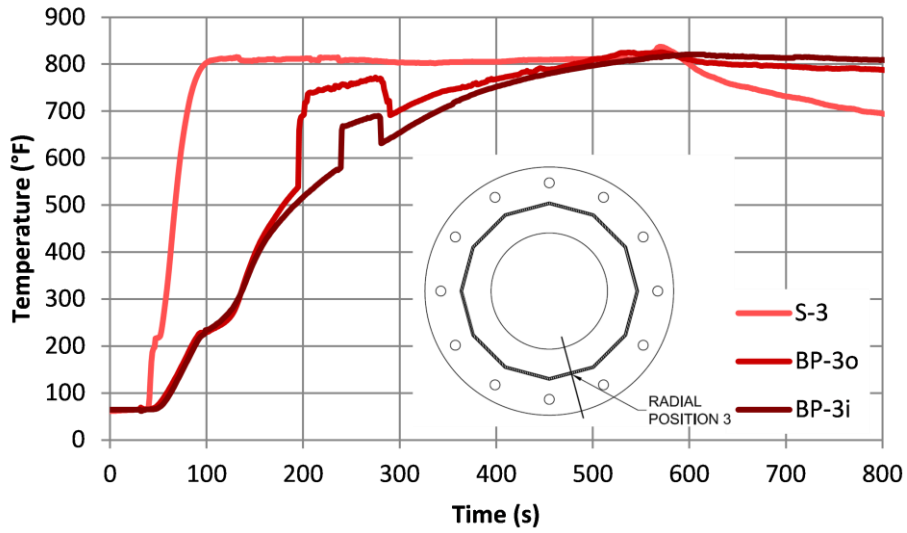**Figure B-23: Temperature vs. time graph of specimen 33-3-12-TX-SG-C during galvanizing at radial location 2**

Figure B-24: Temperature vs. time graph of specimen 33-3-12-TX-SG-C during galvanizing at radial location 3

APPENDIX C. TENSION TEST GRAPHS
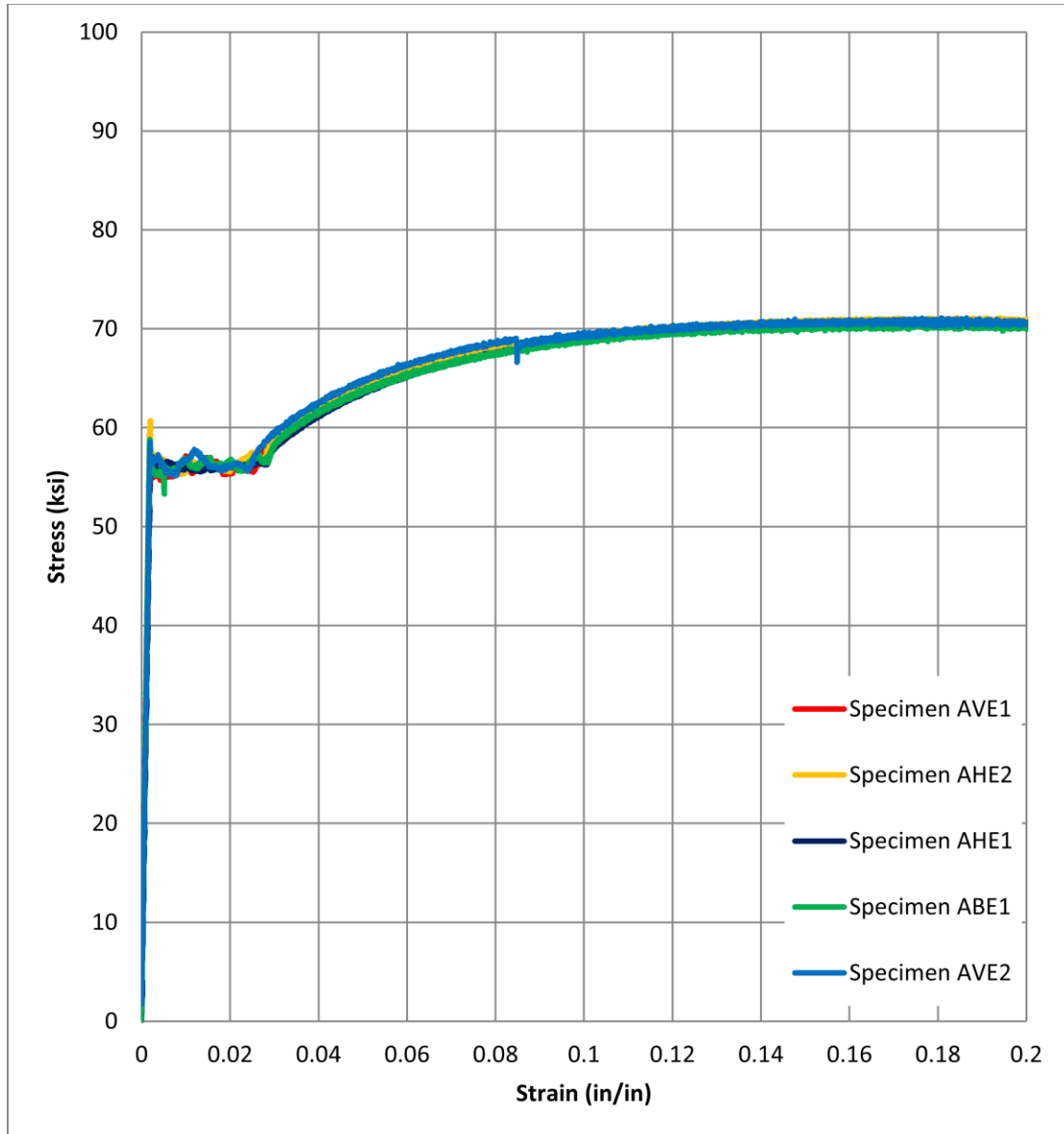
C.1   33-3-12-TXEC-SG-A

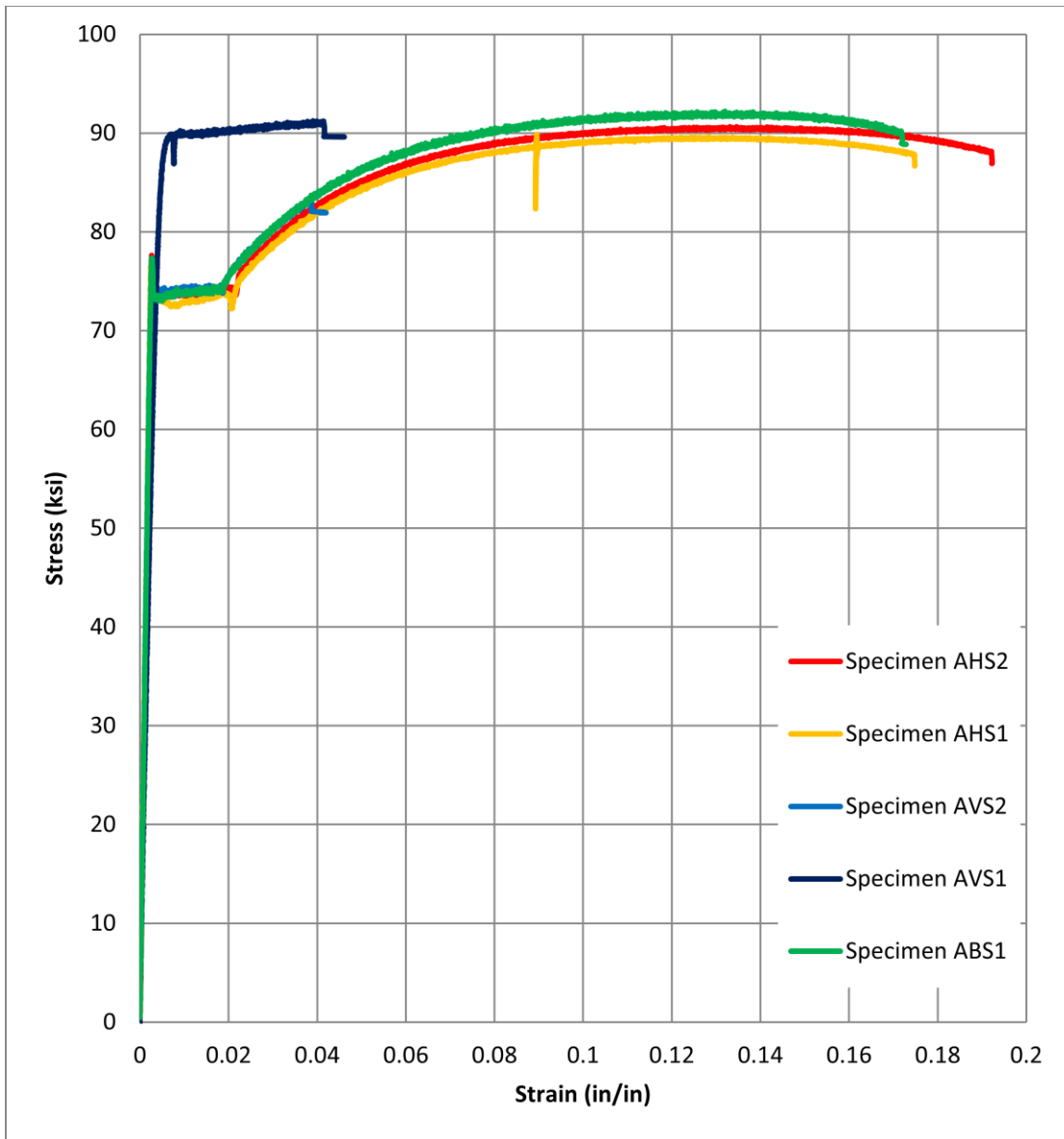**Figure C-1: Stress strain curve for specimen tested from 33-3-12-TXEC-SG-A external collar**

Figure C-2: Stress strain curve for specimen tested from 33-3-12-TXEC-SG-A pole shaft
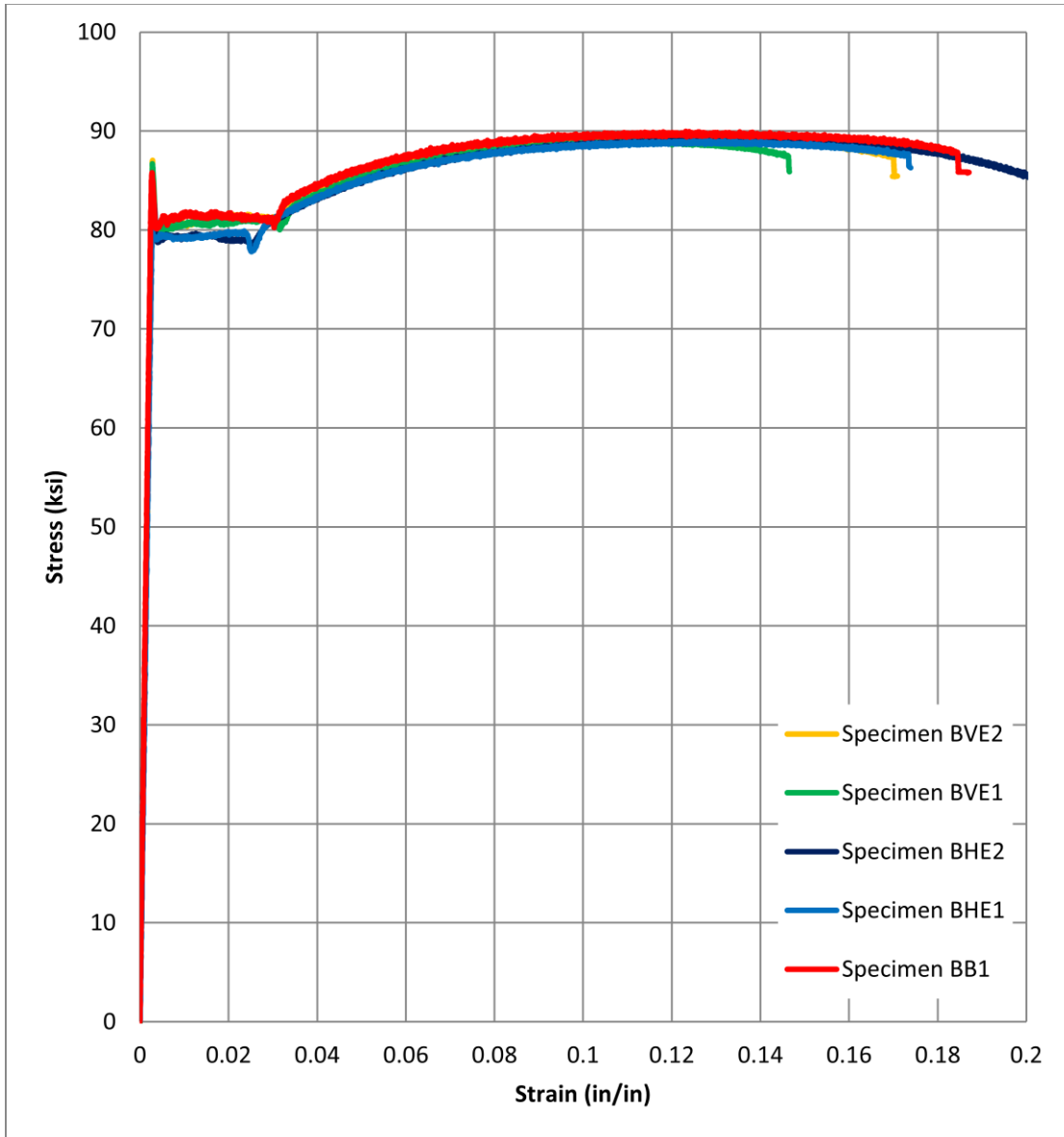
C.2   33-3-12-TXEC-SG-B

Figure C-3: Stress strain curve for specimen tested from 33-3-12-TXEC-SG-B external collar
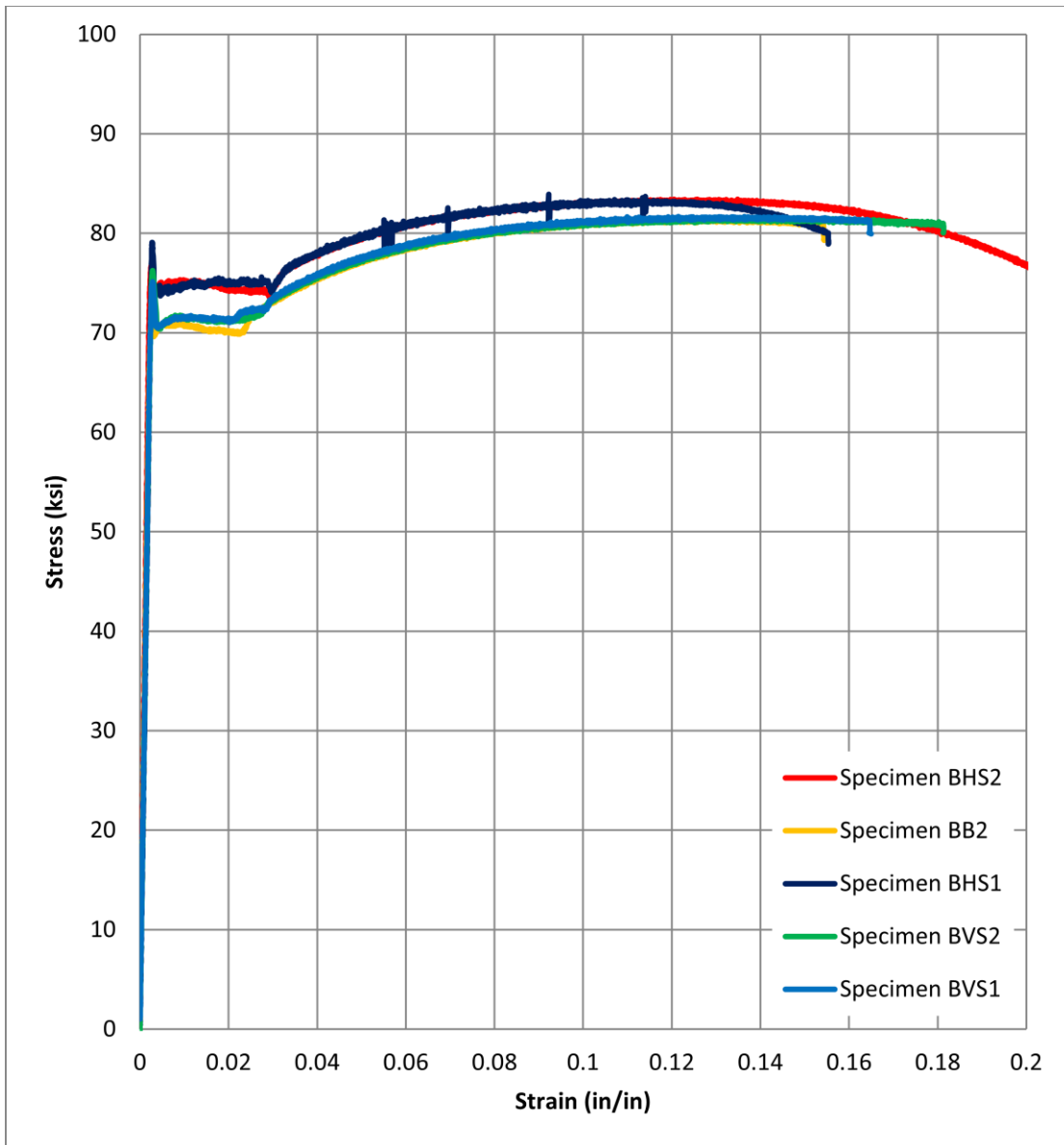
Figure C-4: Stress strain curve for specimen tested from 33-3-12-TXEC-SG-B pole shaft

APPENDIX D. STRAIN TEST RESULTS

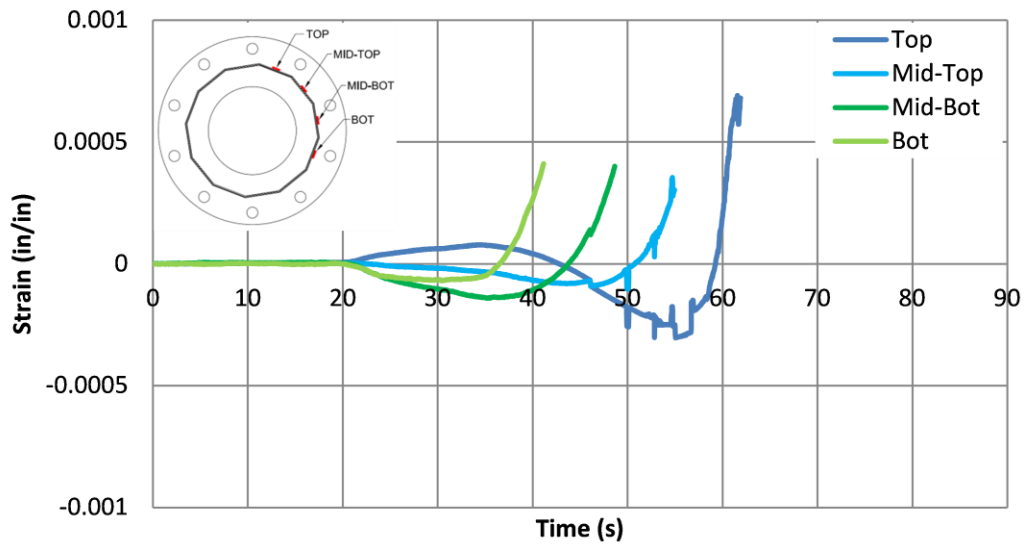## D.1   Specimen 33-3-12-TX-SG-SA

Figure D-1: Strain measurements from specimen 33-3-12-TX-SG-SA
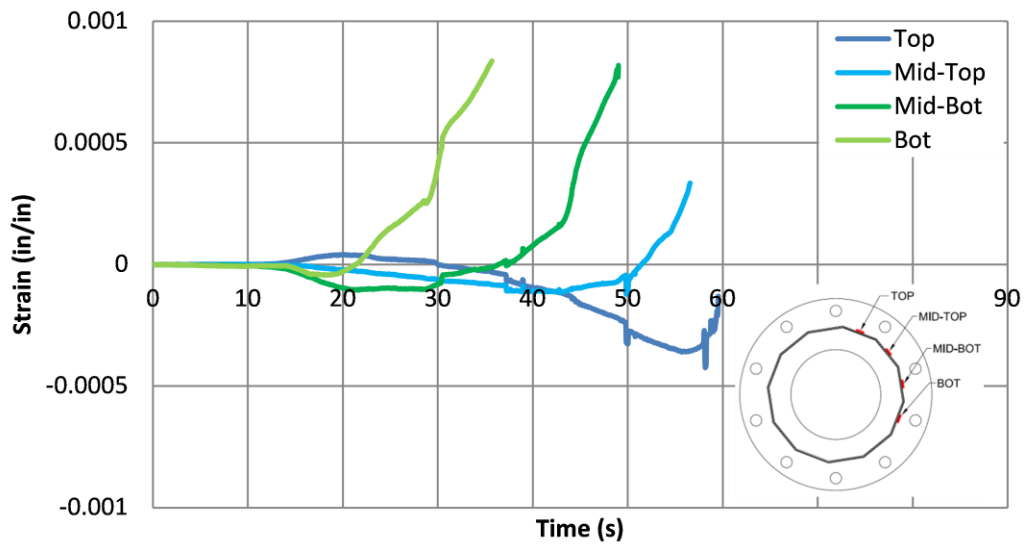
D.2   Specimen 33-3-12-TX-SG-SC

Figure D-2: Strain measurements from specimen 33-3-12-TX-SG-SC

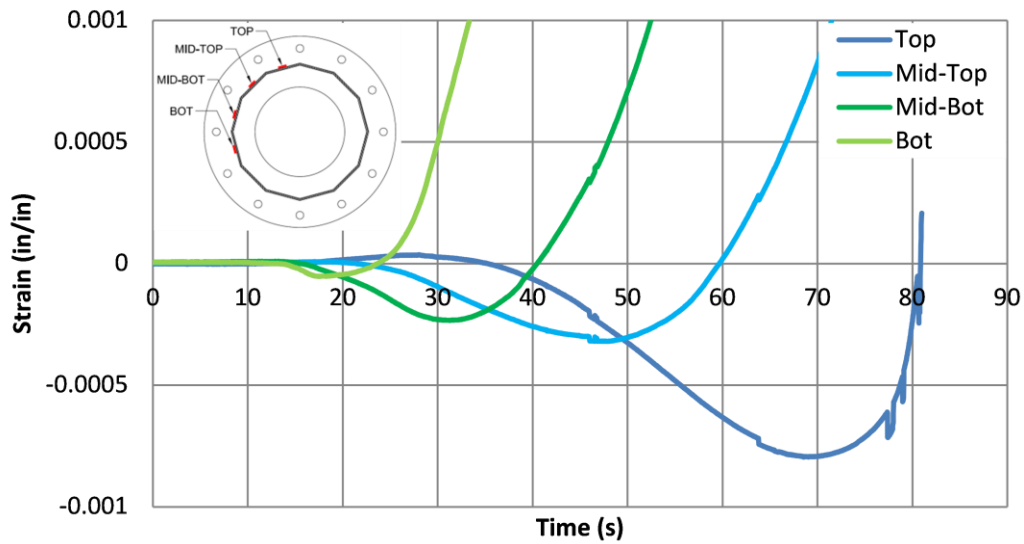## D.3   Specimen 33-3-12-TX-SG-C

Figure D-3: Strain measurements from specimen 33-3-12-TX-SG-C

References

Aichinger, R., Higgins, W. *Toe Cracks in Base Plate Welds – 30 Years Later*. Valmont Industries, Nebraska, 2006.

American Association of State Highway and Transportation Officials, *AASHTO Standard Specifications for Structural Supports for Highway Signs, Luminaries and Traffic Signals*. Fourth Edition, AASHTO, Washington, D.C., 2001.

American Galvanizers Association. <http://www.galvanizeit.org/aga/about-hot-dip-galvanizing/what-is-hot-dip-galvanizing/hdg-process>. Accessed Feb. 27, 2011. Copywrite 2008.

Çengel, Yunus A, and Robert H Turner. *Fundamentals of Thermal-Fluid Sciences*. 2nd ed. 2001. New York: McGraw, 2005.

European Committee for Standardization. Technical Committee CEN/TC 250. "Design of steel structures - Part 1-2: General rules - Structural fire design." *Eurocode 3*. 2003. 15-21, 40-41.

Feldmann, M., Pinger, T., Schäfer, Pope, R., Smith, W., Sedlacek, G. *Hot-dip-zinc-coating of prefabricated structural steel components*. JRC Scientific and Technical Reports, EUR 24286 EN – 2010.

Getting Started with ABAQUS. Version 6.6, Rising Sun Mills, Providence, RI, 2006.

Kinstler, T.J. *Current Knowledge of the Cracking of Steels During Galvanizing*. GalvaScience LLC, Springfield, Alabama, 2006.

Koenigs, Mark Thomas. *Fatigue Resistance of Traffic Signal Mast-Arm Connection Details*. Thesis. The University of Texas at Austin, May 2003.

Ocel, Justin Michael. *The behavior of thin hollow structural section (HSS) to plate connections*. Dissertation. University of Minessota, October, 2006.

Peil, Udo, and Michael Wichers. "Schweißen unter Betriebsbeanspruchung – Werkstoffkennwerte zur Temperaturfeldberechnung für einen S 355 J2 G3." *Steel Construction 74* 4, 2005: 249-257.

Pool, Charles Stephen. *Effect of Galvanization on the Fatigue Strength of High Mast Illumination Poles*. Thesis. The University of Texas at Austin. May 2010.

Reumont, G., Perrot, P., Foct, J. *Thermodynamic study of the galvanizing process in a ZN-0.1%Ni bath*. Journal of Materials Science, Vol. 33, pg. 4759-4768, 1998.

Richman, Nicholas B. *Fatigue Life Investigation of High Performance Mast Arm Base Plate Connections*. M.S. Thesis, Department of Civil Engineering, The University of Texas at Austin, May 2009 .

Rios, Craig Abel. *Fatigue Performance of Multi-Sided High-Mast Lighting Towers*. M.S. Thesis. The University of Texas at Austin, May 2007.

Scheider, I, W Brocks, and A Cornec. "Procedure for the Determination of True Stress-Strain Curves from Tensile Tests with Rectangular Cross-Section Specimens." *Journal of Engineering Materials and Technology* 126, Jan. 2004: 70-76.

Stam, Andrew Philip. *Fatigue Performance of Base Plate Connections Used in High Mast Lighting Towers*. M.S. Thesis. The University of Texas at Austin, May 2009.

Warpinski, Margaret K. *The Effect of Base Connection Geometry on the Fatigue Performance of Welded Socket Connections in Multi-sided High-mast Lighting Towers*. Thesis. Lehigh University, May 2006.

Vita

James Robert Kleineck was born in Dallas, TX and grew up with his family in Mesquite, TX. He attended North Mesquite High School, where he graduated in 2005. Following graduation, James moved down to Austin to pursue his bachelor's degree in Architectural Engineering at The University of Texas at Austin. During his undergraduate education, James worked at Ferguson Structural Engineering Laboratory where he learned that he wanted to pursue a master's degree in civil engineering with an emphasis in structures. Upon graduation, James remained at the University of Texas to work toward his advanced degree.

Following graduation from his master's program, James plans on entering into practice designing buildings with a structural engineering consulting company.

Permanent Address:

4929 Country Club Dr.

Mesquite, TX 75150

This thesis was typed by the author.